JAMMING: MARGINAL STABILITY AND THERMODYNAMIC RIGIDITY

by

R. CAMERON DENNIS

A DISSERTATION

Presented to the Department of Physics
and the Division of Graduate Studies of the University of Oregon
in partial fulfillment of the requirements
for the degree of
Doctor of Philosophy

December 2021

DISSERTATION APPROVAL PAGE

Student: R. Cameron Dennis

Title: Jamming: Marginal Stability and Thermodynamic Rigidity

This dissertation has been accepted and approved in partial fulfillment of the requirements for the Doctor of Philosophy degree in the Department of Physics by:

Raghuveer Parthasarathy	Chair
Eric Corwin	Advisor
Tim Cohen	Core Member
Marina Guenza	Institutional Representative

and

Krista Chronister	Vice Provost for Graduate Studies

Original approval signatures are on file with the University of Oregon Division of Graduate Studies.

Degree awarded December 2021

DISSERTATION ABSTRACT

R. Cameron Dennis

Doctor of Philosophy

Department of Physics

December 2021

Title: Jamming: Marginal Stability and Thermodynamic Rigidity

This dissertation marks a significant step forward in fully understanding glasses and jammed materials as we unify the concept of marginality in amorphous systems, definitively resolve the jamming threshold problem, create new methods for simulating and analyzing polymer packings, and prove a series of salient theorems involving periodic boundary conditions.

We shift the discussion of Gardner marginality to include athermal systems and open the door to broader explorations. For the first time, we show that athermal jammed systems in physically relevant spatial dimensions are controlled by the marginal Gardner phase. The set of over-jammed minima form a hierarchical ultrametric space.

Understanding the physics of the jamming transition is widely relevant because jamming critical points occur in systems forming a universality class. This work takes important steps toward verifying the critical properties of this transition. While previous works have confirmed the criticality of thermodynamic variables, no such tests have been carried out for the distributions of contact forces and interparticle gaps.

We demonstrate that mechanically stable jammed packings of spheres can be made at densities all the way down to zero, not only answering a long-standing question about the lower limit on the density of sphere packings, but demonstrating the shocking result that mechanically rigid packings of spheres can exist at zero density. This result is of widespread importance in materials science research.

A system of athermal soft spheres that interact via a one-sided contact potential is an excellent model for jamming and glasses. However, many glasses we interact with on a daily basis consist of molecular chains. By modifying the soft sphere model, I demonstrate how to create polymer packings and examine their properties.

Most simulations involving glasses and jamming utilize periodic boundary conditions, a simple choice that drastically reduces finite-size effects. However, we find that sometimes there is a stark difference between systems with periodic boundary conditions and the corresponding infinitely repeated lattice representations. We show a series of proofs that put these differences into perspective, providing a foundation for better understanding when periodic boundary conditions are appropriate.

This dissertation includes previously published and unpublished single-authored and co-authored materials.

CURRICULUM VITAE

NAME OF AUTHOR: R. Cameron Dennis

GRADUATE AND UNDERGRADUATE SCHOOLS ATTENDED:

University of Oregon, Eugene, OR
Wabash College, Crawfordsville, IN

DEGREES AWARDED:

Doctor of Philosophy, Physics, 2021, University of Oregon
Bachelor of Arts, Physics, 2016, Wabash College (summa cum laude 4.0)
Bachelor of Arts, Mathematics, 2016, Wabash College (summa cum laude 4.0)

AREAS OF SPECIAL INTEREST:

Soft Condensed Matter, Granular Materials, Active Matter, Biophysics, Network, Phase Transitions, Glasses and Jamming

PROFESSIONAL EXPERIENCE:

Graduate Research Assistant, Physics, University of Oregon, 2016-2021

Graduate Teaching Assistant, Physics, University of Oregon, 2016-2020

Writing Center Tutor, Wabash College, 2014-2016

Physics Tutor, Wabash College, 2013-2016

GRANTS, AWARDS AND HONORS:

Research as Art Winner, ArtSci Oregon, 2019

Departmental Exam Award, University of Oregon Physics Department, 2017

Mackintosh Fellowship, Wabash College, 2016

Phi Beta Kappa Prize, Wabash College, 2015

Fuller Prize, Wabash College Physics Department, 2015

Writing Prize, Wabash College Physics Department, 2015

PUBLICATIONS:

R. C. Dennis & E. I. Corwin, "Jamming energy landscape is hierarchical and ultrametric" *Physical Review Letters*, **124**, 078002 (2020).

Patrick Charbonneau, Eric I. Corwin, R. Cameron Dennis, Rafael Daz Hernndez Rojas, Harukuni Ikeda, Giorgio Parisi, and Federico Ricci-Tersenghi. Finite-size effects in the microscopic critical properties of jammed configurations: A comprehensive study of the effects of different types of disorder. **104**, 014102 (2021).

R. C. Dennis & E. I. Corwin, "Dionysian hard sphere packings are mechanically stable at vanishingly low densities" Forthcoming (2021)

R. C. Dennis, "Methods for creation and linear elastic response analysis of packings of semi-flexible soft polymers and chains" Forthcoming (2021)

R. C. Dennis, V. F. Hagh, E. I. Corwin, "Properties of Amorphous Materials Under Periodic Boundary Conditions" Forthcoming (2021)

ACKNOWLEDGEMENTS

I would like to thank..

– my parents for always believing in me and continuing to be supportive throughout my life. I've always felt limitless with their constant encouragement and share this victory with both of them.

– my advisor, Eric Corwin, for the myriad *of* valuable lessons he taught me throughout my time at the University of Oregon. He was always there to give advice when I needed it and to help me get back on track when I veered from my goals. Most important of all, he taught me how exciting research can be. There is so much joy in exploring problems and contributing to the world's scientific knowledge.

– Dennis Krause. I have collaborated with many brilliant people and will collaborate with many more, but he was the first and I owe him a lot for starting me on the path I've been on for the past nine years.

– Jim Brown for teaching me how to think like a physicist and always challenging me beyond what was required.

– Danielle McDermott for her faith in me and her encouragement to continue with my physics education. Without Dr. McDermott, I would never have discovered my love for soft matter physics.

– James Sartor for his feedback, advice, and discussions throughout my time here. He is a superb scientist and friend.

– Philip Jahl for always reminding me to believe in myself.

– Varda Faghir Hagh for being an exceptional role model throughout my time here

– Raghu Parthasarathy for being supportive and helpful to all of us graduate students

– Andrea Liu and Lisa Manning for being incredible scientific role models and for taking me on as a postdoc

– my partner, Olivia, for being a beautiful light during the dark year of 2020. She has been such a supportive and reliable person throughout the tumultuous ending of my PhD.

This work was supported by the National Science Foundation (NSF) Career Award DMR-1255370, and the Simons Foundation No. 454939.

TABLE OF CONTENTS

LIST OF FIGURES

Figure Page

CHAPTER I

INTRODUCTION

I love doing research on glasses because it's so easy. You see, glass is just a very viscous liquid. That's why the beautiful stained glass windows in cathedrals are thicker at the bottom than at the top. All of these windows will eventually need to be replaced before they turn into iridescent pools on the ground. Similarly, if you visit a museum with ancient Mesopotamian glass jewelry, you'll notice that much of it has flowed and congealed into a singular mass. But if glass is simply a liquid that flows very slowly, why are so many physicists studying it? Well, because everything I just said is a lie.

When mummies come back to life, they will be quite relieved to find their glass artwork is precisely as they left it and not a puddle. But I can't blame anyone for perpetuating these myths. The window pane myth for example is an exceptionally appealing and simple explanation for something that is actually quite complicated.

So then what is a glass and why do we care? To begin to answer this question, let's consider a material that everyone is a little more comfortable with: water. We've all seen water in the process of freezing: it gets cold and then some small patches of ice start to form before the whole thing eventually becomes rock solid. So what's happening here? As the water is cooled, the molecules start to organize themselves into a nice crystalline arrangement. Water molecules in a liquid state are arranged without any structures–they slip and slide past each other easily, going wherever they want. Water molecules in an ice crystal on the other hand are

arranged in a nice repeated crystalline pattern and dance in place, bumping into the neighbors that surround them.

So are glasses like liquid water or are they like solid ice? The answer is both...and neither. The molecules of glass, just like the molecules of liquid water, are arranged amorphously–they don't have any structure. But the molecules of glass, like the molecules in ice, are caged by their neighbors and can only dance in place, unable to explore as much space as a molecule in a liquid can. Glass is a solid. It doesn't flow and it shatters if you put too much stress on it.

Taking these ideas one step further, we know that if you heat up a piece of glass, it becomes soft and pliable, transitioning into a substance that is liquid and flows. The hotter the liquid glass, the less viscous it becomes. You might expect that as liquid glass is cooled, it just becomes more and more viscous until eventually we just deem it solid. This is where the idea that glass is a liquid comes from, but as I keep saying, this isn't true! There really is a transition from liquid to solid that happens. If you believe this (and you should) then you might think that the glass transition is just like the transition from liquid water to solid ice, but this also isn't true. The glass transition is something distinct and different and while there has been a plethora of research in understanding this transition, we still have a lot to learn about it.

One way to attack this glass problem is to think about amorphous systems that don't have temperature. The particles don't jiggle around and bump into each other. Some examples of this are grains of sand and rice. The sand on the beach is solid; you can stand on it and it supports your weight. The sand on the beach is liquid; you can fill a bucket with it and pour it out. When you were a kid, did you ever go to a party that had a big jar of candy and a sign beseeching you to

guess how many pieces the jar contains? If the candies were stacked in a nice even cube, you could just count the number of candies on one side and cube the result, but the candies are never arranged nicely, they're always amorphously filling the jar. This little game is an example of a concept called *jamming*. If you pick up the jar of candy and shake it, either the jar rattles as the candy moves around, or the jar is silent and the candy is packed so tight it can't move. The latter situation is jammed and the former is unjammed. Jamming is strongly related to the glass problem because of the amorphicity. And jamming, much like the glass, has a transition associated with it. If your jar of candy rattles, you can simply add another candy to it. If you repeat this process, your jar will go from rattling to slient: from unjammed to jammed. This is called the jamming transition and is the subject of much of my research.

In chapter II of this dissertation, I will share with you a manuscript that was published in Physical Review Letters which will explain jamming more thoroughly and show an interesting connection between glasses and jammed solids. There is a complicated phase transition that glasses can go through called the Gardner phase transition. In this manuscript I show that jammed packings of spheres are marginal as well. Marginal stability is an interesting, albeit confusing concept. One way to understand the marginal phase is by considering a jammed pile of sand grains. Sand grains in a pile don't move around; they're happy where they are–stable. However, if you gently push on a pile of sand, an avalanche will occur and the sand grains will move and rearrange. However, the pile of sand before and after the soft push are the same macroscopically. We therefore say that the pile of sand is both jammed and marginally stable.

Chapter III is a collaborative, comprehensive study on finite size effects. For real finite glasses, theorists have been unsuccessful in writing down a theory that explains their behaviors. However, a mean-field theory has been developed for infinite dimensional space. Since we only really care about two and three dimensional space, it may seem like this is a waste of time; however it turns out that this mean-field theory is extremely successful at describing things that we actually see in two and three dimensions. We look at a few different types of finite simulations of jamming and compare the theoretical predictions for the distributions of particle gaps and interparticle forces. We show that these agree with the mean-field predictions which means that they are all part of the same universality class.

Chapter IV is about a fundamental property of jamming: the jamming threshold. If you can pick up that jar of candy we talked about a minute ago and it doesn't rattle, we called that jammed. If you're careful about how you pack those candies into the jar, you can fill more of the jar volume than if you were to throw them in haphazardly. Likewise, if you're very careful, you can also make a jammed structure where there is more free space in the jar. But there must be a limit, right? The lowest density one can achieve is called the jamming threshold. We show in this paper that the jamming threshold is precisely zero, which is a counter-intuitive and fascinating result.

Chapter V is a single-author methods paper. In my other projects and indeed in the study of jamming at large, sphere packings are often used. The reason for this is that they are easy to deal with and still give rich, beautiful physics. However, most glasses we encounter on a daily basis are made of polymer chains. This paper shows how to create packings of semi-flexible polymers (clusters of

spheres that are glued together and can't be broken apart). The paper also goes into great detail on how to analyze the structural properties of these packings. The goal of this research is to create a slightly more realistic model that can be used to better understand the polymer glass transition and the elastic properties of polymeric systems.

Chapter VI is a project that was first proposed by Varda Fagir Hagh. This project was a collaborative effort between Varda, me, and Eric Corwin. In jamming physics, we often use something called *periodic boundary conditions* which is like pac-man's world. If pac-man goes all the way to the left of the screen, he suddenly shows up on the right. Likewise, the left side of packings of spheres interacts with the right side. We think of these packings as a representation that tiles all of space. However, we show why this is a problematic idea. If you can pick up your packing and shake it without the particles rattling around, then the packing is jammed. However, if you take this same packing and tile all of space with it, this may no longer be true.

These chapters represent manuscripts in various stages of publication and are presented in a format that has only been slightly altered from their published or pre-published formats.

Studying amorphous materials has been an immensely satisfying endeavor these past few years and I am fortunate and excited to continue this research.

CHAPTER II

JAMMING ENERGY LANDSCAPE IS HIERARCHICAL AND ULTRAMETRIC

2.1. Introduction

The energy landscape surrounding a crystalline material clearly reflects the underlying crystal symmetries. Likewise, the energy landscape surrounding an amorphous material must reflect the replica symmetries underlying amorphous systems. The replica theory of glasses has shown that in the mean field limit, amorphous systems can exist in the liquid phase, the stable glass phase, or the marginal Gardner phase [2, 3, 4, 5, 6, 7, 8, 9]. The energy landscape of the liquid phase is a single smooth basin, reflecting the unbroken replica symmetry of an ergodic phase. In the stable glass phase, this replica symmetry is broken and the landscape consists of many smooth basins separated by energy barriers [8]. However, within any individual basin, replica symmetry is still present. In the marginal Gardner phase, the replica symmetry is infinitely broken as each sub-basin is itself broken up into many sub-basins *ad infinitum* [5, 7, 10, 11, 12, 13, 14, 15]. In the mean field framework, jamming is predicted to lie within the marginal Gardner phase [11, 12, 13, 15, 16]. Indirect evidence for this phase in thermal systems has been observed in numerical simulations [17, 18, 19, 20, 21, 22, 23], in two dimensional pseudo-thermal granular systems [24], and in thermal colloidal systems [25]. The mean field result is applicable to low dimensional systems as evidenced by a recent result demonstrating through thermal exploration that the free energy landscape of quenched soft spheres has a hierarchical structure [23]. Similarly, the free energy landscape of thermal disks at low temperatures

has been observed to be hierarchical [22]. However, it is unknown how well this theory relates to physically relevant three dimensional athermal jammed packings [26, 27, 28, 29] for which not only are dynamics absent, but the system need not be created by an equilibrium process, and for which all behavior is solely determined by geometry. In this paper, we directly measure the Gardner phase in over-jammed systems by constructing the distance metric between nearby minima and characterizing its hierarchy and ultrametricity. We find that for a range of pressures, jammed systems are both hierarchical and ultrametric.

2.2. Background

As illustrated in Figure 2.1, the single replica symmetry breaking (1RSB) solution reflects the fact that a stable glass phase is characterized by *distinct*, infinitely long-lived energy basins. The solution with infinitely many distinct basins-within-basins representing the marginal Gardner phase is called the fullRSB solution [2, 6, 30]. The hierarchical structure of a marginal Gardner phase results in minima forming a tree-like structure in phase space for which minima within a given sub-basin will all be much closer to one another than they will be to minima within any other sub-basin [4]. This feature is codified by the ultrametric inequality [31, 32] which states that the distance d between any three configurations a, b, and c must satisfy

$$d\left(a,c\right) \leq \max\left[d\left(a,b\right), d\left(b,c\right)\right]. \tag{2.1}$$

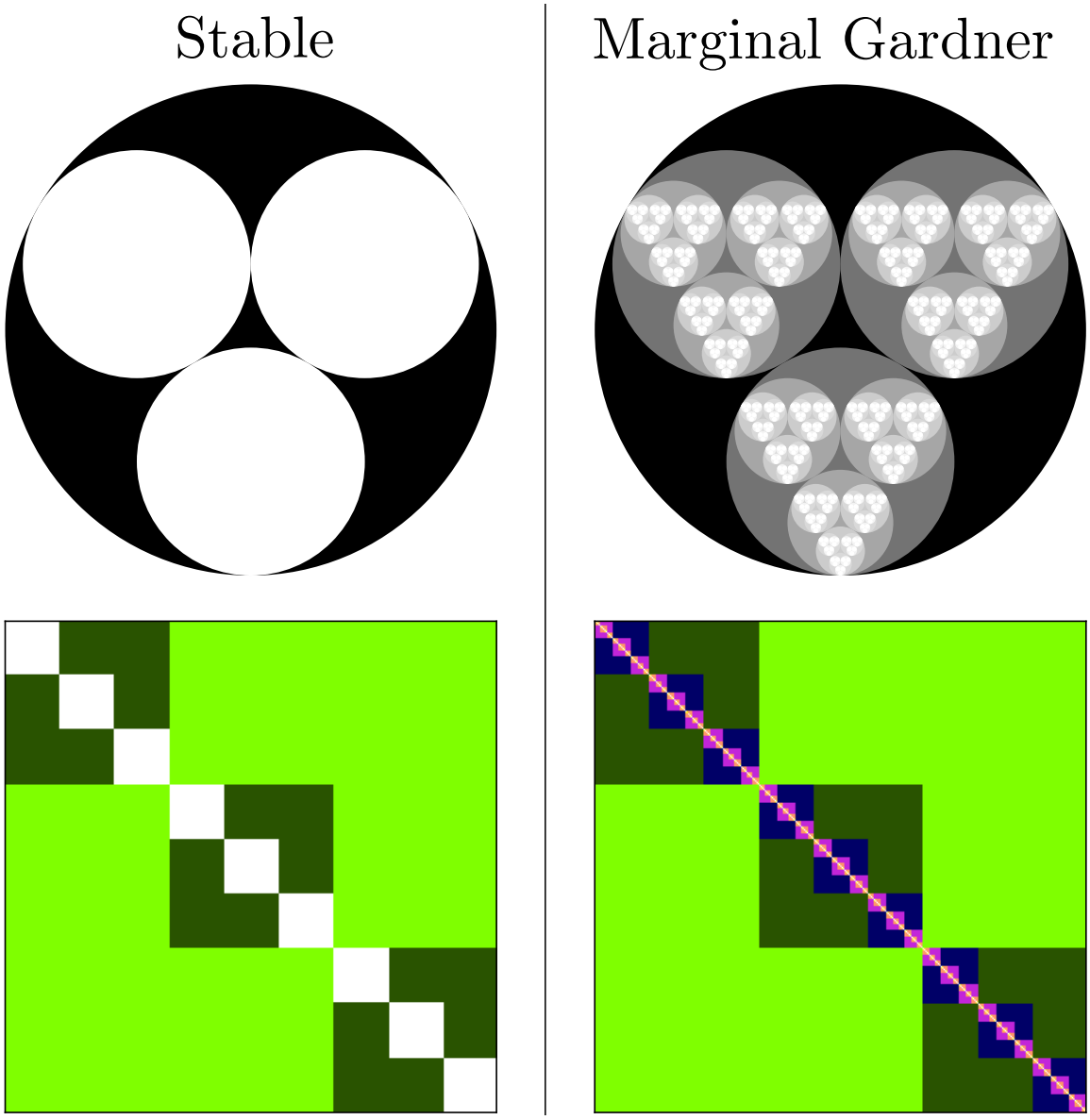

FIGURE 2.1. Above: two dimensional schematic illustrations of the energy landscape present in the stable (1RSB) and marginal Gardner (fullRSB) phases, below: their respective metrics. The ij entry in the metric describes the distance between minimum i and minimum j. The stable system has two levels of distinct infinitely long-lived free energy basins, shown as the set of circles contained within a larger circle. The metric for the stable phase likewise reflects this hierarchy, shown schematically below. In the marginal Gardner system, every sub-basin has sub-basins forming a fractal energy landscape. The metric for such a landscape reflects marginality and is shown schematically below. Note that we depict each basin as having the same number of sub-basins, but marginal systems do not generally have this feature.

2.3. Methods

We construct jammed packings of N monodisperse soft spheres interacting through a harmonic contact potential in three dimensions using the FIRE algorithm [33] as implemented by the pyCudaPacking software [29, 34, 35]. In order to unambiguously distinguish nearby minima in the energy landscape, all calculations are done with quad precision floating point numbers and minimization is only halted once the maximum unbalanced force on any particle is less than 10^{-20} in natural units. Systems are created in a cube of side length 1 with periodic boundary conditions and at a large initial packing fraction $\phi = 0.8$. These packings are then brought to a specified pressure [36] through an iterative process exploiting the known scaling between packing fraction and pressure for over-jammed systems [37].

In sufficiently small systems ($N \sim 10$ in two dimensions), one can sample the entire energy landscape, enumerate all minima, and use these minima to construct the metric for the landscape [38, 39]. However, this quickly becomes intractable as the number of minima increases exponentially with increasing N. Choosing energy minima at random results in a small uncorrelated sample which will trivially not reveal any hierarchical structure as it is extraordinarily unlikely that two minima will be a part of the same deep sub-basin [40, 41]. Instead, we search for correlated samples with a small number of minima which are close together in configuration space and thus have the power to reveal any existing hierarchy.

To explore behavior as a function of distance to jamming, we create initial systems at logarithmically spaced pressures, p, running from 10^{-1} down to $10^{-5.5}$ in natural units. Given a system at a specified pressure, we explore the nearby minima that characterize the local energy landscape by repeatedly perturbing the

initial conditions of the original minimum and re-minimizing. Each perturbation is chosen randomly from a Gaussian distribution and amounts to moving each particle a random distance in a random direction. Due to the random nature of the perturbation, there will be a small component of global particle translation. To remove this we subtract off the global translation when calculating ε, the magnitude of the perturbation. Further, this magnitude is normalized by the typical interparticle spacing, $N^{-1/3}$, to remove the trivial dependence on the number of particles in the system in a way which is independent of the system's packing fraction.

Depending on the initial pressure, many to most nearby perturbed systems will return to the original configuration. To adequately sample the nearby landscape, we continue to perturb the original minimum until we have found 500 distinct minima (with the exception of the data presented in Figure 2.4 for which 5000 minima were found).

Finding the metric for nearby minima using the perturbation technique requires choosing a length scale for the perturbation. A perturbation which is too small will frequently lead back to the original minimum. A perturbation which is too large will result in minima which do not fall within the same top-level superbasin and are not sufficiently nearby in configuration space to properly probe the hierarchical structure of the landscape. Because the configuration space is Nd dimensional, sampling a small spherical volume of the space biases points to the surface of the sphere. Instead, to better sample nearby minima, the length of the perturbation ε is chosen from a uniform distribution between 0 and $\varepsilon_{\max}$.

Figure 2.2 shows the magnitude of the initial perturbation, scaled by $\sqrt{N}$, plotted against the resulting normalized distances between the original system and

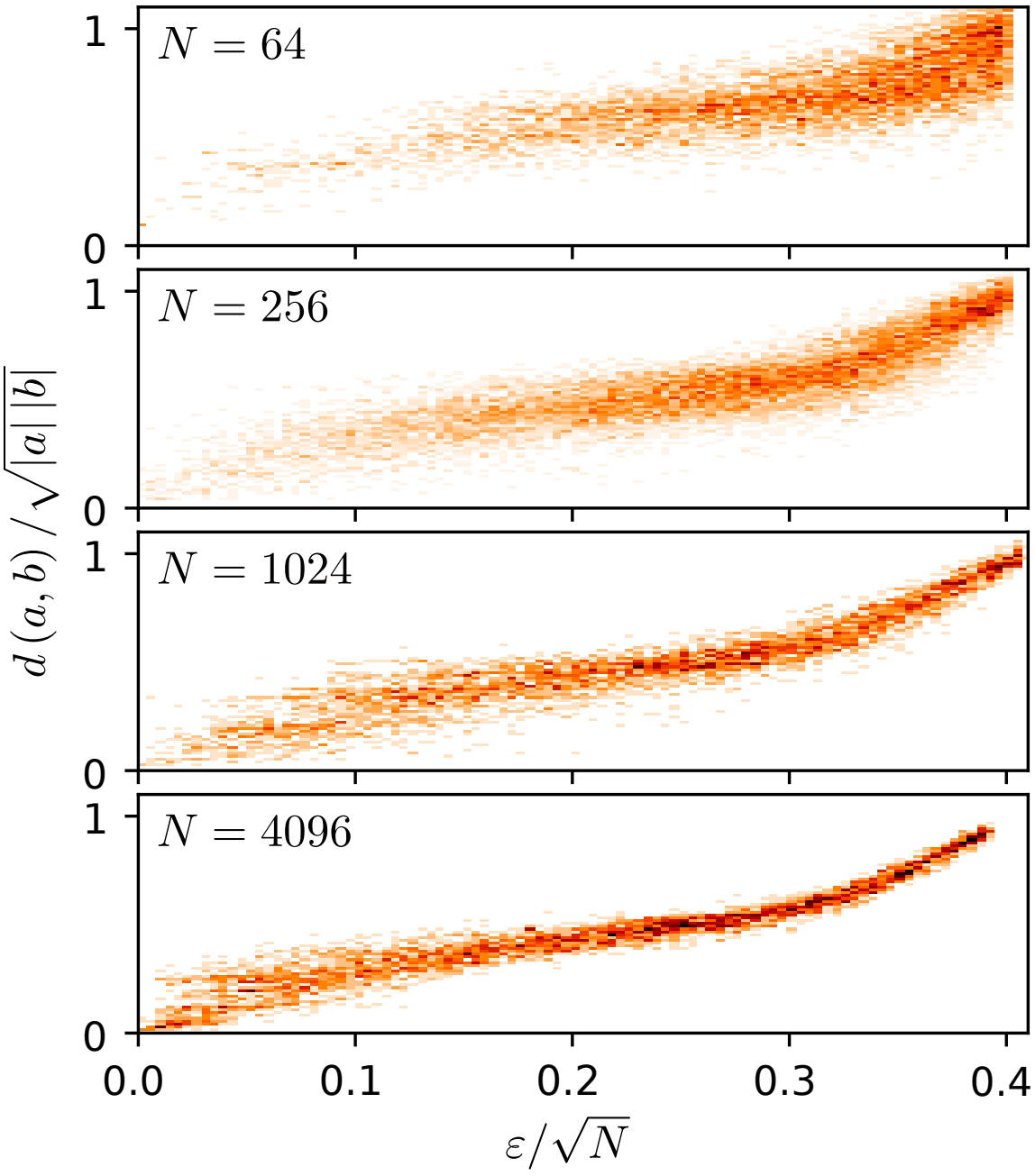

FIGURE 2.2. Two dimensional histograms of the distribution of normalized metric distance to the original packing as a function of the size of the perturbation. The original packing is perturbed by a Gaussian random vector with length ε and then minimized. The distance between the original minimum and this newly discovered minimum, $d(a,b)$, is found. This distance is normalized by $\sqrt{|a|\,|b|}$ where the absolute value of a system $|a|$, is defined as $d(a,0)$ and 0 is the contact network containing all zeros. From the top, plots for packings with 64, 256, 1024, and 4096 particles at pressure $p = 10^{-3}$. We see that these curves all take a similar functional form and have a normalized metric distance of about 1 at $0.4\sqrt{N}$ which is thus a natural value for $\varepsilon_{\max}$.

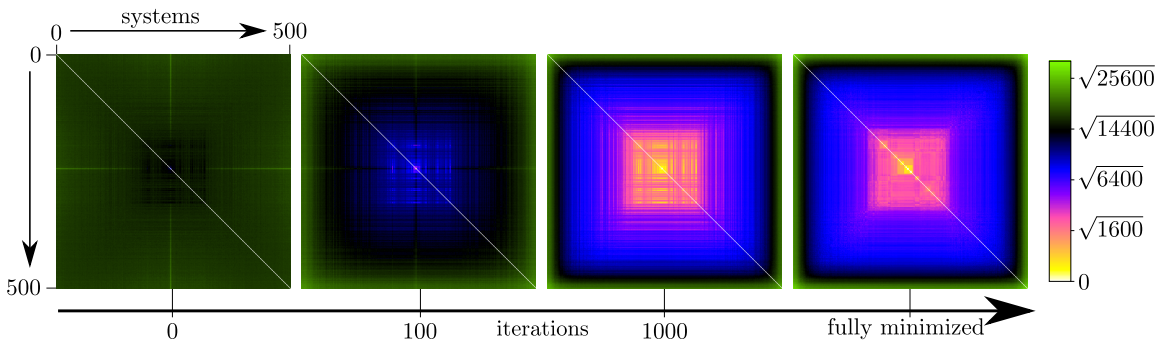

FIGURE 2.3. Evolution of hierarchy with minimization. 500 configurations with $N = 4096$ are prepared by perturbing a random minimum at a pressure 10^{-3}. The metric distance between every pair of configurations, as given in equation 2.2, is shown for 0, 100, and 1000 minimization iterations as well as for fully minimized systems. The color scale reflects the metric distance is labelled by square rooted numbers, reflecting the fact that the metric distance is roughly the square root of the number of changed contacts between two systems for $d(a, b) < \sqrt{N}$.

the minimized perturbed system. A scaled distance of one means that the number of stable contacts that differ between two systems is comparable to the number of stable contacts present within each system. Systems that are greater than this distance bear no more structural relationship and are thus in different top-level basins, making this a natural cutoff for exploring the hierarchical structure of the local energy landscape. The relationship between distance and initial perturbation becomes sharper with increasing N and does not depend strongly on pressure. Exploiting this empirical relationship, we set $\varepsilon_{\max} = 0.4\sqrt{N}$.

Given a set of nearby minima, we construct the metric d by calculating the distance between every pair of minima. To avoid the ambiguity introduced by rattlers and by global drifts, we define the distance based on the stable contact vector network within each system. The stable contact vector between particle i and particle j for configuration a is denoted as $\vec{C}_a^{ij}$. If two particles are not in contact, the contact vector between them is taken to be $\vec{0}$. The distance between

two systems a and b is

$$d\left(a,b\right) \equiv \frac{1}{\langle\sigma\rangle}\sqrt{\sum_{ij}\left(\vec{C}_a^{ij} - \vec{C}_b^{ij}\right)^2} \tag{2.2}$$

where σ is the diameter of a particle. This metric has the convenient property that $d(a,b)$ will be approximately equal to the square root of the number of contacts that differ between the two minima for $d(a,b) < \sqrt{N}$.

For any set of elements with a metric, one can construct a new ultrametric by changing the pairwise distances. There exists a family of ultrametrics for which every distance is smaller than that found in the original metric. Of these, the ultrametric that is closest to the original metric is called the subdominant ultrametric, $d^<$, and can be constructed from the original metric using a minimum spanning tree [42] as detailed in the supplementary information. We characterize the generalized distance between the subdominant ultrametric and the original metric as

$$\mathcal{D} \equiv \sqrt{\left\langle\left(d(a,b) - d^<(a,b)\right)^2\right\rangle} \tag{2.3}$$

where the angle brackets denote an average taken over every pair of a and b. $\mathcal{D} = 0$ indicates a precisely ultrametric system.

2.4. Results

Development of hierarchy upon minimization – Figure 2.3 shows the evolution of the metric between distinct nearby minima of $N = 4096$ particles as a function of iterations of the minimization protocol. These 500 minima are all initially created by the above perturbation process around an arbitrarily chosen initial

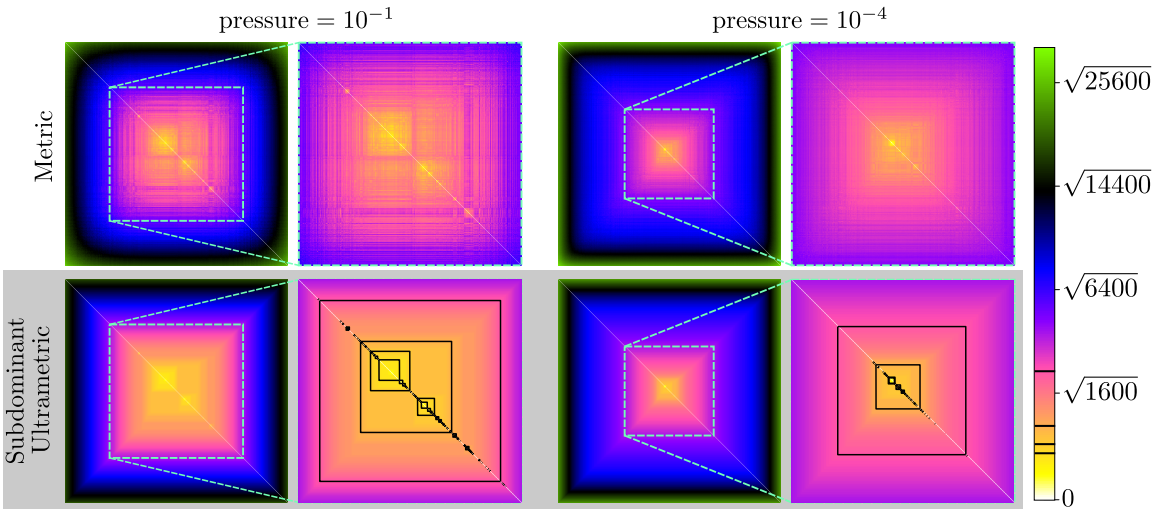

FIGURE 2.4. Metrics (top) and corresponding subdominant ultrametrics (bottom) as a function of pressure constructed from 5000 systems with $N = 4096$ particles. Next to each metric and ultrametric is a blowup of the region for which the subdominant ultrametric distance is less than $\sqrt{4096}$ which amounts to approximately 1 contact per particle. Contours of the subdominant ultrametric are overlayed to highlight the hierarchy and their values are shown on the color bar. The color scheme is the same as in Figure 2.3.

minimum. The simple nature of this random perturbation is revealed in the first panel which shows every system is initially nearly equidistant (shown in black and dark green). After 100 iterations (second panel) of minimization, the structure of a basin (shown in black and blue) begins to appear as some systems relax towards the initial minimum by reforming contacts; meanwhile others relax away by forming different contacts and fall into distinct super-basins (shown in lighter green). After 1000 iterations (third panel), the hierarchical structure begins to appear but only becomes fully realized once systems are fully minimized (final panel). The metrics are all sorted using the single link clustering algorithm [43] on the subdominant ultrametric of the fully minimized systems.

The hierarchical structure at different pressures – We plot the metric and corresponding subdominant ultrametric for minima of $N = 4096$ particles far from

jamming, $p = 10^{-1}$, and those closer to jamming, $p = 10^{-4}$, in Figure 2.4. These metrics are each constructed from 5000 distinct nearby minima. As jamming is approached, we observe the metric to become more similar to the subdominant ultrametric and we see that ever fewer minima fall into the same sub-basins. Visually, systems at a low pressure have a metric that is closer to the subdominant ultrametric than do those at high pressure. This can be observed in the quality of the color scale matching and the sharpness of the boxes corresponding to sub-basins. For the high pressure metric, three-fifths of all systems differ from one another by less than one contact per particle whereas at low pressure about two-fifths of the systems differ by less than this amount. Once perturbed, the positions of particles for low pressure systems do not need to change as much before finding a new minimum. As the pressure is decreased, the number of nearby minima explodes leading to a shrinking of the region that can be densely sampled. Both of these results arise from the increasingly rough and hierarchical energy landscape upon the approach to jamming.

We quantify the qualitative result of increasing ultrametricity with decreasing pressure in Figure 2.5 by plotting $\mathcal{D}$ as a function of scaled pressure, N^2p, which can be interpreted as the distance to jamming [44]. We see that for all system sizes $\mathcal{D}$ collapses onto a master curve which achieves a plateau value of about 2.7 as N^2p goes to zero. This means that on average the distance between any pair of minima will be bigger than the distance needed for ultrametricity by about 2.7. However, the distance between any pair of minima itself scales with $\sqrt{N}$ so this *fractional* excess of distance will tend to zero as N becomes large. Therefore in the thermodynamic limit the metric becomes precisely ultrametric for all of the pressures explored.

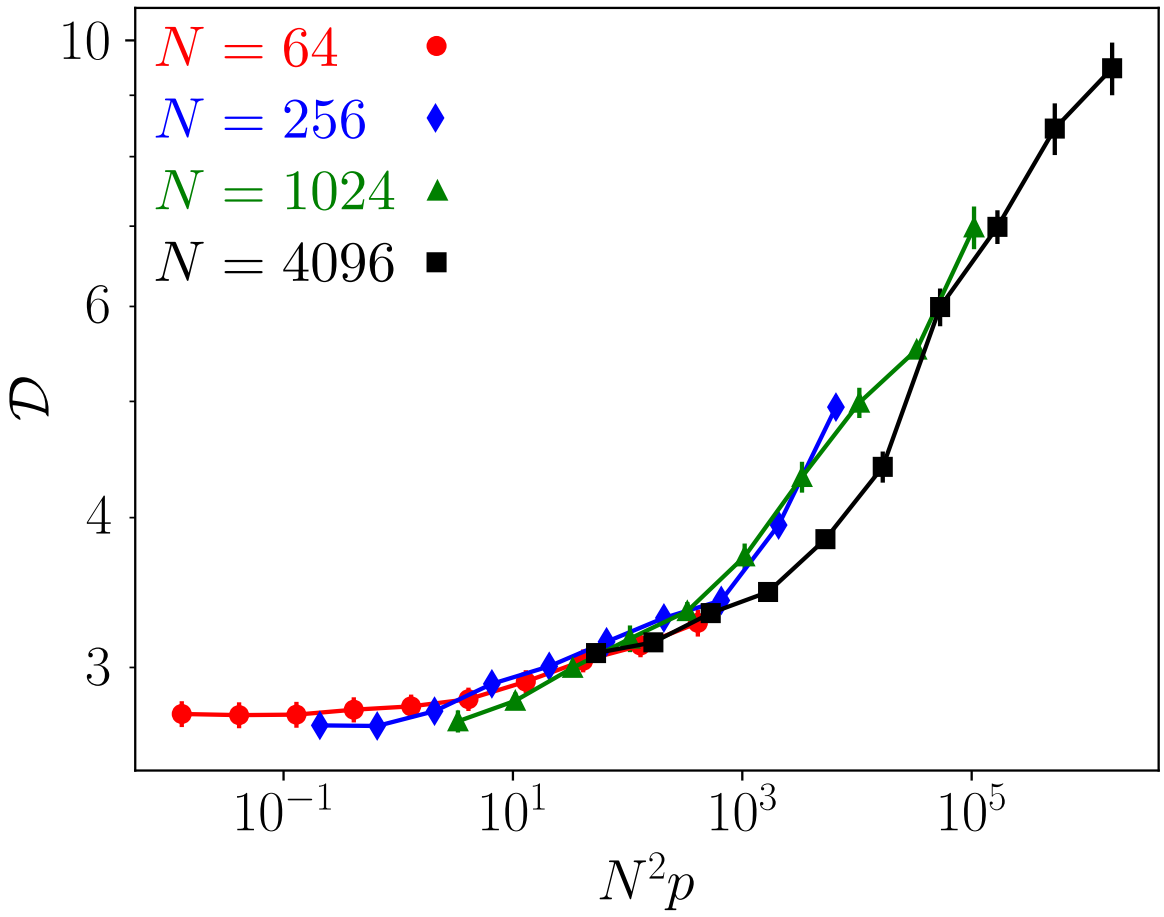

FIGURE 2.5. The generalized distance between the subdominant ultrametric and the original metric, $\mathcal{D}$, as a function of pressure and system size. The number of systems over which each point is averaged is chosen such that the standard error bars fall below a threshold. Systems of different sizes fall on a master curve.

2.5. Conclusions

The structure of the distance metric between minima provides the first evidence that the energy landscape of over-jammed three dimensional configurations becomes hierarchical and ultrametric in the thermodynamic limit for all pressures sampled. In this limit, the marginal Gardner phase arises as strictly a consequence of geometry with no recourse to thermal fluctuations. It is far from clear that this hierarchy and ultrametricity arises for such low-dimensional configurations, especially with finite numbers of particles. This result points to the universality of the marginal Gardner phase within amorphous materials as it has now been measured within athermal materials in addition to the already known thermal [22, 23] and mean-field limits [3]. By exploring the energy landscape at zero temperature and never with any sense of thermal exploration, we have sampled a spatially localized region of phase space. Our results demonstrate that the Gardner phenomenology is not just restricted to the easily accessible regions of configuration space that are seen in thermal materials, but is instead present everywhere.

This research demonstrates that Gardner physics can be observed in athermal out-of-equilibrium systems. Furthermore, that this result can be seen in an athermal system demonstrates that the Gardner transition controls not only the free energy landscape but also the underlying energy landscape. As such, Gardner physics should be amenable to experimental tests which need not rely on thermal systems. This innovation marks a significant step forward in fully understanding glasses and jammed materials as we unify the concept of marginality in amorphous systems.

Acknowledgments – We thank Horst-Holger Boltz, Peter Morse, Sid Nagel, and Camille Scalliet for useful discussions. This work benefited from access to the University of Oregon high performance computer, Talapas. This work was supported by National Science Foundation (NSF) Career Award DMR-1255370 and the Simons Foundation No. 454939.

2.6. Supplementary Materials

2.6.1. The Subdominant Ultrametric

We present here a simple outline of the algorithm for creating the subdominant ultrametric and provide an intuitive explanation for how it works. Given a metric, d, the corresponding subdominant ultrametric, $d^<$, can be found with the following algorithm [42]:

1. The metric, d, is a symmetric matrix of pairwise distances between minima. This can be reinterpreted as an edge-weighted graph where the nodes are the minima and the edge weights are the distances between minima.

2. We compute the minimum spanning tree of this graph, which is simply the network with the minimum possible total edge weight (sum of distance values) which connects every node into a single tree. The minimum spanning tree is unique [45] and has the property that every pair of nodes has only one path connecting them.

3. The subdominant ultrametric, $d^<$, is created as a symmetric matrix with entries $d^<_{ij}$ determined by the maximum edge weight in the path from node i to node j in the minimum spanning tree.

The hierarchical nature of $d^<$ derives from that of the minimum spanning tree. The maximum condition ensures that the resulting metric will be ultrametric as it is a direct enforcement of the ultrametric inequality (Equation 1 of the text). Given any triplet of minima the constructed subdominant ultrametric $d^<$ will produce a triangle with one short side and two equal long sides. This is an equivalent definition of the ultrametric inequality given in the manuscript. This explanation demonstrates why this algorithm returns an ultrametric which always contains distances that are less than or equal to the corresponding metric entries. However, the proof that this is the largest possible ultrametric to satisfy this criterion is less intuitively obvious and can be found in the original reference [42].

2.6.1.1. Uniqueness of the Subdominant Ultrametric

If all of the edge-weights in our metric are distinct, the minimum spanning tree will be unique [45]. Our metrics come from amorphous systems with unique edge-weights and unique minimum spanning trees. Additionally, the subdominant ultrametric is always unique whether or not this condition is met because while degenerate edge-weights results in multiple minimum spanning trees, the maximum edge-weight along the path between every pair of nodes will be the same [42].

CHAPTER III

FINITE SIZE EFFECTS IN THE MICROSCOPIC CRITICAL PROPERTIES OF JAMMED CONFIGURATIONS: A COMPREHENSIVE STUDY OF THE EFFECTS OF DIFFERENT TYPES OF DISORDER

3.1. Introduction

Jammed systems may lack dynamics, but their study is far from motionless. A surge of physical interest over the last couple of decades has indeed led to marked advances [8, 10, 46, 47, 48, 49, 50, 51]. This sustained interest stems partly from jamming being observed in systems as varied as grains, foams, and emulsions, and partly from jamming exhibiting features encompassed in few universality classes. The mix of ubiquity and universality has motivated the search for a common framework to explain the pervasiveness of jammed systems and their properties, starting with the seminal works of Liu, Nagel and co-workers [26, 52]. It has since become clear that although different systems reach jamming by tuning different physical variables, several properties *near* and *at* the onset of jamming are shared by all of them. In other words, the same underlying physics should be responsible for the jamming phenomenology. Even though a fully comprehensive theory remains to be formulated, a major step forward has been the discovery that this jamming point is critical and gives rise to a phase transition, albeit an out-of-equilibrium one [28].

Attempts to better understand jamming [47] commonly focus on systems of frictionless spherical particles[49], which are central to a fairly wide universality class (see below). An outstanding example of the theoretical analysis that can

be achieved by such geometric simplification is the recently developed mean-field (MF) theory [5, 6, 7, 8, 46, 53] that describes –exactly, in the infinite-dimensional limit– the behavior of glass-forming liquids from the point they fall out of equilibrium up to jamming. Even though one might expect this theory only to be valid in high spatial dimensions, near jamming it describes many of the critical properties observed in dimensions as low as $d = 2$ and $d = 3$[8, 37, 46, 54]. (A different criticality is observed in quasi-one-dimensional systems [55, 56].) Jamming criticality is peculiar because not only thermodynamic variables, *e.g.* the pressure or bulk and shear moduli, but also collective quantities, such as the mean square displacement and the average contact number, scale critically with the distance from the jamming point. More specifically, denoting the configuration density (or packing fraction) ϕ and its value at the onset of jamming ϕ_J, several quantities either jump discontinuously or scale as power laws, $|\phi - \phi_J|^\mu$, as the jamming point is approached [26, 48, 57]. Although ϕ_J depends sensitively on the preparation protocol –thus giving rise to a density continuum of jamming points [17, 49, 58, 59, 60, 61]– μ is often surprisingly independent of dimensionality and polydispersity[26]. And even though different interaction potentials may yield different exponents for a given quantity, this dependence can often be trivially accounted for [48, 50, 57]. Importantly, once a jammed state is reached for a given potential, the resulting configuration is an equally valid jammed state for any other potential [37] .

However broad this universality class may be, it does not prevent μ from depending on whether the jamming point is approached either from below (*i.e.* from the under-compressed (UC) phase, $\phi \to \phi_J^-$) or from above (over-compressed (OC) phase, $\phi \to \phi_J^+$). A salient example is pressure, P, which scales as

$P \sim |\phi - \phi_J|^{\pm 1}$ [26, 62], i.e., $\mu_\pm = \pm 1$ as $\phi \to \phi_J^\pm$. In the UC case, pressure thus diverges as density approaches ϕ_J, as found in granular materials or glass-formers made out of infinitely hard particles [10]. Conversely, in the OC case, pressure vanishes linearly as the packing fraction is brought down to ϕ_J, as found in soft-harmonic particles [26]. Another important example is the average contact number, $\overline{z}$. Simulations of harmonic soft spheres, for instance, show that $\overline{z}$ exhibits a discontinuity exactly as $\phi \to \phi_J^-$, and then grows as $\overline{z}(\phi) - \overline{z}(\phi_J) \sim (\phi - \phi_J)^{1/2}$ for $\phi > \phi_J$ [26]. This discontinuity can be related to the condition that the number of contacts in a configuration should exactly match its number of degrees of freedom, *i.e.*, the onset of isostaticity [48, 50, 63]. Recent studies have further verified the expected finite-size scaling of P, $\overline{z}$, and the bulk and shear moduli for a wide variety of potentials in $d = 2$ and 3 [44, 64]. A Widom-like scaling function has further been derived for these variables as well as for the configurational energy and shear stress [65]. Furthermore, various studies have identified correlation lengths associated to the characteristic length scales of vibrational response to perturbations [66, 67], the fluctuations in the number of contacts [68, 69], and the fluctuations of particle mobility [57], all of which diverge at the jamming point. These observations for thermodynamic variables and bulk properties provide some of the strongest evidence in support of the critical nature of the jamming transition.

Remarkably, some of the *microscopic* structural properties of jammed configurations, such as the distributions of contact forces and interparticle gaps, are also expected to exhibit non-trivial critical scalings. In particular, in a jammed configuration of N spherical particles with center positions $\{\mathbf{r}_i\}_{i=1}^N$ and diameters $\{\sigma_i\}_{i=1}^N$, one can define a dimensionless gap between any pair of particles, $h_{ij} =$

$\frac{|\mathbf{r}_i - \mathbf{r}_j|}{\sigma_{ij}} - 1$, with $\sigma_{ij} = (\sigma_i + \sigma_j)/2$. Because jammed packings are disordered, gap values are randomly distributed, but theoretical predictions [6] state that the distribution of small gaps should scale as

$$g(h) \sim h^{-\gamma}, \qquad \text{with } \gamma = 0.41269\ldots \tag{3.1}$$

Similarly, the distribution of small contact forces is predicted to scale algebraically, $p(f) \sim f^{\theta}$, but initial reports found a strong dependence of θ on dimensionality and jamming protocol, in apparent contradiction with the theoretical expectation [70]. This paradox was resolved by recognizing that two different types of forces contribute in this regime [37, 70]. Opening the contact between a pair of particles can indeed give rise to two distinct responses: (i) a localized rearrangement of neighboring particles; or (ii) a displacement field that extends over the whole configuration, without decaying with distance. The former is associated with a buckling motion, and hence remains localized; the latter is associated with a correlation length of the same order as the system size, and hence is a clear example of the criticality of jammed packings. Considering these two types of forces separately yields two power laws with different exponents,

$$p(f_\ell) \sim f_\ell^{\theta_\ell}, \qquad \text{with } \theta_\ell \simeq 0.17, \tag{3.2a}$$

$$p(f_e) \sim f_e^{\theta_e}, \qquad \text{with } \theta_e = 0.42311\ldots; \tag{3.2b}$$

for localized and extended excitations, respectively. The ability of MF theory [6, 8, 46] to predict the non-trivial values of γ and θ_e is considered a major analytical success. MF theory, however, does not directly predict θ_ℓ, because bucklers are an intrinsically low-dimensional feature [37], and are therefore absent from the $d \to \infty$

description. The critical exponents of gaps and contact forces are also of utmost importance because they are associated with the mechanical stability of jammed packings. By considering the displacement field that follows opening one of the two types of contacts as well as the ensuing closure of gaps to form stabilizing contacts, a pair of inequalities between γ, θ_ℓ, and θ_e can be derived [54, 71],

$$\gamma \geq \frac{1-\theta_\ell}{2}, \tag{3.3a}$$

$$\gamma \geq \frac{1}{2+\theta_e} \ . \tag{3.3b}$$

MF theory values as well as numerical simulations indicate that both inequalities are in fact saturated, implying that jammed packings are *marginally* stable [71, 72]. This result is consistent with the MF description, which always locates the jamming point within a critical Gardner phase that emerges deep in the glass phase and is characterized by the emergence of marginally stable states [5, 6, 8, 17, 46, 73].

The picture that coalesces from putting together the exact MF description with the critical scalings for thermodynamic and other variables, and from considering the robustness of numerical experiments for several dimensions and for different protocols [8, 10, 28, 37], suggests that the jamming transition of spherical particles properly defines a universality class. We now know that this class should encompass a broad range of problems and models beyond spherical particles, including the perceptron [74, 75], neural networks [76, 77, 78], statistical inference [79], and the SAT-UNSAT transition in continuous constraint satisfaction problems [80, 81]. Recent works have shown that universality persists even when the interactions are non-analytic, for instance, due to discontinuous forces [75, 82].

Yet, a careful analysis of the values of θ_ℓ, θ_e, and γ inferred from numerical simulations has not systematically been carried out. Conducting such an analysis is especially important considering that packings of slightly polydisperse crystals are reported to exhibit a microstructure characterized by exponents that differ considerably from those of Eqs. (3.1) and (3.2) [83, 84]. Additionally, recent works have shown that many of the salient features of spherical packings depend sensitively on particle shape. For instance, introducing even an infinitesimal amount of asphericity changes the universality class [85, 86], in which the isostatic condition no longer holds. An assessment of the extent of the jamming universality class and an accurate test of its many theoretical predictions are therefore in order [73].

In this work we systematically analyze the finite-size scaling of the distributions of interparticle gaps and contact forces. These distributions are one of the fundamental consequences of the presumed non-trivial critical behavior of jammed packings, hence their testing is a key step toward rigorously validating a whole set of critical properties. Although a similar analysis has been carried out for the perceptron [87] and for the gaps distribution of a two-dimensional binary mixture [85], no systematic result exists for jammed packings of spherical particles nor for amorphous packings with other sources of disorder. Here, in addition to analyzing the most common cases of jammed configurations, *i.e.* $2d$ polydisperse and $3d$ monodisperse packings, we consider two additional sets of jammed packings: (i) polydisperse spheres in a crystalline FCC structure; and (ii) Mari-Kurchan (MK) hard spheres with random shifts distributed uniformly over space [88]. By examining the impact of different sources of disorder, we attempt to define precisely which are the most robust features of jamming criticality, and

thus better demarcate its physical universality. The rest of this paper is organized as follows. In Sec. 3.2 we describe the models used and the algorithms employed to produce jammed configurations and extract the relevant structural information, *i.e.* the interparticle gaps, h, and contact forces associated with extended, f_e, and localized, f_ℓ, displacement fields. We also explain how finite-size effects in the distributions of these structural variables are considered. In Sec. 3.3 we present a detailed analysis of the finite size effects in jammed configurations of monodisperse spherical particles in $3d$, where we reveal the striking contrast of such effects on the distributions f_e and h. Then, in Sec. 3.4 we present a similar analysis for the other types of systems considered, finding important differences with the results for $d = 3$ spherical systems. We nevertheless argue that most of these differences can be explained from the other scaling corrections described in Sec. 3.2.4. Because theory and previous numerical studies suggest that f_e and h are critically correlated across the whole system, we first consider these two quantities. The distribution of localized forces, f_ℓ, associated with buckling effects is expected to be independent of system size, hence its analysis is postponed to Sec. 3.5. A discussion and brief conclusion are given in Sec. 3.6.

3.2. Numerical methods, models systems, and finite-size scaling

In this section, we describe the numerical techniques used to produce jammed sphere packings, coming from either the OC or the UC phase. Studying independently these two regimes is useful because –as for other critical points– there is no reason *a priori* to assume that the scalings from above and below ϕ_J are the same. Because each of these two phases is identified with different materials, namely granular matter (from the UC regime) and glasses, foams, and colloids

(from the OC phase), this verification is an important test of materials universality. We also describe the other models considered, which are chosen to better appraise the extent of the jamming universality class. The methodology employed to analyze the system size dependence on the distributions of the microstructural variables, Eqs. (3.1) and (3.2), is also detailed.

3.2.1. Jammed states from the OC phase

We first consider three-dimensional configurations of N spheres of equal diameter, *i.e* $\sigma_{ij} = \sigma \; \forall i, j = 1, \ldots, N$, in a cubic box under periodic boundary conditions. In a certain sense, this choice is the minimal model with which to produce jammed packings. Lower-dimensionality systems inevitably crystallize unless polydisperse mixtures are used, but ordering can be avoided for monodisperse spheres in $d \geq 3$. Sphere positions then serve as the only source of disorder. Given the set of vectors of positions $\{\mathbf{r}_i\}_{i=1}^N$, the jamming point starting from the OC phase is obtained for the harmonic contact potential,

$$U\big(\{\mathbf{r}_i\}_{i=1}^N\big) = \frac{\epsilon}{2} \sum_{i,j} (\sigma - |\mathbf{r}_i - \mathbf{r}_j|)^2 \; \Theta(\sigma - |\mathbf{r}_i - \mathbf{r}_j|), \tag{3.4}$$

where ϵ is a constant that defines the energy scale) and Θ is the Heaviside step function. Hence, a pair of particles only interacts if there is an overlap between them. Starting in the OC phase with $\phi > \phi_J$ ($\phi = 1.02$ in two dimensions (see below) and $\phi = 0.792$ in three dimensions) and a uniformly random distribution of spheres in a square box, a series of energy minimization steps and packing fraction reduction steps are performed until the system has just a single state of self stress, which is where jamming criticality occurs [54, 58, 71, 89]. Such

a state is characterized for having one contact above isostaticity, *i.e.* when the total number of constraints in a system, N_c, matches its number of degrees of freedom, N_{dof}. A single state of self stress is required for critical jamming in order to achieve a finite bulk modulus [44, 90]. Put differently, the system density is an additional variable that needs to be fixed, and thus requires one additional contact above isostaticity [91]. At a given density the FIRE algorithm, a damped dynamics method, is used to achieve force balance in the configuration [33]. The energy of the configuration is then calculated and the known scaling relation, $U \propto (\phi - \phi_J)^2$ [37], is used to determine by how much the sphere radii should be uniformly decreased to reduce the system energy by a fixed fraction. After several iterations of this procedure, the packing has precisely $N_c = N_s d - d + 1$ contacts where N_s is the number of stable particles and thus $N_{dof} = d(N_s - 1)$ corresponds to the number of degrees of freedom in a system under periodic boundary conditions. A small fraction of particles, termed rattlers, remain unconstrained at jamming and do not contribute to the overall rigidity of the packing[37, 64, 91], thus $N_s = N - N_r$, with N_r denoting the amount of rattlers in a given configuration. In a d-dimensional system, these rattlers can be identified as particles with fewer than $d + 1$ contacts. Although N_r changes from one configuration to another, N_r/N always lies within a small range of $\sim 2 - 3\%$. Only the total number of particles in the system, N, is thus reported. After removing rattlers, the dynamical matrix [50] is used to ensure that the packing is jammed. This algorithm is implemented in the pyCudaPacking software using general purpose graphical processing units and quad-precision calculations [29, 34, 35]. Given that our configurations are not subject to any external force, once the jamming point is reached the N_c dimensional vector of forces magnitudes, $\underline{\boldsymbol{f}}$, is obtained as the non-zero solution to

the set of linear equations that impose the condition of mechanical equilibrium[37]:

$$\mathcal{S}^T \underline{\boldsymbol{f}} = 0\,; \quad \mathcal{S}^{\alpha k}_{\langle ij \rangle} = (\delta_{jk} - \delta_{ik}) n^{\alpha}_{ij}\,. \tag{3.5}$$

In this last equation, $\langle ij \rangle$ with $i < j$ is the index of a contact, $\mathbf{n}_{ij}$ is the unit contact vector pointing from particle i to j, and $\alpha = 1, \ldots, d$ indexes its components. (The single state of self stress that results guarantees that $\underline{\boldsymbol{f}}$ is unique.) Contributions associated with localized buckling displacements, f_ℓ, are then separated from those that produce extended excitations, f_e, using the fact that (with high probability) bucklers are particles with $z_\ell = d + 1$ contacts [37]. The set $\{f_\ell\}$ is thus taken as the set of forces applied on particles with z_ℓ contacts, while $\{f_e\}$ is its complement.

3.2.2. Jammed states from the UC phase

For configurations initially in the UC regime, an infinitely hard-sphere potential is used and a combination of molecular dynamics (MD) and linear optimization algorithms are employed to approach ϕ_J from below. More precisely, we start from a low-density configuration of particles with random positions and use event-driven MD with a Lubachevsky–Stillinger (MD-LS) growth protocol [59] to increase the (reduced) pressure up to $P = 500$. This first step is performed with a fast compression rate in order to avoid any partial crystallization and is then followed by a second, much slower, growth protocol until $P \gtrsim 10^7$. In this way, the MD-LS protocol compresses a low density fluid into an out-of-equilibrium glass at a very high pressure, while still closely following the (phenomenological) equation of state [10, 17, 59]. The high pressure configuration is then used as input for the

sequential Linear Programming (LP) algorithm used in Refs. [92, 93] to produce jammed packings. At each step, the LP algorithm finds the optimal rearrangement of particles that maximizes their radius, considering a linearized version of the non-overlapping constraint between any pair of particles. Upon convergence, this algorithm produces a jammed configuration, because neither particle displacements nor size increases are possible. This approach also allows to easily build the full network of contacts at jamming, because genuine contact forces can be identified, up to a proportionality factor, from the active dual variables associated to the non-overlapping constraints. As with the OC phase, rattlers are removed and only systems with a single state of self stress are considered. Moreover, it is easy to show that the contact forces thus obtained also satisfy Eq. (3.5), and therefore our hard-sphere packings are well defined jammed states.

Using either of the two methods to reach jamming we find that all our configurations have a similar final density, $\phi_J \approx 0.64$, which corresponds to inherent structures of systems that are quenched relatively quickly[10, 26, 46, 48, 49, 50, 58, 59, 92, 93, 94]. (Fluctuations around the average value of ϕ_J decrease for larger system sizes, as first reported in Ref. [26].) Some remarks about the differences of the two protocols are nevertheless in order. First, note that independently of how a jammed packing is realized, it must be a minimum of the corresponding free energy [6]. And indeed, both of our protocols are implemented to perform such minimization, although in markedly different circumstances. For instance, critical jamming occurs in the $T \to 0$ limit when coming from the OC phase, so the free energy is minimized by finding a energetic ground state of the configuration. The FIRE algorithm allows to perform such energy minimization, and by iteratively decompressing the system until overlaps vanish, we guarantee that the final

configuration is also valid when $T = 0$. For hard spheres, by contrast, only the entropic contribution to the free energy matters, because the interaction energy is necessarily zero and the kinetic contribution is trivial. Correspondingly, our MD-LS+LP method proceeds by maximizing the entropy of the configuration as the free volume per particle vanishes [95].

But it should be mentioned that harmonic[96] and logarithmic contact potentials[94, 97] can also be used to produce jammed packings from the UC phase. In our case however, the two different protocols we implemented to reach free energy minima are conceived to follow the specific route of the systems we aim to model: (OC) thermal glass formers, soft particles etc., or (UC) grains, rigid particles and other athermal systems.

3.2.3. Other models of jammed packings

We also investigate the jamming point of three other models.

Polydisperse disks: Previous studies strongly suggest that the upper critical dimension of the exact MF theory is $d = 2$ [37, 54, 64]. However, as mentioned above, particles of different sizes must then be utilized to inhibit crystallization. An additional source of disorder is thus introduced by extracting particle radii from a log-normal distribution to achieve a polydispersity–defined as the ratio of standard deviation to mean–of 20%. This was achieved by generating a Gaussian random number, R, with parameters $\mu = 0$ and $\sigma = \sqrt{\ln(0.2^2 + 1)}$ and setting the radii to be e^R. (Note that the radii distribution parameters should not be confused with the particle diameter used in monodisperse systems.) These soft harmonic spheres are initially in the OC regime, and thus the FIRE-based algorithm is used to bring

configurations to their jamming point via repeated quenching and decompression steps.

Crystalline polydisperse spheres: Removing randomness from particle positions while keeping size polydispersity as the main source of disorder is achieved by generating jammed packings on the sites of a regular face-centered cubic (FCC) lattice. Radii are drawn from a log-normal distribution with a polydispersity of 3%. These nearly crystalline packings are brought to critical jamming using the quenching and decompressing FIRE-based protocols for soft spheres initially in the OC phase. Although this type of system displays many of the features associated with traditional glasses [83], its distributions of forces and gaps often markedly differ from those predicted by MF theory [83, 84]. By using a system with a different crystalline symmetry we aim to quantify such discrepancy.

Monodisperse Mari-Kurchan (MK) spheres: The MK model is a MF reference given that, by construction, the properties of MK configurations are roughly independent of dimension. Specifically, we consider $d = 3$ systems of monodisperse spheres that interact according to a randomly shifted distance, $D(\mathbf{r}_i, \mathbf{r}_j) = |\mathbf{r}_i - \mathbf{r}_j + \mathbf{A}_{ij}|$, where $\mathbf{A}_{ij}$ is a quenched random vector drawn uniformly from the total system volume. Introducing random shifts, $\mathbf{A}_{ij}$, suppresses almost completely correlations due to short loops on the interaction graph. Even if $D(\mathbf{r}_i, \mathbf{r}_j) = D(\mathbf{r}_j, \mathbf{r}_k) = \sigma$ it is very unlikely that $D(\mathbf{r}_i, \mathbf{r}_k) \simeq \sigma$. In other words, while for particles interacting via the usual Euclidean distance neighbours of a given particle are likely also neighbours, in the MK model, almost certainly, they are not. Because this property is also the case for systems using the Euclidean distance in the $d \to \infty$ limit, it is expected that the microscopic structural properties of MK jammed configurations should follow the MF theory predictions

closely. Besides, it has already been verified that the MK model exhibits several features of more usual glass formers [98], that a Gardner transition also occurs deep in the glass phase [99], and that contact number fluctuations are critically correlated at jamming [69]. Consequently, any deviation from MF predictions observed for this system can safely be attributed to finite-size corrections, which makes the MK model a particularly useful reference to explain the contrasting scaling effects in the distributions of gaps and contact forces (Sec. 3.6). For this model, we consider hard sphere configurations initially in the UC phase, and use the MD-LS and LP algorithms to reach their corresponding jamming point, after going through the liquid and glass phases[98, 99].

3.2.4. Expected finite-size scalings

To ensure that we sampled all the systems of a given type with the same accuracy, M_N independent configurations are produced for a fixed value of N, such that data of $N \times M_N \gtrsim 10^6$ particles is obtained. (Specific values for each system are given below.) Forces and gaps can then be studied across many orders of magnitude, and finite-size corrections can be systematically identified. Because testing for power-law distributions using logarithmic binning of the probability density function (pdf) leads to poor comparisons (due to the loss of resolution when grouping data in a single bin to produce a smooth trend [100]), the cumulative distribution function (cdf) is considered instead. Note that if a random variable x is distributed according to a pdf of the form $\rho(x) \sim x^\alpha$ for $\alpha > -1$, then its cdf follows $c(x) \sim x^{1+\alpha}$.

When fitting a distribution to empirical data it should be considered that even if x ideally follows such a distribution all the way down to $x \to 0$,

finite sampling inevitably leads to deviations. Here, the situation is further complicated by our consideration of marginals of correlated variables. Gaps and forces distributions of finite N configurations are indeed prone to exhibit deviations from their expected form due to both finite sampling and system-wide correlations. Fortunately, introducing a scaling function, as is usually done in the study of critical phenomena [101, 102], can account for both effects, and hence the dependence of the cdf on system size can be carefully teased out.

To derive the size scaling of the distributions of x, we first note that in a sample of size $N \gg 1$, we can estimate the order of the smallest value observed in the data, $x_{\min}$, from the probability mass assigned to the extremes of the distribution:

$$\int_0^{x_{\min}} \rho(x)\,\mathrm{d}x \sim x_{\min}^{1+\alpha} \sim \frac{1}{N}. \tag{3.6}$$

In other words, $x_{\min}$ can be estimated from the weight assigned to the extremal value of the empiric cdf, whence it follows that $x_{\min} \sim N^{-1/(1+\alpha)}$. Note that strictly speaking in this last equation N should be replaced by N_c when analyzing, for instance, the distribution of contact forces. However, given that $N_c \sim dN$ and that we are mostly concerned with the scaling exponent, we can safely neglect the associated proportionality constants. The behavior of the gap distribution is expected to be similar, in that the amount of particles almost in contact should be self-averaging. Next, we follow the traditional path for analyzing size scaling and write the pdf as

$$\rho(x) \sim N^{\beta}\tilde{\rho}\Big(xN^{\frac{1}{1+\alpha}}\Big) \tag{3.7}$$

where $\tilde{\rho}$ is the scaling function of the pdf such that $\tilde{\rho}(x) \sim x^{\alpha}$ for $x \gtrsim 1$. The exponent β can be easily determined by requiring that $\rho(x)$ exhibits no N

dependence for a large enough value of x, given that if $N^{\frac{1}{1+\alpha}}\ x \gg 1$ the data should follow the expected power-law scaling for any N. We thus get that $\beta = -\frac{\alpha}{1+\alpha}$, whence the expressions used for the scalings studied in Ref. [87] are recovered. For the cumulative distributions, repeating the above analysis for $c(x) \sim N^{-\delta}\tilde{c}\Big(xN^{\frac{1}{1+\alpha}}\Big)$ gives $\tilde{c}(x) \sim x^{1+\alpha}$, and it immediately follows that $\delta = 1$, whence the relevant scaling relation is

$$c(x) \sim N^{-1}\ \tilde{c}\Big(xN^{\frac{1}{1+\alpha}}\Big). \tag{3.8}$$

Using the correct α should remove any dependence on N. Data for different system sizes should then be rescaled such that they follow a common curve, $\tilde{c}$. Finding a good collapse of the curves for different N thus indicates that deviations from the expected power laws fall outside the thermodynamic limit, but are not caused by the variables following a different power-law scaling. Additionally, showing that the system size influences the cdf of a given variable strongly evinces that such a variable is correlated across the whole system. Hence, an upper bound to the correlation length can then be estimated.

We want to stress that for microscopic variables of jammed configurations the situation is conceptually different from that of standard critical phenomena, because the systems are already *at* the critical point. We here do not investigate how the distributions of contact forces and gaps converge to their expected distributions as we move away from ϕ_J, but instead analyze how the system size affects the range over which power-law scalings are followed. As a result, most techniques for size scaling analysis (*i.e.* computing $\gamma(N)$ and $\theta_e(N)$ by isolating the non-singular contribution of an appropriate scaling function *away* from ϕ_J and then extrapolating to $N \to \infty$) are inapplicable. Equation (3.8) can nevertheless

be used to estimate the scaling functions of the cdf of gaps and forces obtained by integrating Eqs. (3.1) and (3.2), respectively.

At the upper critical dimension $d = 2$, we expect a logarithmic correction to the size scaling law [64, 103, 104, 105],

$$\rho(x) \sim x^{\alpha}(-\ln x)^{\xi}, \text{for } x \ll 1. \tag{3.9}$$

We can then estimate $x_{\min}$ as

$$\int_0^{x_{\min}} \rho(x)dx \sim x_{\min}^{\alpha+1}\,(-\ln x_{\min})^{\xi} \sim \frac{1}{N}, \tag{3.10}$$

leading to

$$x_{\min} \sim N^{-\frac{1}{1+\alpha}}(-\ln x_{\min})^{-\frac{\xi}{1+\alpha}} \sim N^{-\frac{1}{1+\alpha}}(\ln N)^{-\frac{\xi}{1+\alpha}}. \tag{3.11}$$

Repeating the same argument as above, we get

$$c(x) \sim N^{-1}(\ln N)^{-\xi}\ \tilde{c}\left(xN^{\frac{1}{1+\alpha}}(\ln N)^{\frac{\xi}{1+\alpha}}\right), \tag{3.12}$$

where the pre-factor is chosen such that $c(x)$ does not depend on N for $x \gg x_{\min}$. For the cases considered in this work, no theoretical prediction exists for the value of ξ, and hence it here serves as a fitting parameter.

We consider yet another correction to Eq. (3.7) that can also be derived from MF theory. Given that jammed configurations have one extra contact than N_{dof} (see Sec. 3.2.1), the power laws of the microstructural critical variables should be cut off at very small values [80, 85, 106]. MF theory predicts that interparticle gaps are distributed as $h^{-\gamma}$ only for values larger than a cut-off $h^{\star} \sim \delta z^{\frac{1}{1-\gamma}}$, where δz is the excess of contacts in a system with respect to isostaticity. In our case, $\delta z \sim$

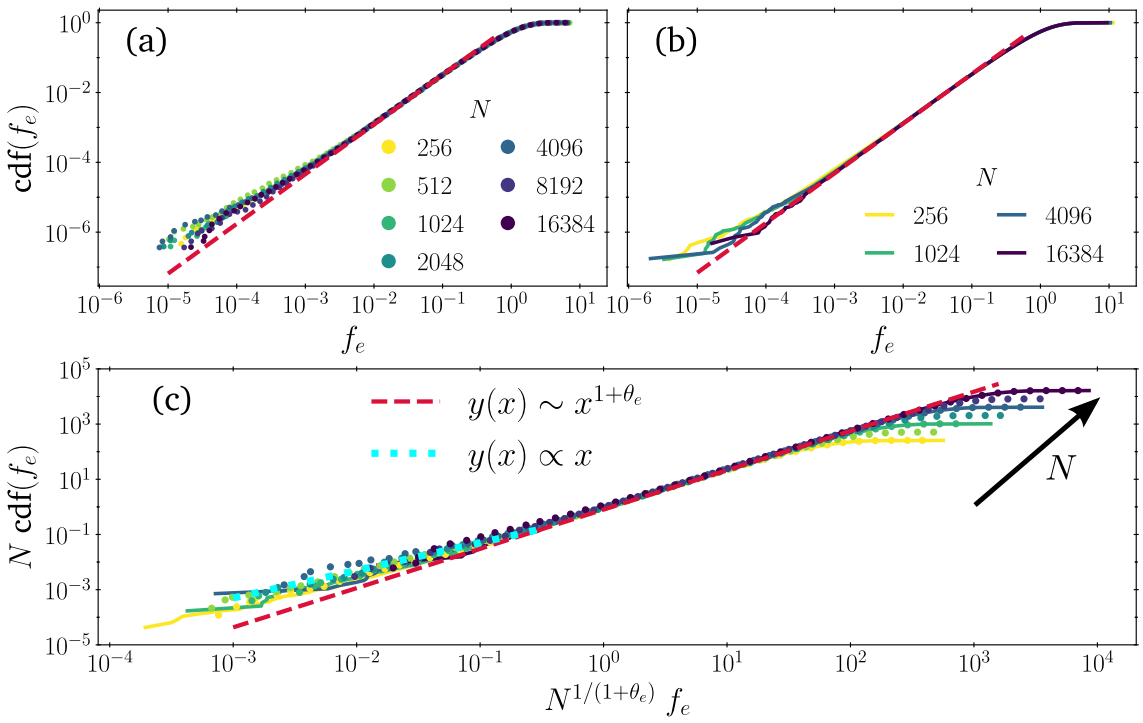

FIGURE 3.1. Cumulative distributions of extended contact forces associated with extensive excitations of monodisperse configurations of frictionless spheres for different system sizes N, as their jamming point is reached (a) from below (UC) and (b) from above (OC). To better distinguish between the two different regimes, results belonging to the UC (OC) phase are identified by circular markers (solid lines). (c) Rescaling (a) and (b) according to Eq. (3.8) clearly collapses the data. The red dashed line corresponds to the power-law scaling of Eq. (3.3b), and shows an excellent agreement between the MF predictions and our numerical results. The coincidence of results from the UC phase and OC phase for various N confirms that θ_e is the same when jamming is reached from either direction. In the left tail of the distributions of panel (c) we also include a comparison with the linear scaling (cyan dotted) expected for very small values, following Eq. (3.14). When put together, these two behaviors match the predictions given in Eq. (3.15).

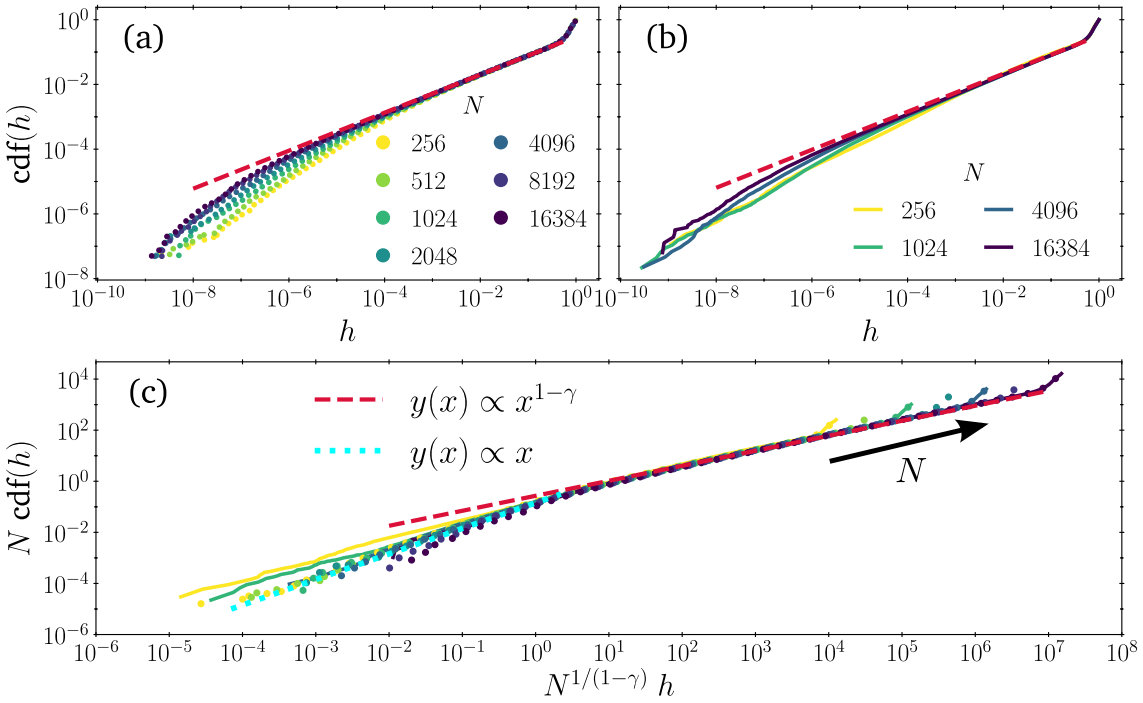

FIGURE 3.2. Cumulative distributions of interparticle gaps for the same configurations as in Fig. 3.1, as their jamming point is reached (a) from below (UC) and (b) from above (OC). (c) Rescaling (a) and (b) according to Eq. (3.8) shows that finite-size corrections can be accounted for in all cases. For comparison, the power-law scaling derived from MF theory, Eq. (3.1), is also shown (red dashed line). Once again, the fact that datasets from both phases, *i.e.* UC (markers) and OC (lines), neatly superimpose confirms that the exponents at the jamming point are the same, independently of how ϕ_J is approached. Additionally, the secondary scaling regime $g(h) \sim 1$ of Eq. (3.13), also predicted by MF theory, can be observed for very small values. Its associated linear cdf is shown (cyan dotted line). These two regimes confirm that the scaling function agrees with our prediction in Eq. (3.15).

$1/N$, so instead of Eq. (3.1) the pdf describing the distribution of h reads,

$$g(h) \sim \begin{cases} N^{\frac{\gamma}{1-\gamma}}\ g_0\Big(hN^{\frac{1}{1-\gamma}}\Big), & hN^{\frac{1}{1-\gamma}} \ll 1 \\ h^{-\gamma}, & hN^{\frac{1}{1-\gamma}} \gtrsim 1 \end{cases} ; \tag{3.13}$$

where $g_0(x) \sim 1$ for $x \ll 1$[85]. Analogously, for extended forces Eq. (3.2b) should be replaced by

$$p(f) \sim \begin{cases} N^{\frac{-\theta_e}{1+\theta_e}}\ p_0\Big(fN^{\frac{1}{1+\theta_e}}\Big), & fN^{\frac{1}{1+\theta_e}} \ll 1 \\ f^{\theta_e}, & fN^{\frac{1}{1+\theta_e}} \gtrsim 1 \end{cases} , \tag{3.14}$$

where $p_0(x) \sim 1$ for very small values is to be expected. Equations (3.13) and (3.14) are indeed consistent with Eq. (3.7) and, repeating the same arguments as above, it is straightforward to derive that both regimes can be captured by Eq. (3.8) using a single scaling function, such that

$$\tilde{c}(x) \sim \begin{cases} x\,, & x \ll 1 \\ x^{1+\alpha}\,, & x \gg 1 \end{cases} . \tag{3.15}$$

That is, using the correct α in Eq. (3.8) accounts for size effects that give rise to deviations from the main power-law scaling as well as the appearance of the linear regime in the left tails. By plotting Nc as a function of $N^{\frac{1}{1+\alpha}}x$ both corrections can thus be tested from a single scaling collapse.

3.3. Finite-size effects in $d = 3$ systems

We first consider systems of monodisperse particles in $d = 3$ by generating, for each N, M_N independent packings, such that $N \times M_N \simeq 2.2 \times 10^6$ (5.5×10^6) particles are considered when the jamming point is approached from the UC

(OC) phase. Figure 3.1 shows the distributions of f_e obtained coming from below (UC, panel (a)) and from above (OC, panel (b)). Comparing the results with the theoretical prediction for the power-law scaling reveals an outstanding agreement over at least three decades. More importantly, no visible signature of finite-size corrections can be detected over the range of N considered. To verify more stringently the absence of finite-size effects, we attempted to collapse the different curves by rescaling the extended forces and their cdf following Eq. (3.8), obtaining the curves reported in panel (c). This last figure evinces that the same critical distribution of forces is found independently of whether the jamming point is generated from the UC or OC regimes. Yet, it is clear that our packings exhibit an excess of very small forces (an effect more noticeable when jamming is reached from below; see Fig. 3.1a), echoing earlier observations [37, 54, 83, 87]. Note that the scaling of Eq. (3.8) does not remove these deviations from the predicted distribution. Note also that these deviations roughly occur for the same scaled force, $N^{\frac{1}{1+\theta_e}} f_e \lesssim 1$. It is therefore likely that forces are subject to size effects caused by the onset of a second power law, $p(f) \sim 1$ (see Eq. (3.14)). We get back to this point below.

Figure 3.2 presents the corresponding cumulative distributions of gaps. The data are also in very good agreement with the predicted scaling of Eq. (3.1), independently of the direction in which jamming is approached. More importantly, the distributions of h are strongly dependent on system size. In contrast to $p(f_e)$, the scaling correction given in Eq. (3.8) using the MF value of γ precisely corrects for such effects over almost *seven* orders of magnitude (Fig. 3.2c). The growing deficit of very small gaps as the system size decreases is another manifestation of the cut-off of the main power law of $g(h)$. It leads to a secondary linear regime,

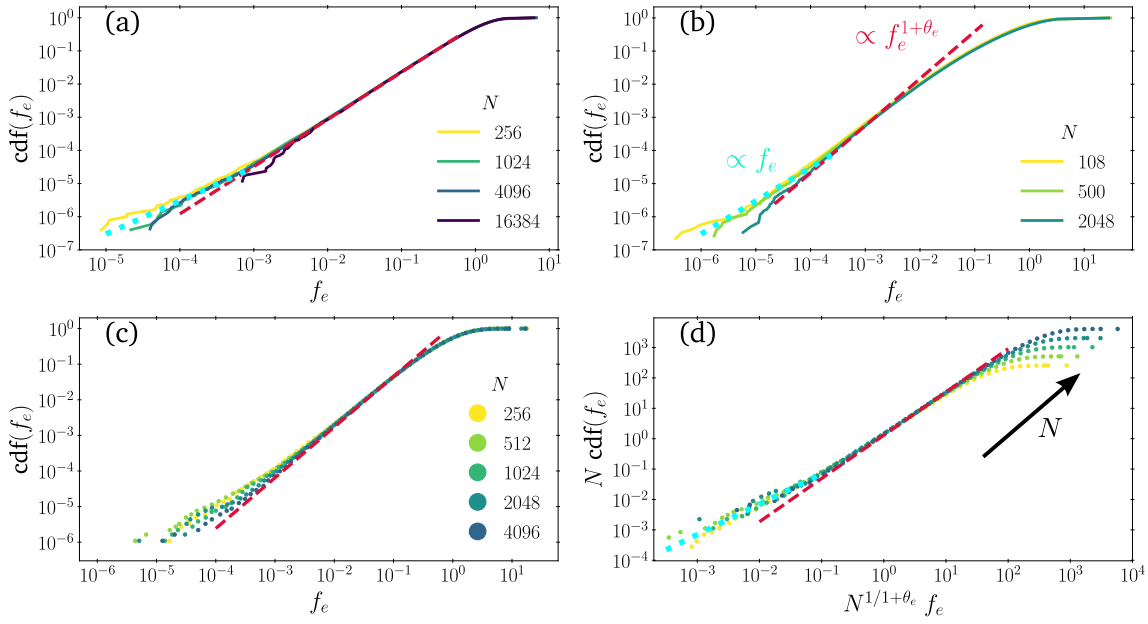

FIGURE 3.3. Cumulative distributions of f_e for jammed configurations of (a) $d = 2$ polydisperse disks packings, (b) polydisperse spheres with a FCC crystalline structure, and (c) packings using the $d = 3$ MK model. Panel (d) depicts the same data from the MK model, rescaled according to Eq. (3.8); see text for details. Data in the upper (resp. lower) panels were produced as jamming was approached from above (resp. below). The expected power law, Eq. (3.2b) is shown (red dashed lines), as is the secondary linear regime, see Eq. (3.14) (cyan dotted lines).

as given in Eq. (3.13), that is in agreement with the numerical results (Fig. 3.2c). This indicates that distances between nearby spheres are significantly modified in finite-size configurations and, consequently, so is the distribution of gaps. This phenomenon is physically interesting. Heuristically, the finite N influence on $g(h)$ can be understood by relying on the marginal stability of jammed packings. In the thermodynamic limit, a system has always enough space to relax any perturbation caused by a contact opening, and hence is always able to re-accommodate particle positions–even if this requires bringing many of them infinitesimally close to each other–in order to guarantee stability. In a finite system, by contrast, no such unconstrained relaxation can take place. Rearranging an extensive fraction of particles necessarily influences the pair of spheres involved in the contact just opened. There is therefore a certain scale, below which the occurrence of small gaps is disfavoured. If the system were further relaxed, then at least one extra contact would form.

At this point, we wish to stress that our results demonstrate the existence of two different types of finite-size corrections to the distributions of extended forces and gaps. The first is a consequence of large scale correlations and can thus be readily taken into account by the scaling of the cdf given in Eq. (3.8). Although this correction is practically absent in the forces distribution, for $g(h)$ it is the main source of deviation from the theoretical prediction. The second is a consequence of the critical scalings of Eqs. (3.1) and (3.2b) being cut off at very small values. This effect, which is very likely related to the excess contact with respect to N_{dof} (see Sec. 3.2.4), affects both microstructural variables and can also be teased out reasonably well using the scaling advanced in Eq. (3.8). We get back to this point in Sec. 3.4, after having considered its signature in other models.

Before concluding this section, it is worth emphasizing that our numerical results are in excellent agreement with the MF, $d \to \infty$ predictions for the power-law scaling of the distributions of both the extended forces and the interparticle gaps. These results confirm that the jamming criticality of these microstructural variables is robust with respect to changes in the systems dimensionality, all the way down to $d = 3$, in agreement with earlier albeit less accurate studies [28, 54, 70]. Because results from both OC and UC phases superimpose onto each other, we further conclude that the critical behavior is controlled by the same exponents on both sides of the jamming point.

3.4. Finite-size effects in other disordered systems

We next consider the finite-size scaling of the force and gap distributions at jamming for the three other models mentioned above: (i) polydisperse disks, (ii) crystalline polydisperse spheres, and (iii) monodisperse MK spheres. From Sec. 3.3, we understand that the direction of approach to the jamming point does not influence on the criticality of microstructural variables, so only one such direction is considered for each mode. The first two approach the jamming point from the OC phase with $N \times M_N \simeq 5 \times 10^6$ particles, and the third from the UC phase with $N \times M_N \simeq 10^6$.

Despite the marked differences between the three models, their distributions of f_e all follow the MF predictions very closely (Fig. 3.3). (a) The $d = 2$ packings show a very good agreement with the cdf derived from Eq. (3.2b) over most of the accessible range. (b) Results for the FCC symmetry also follow the expected scaling, but because its onset takes place at smaller forces, the range of consistency with the MF power-law scaling is correspondingly reduced. (c)

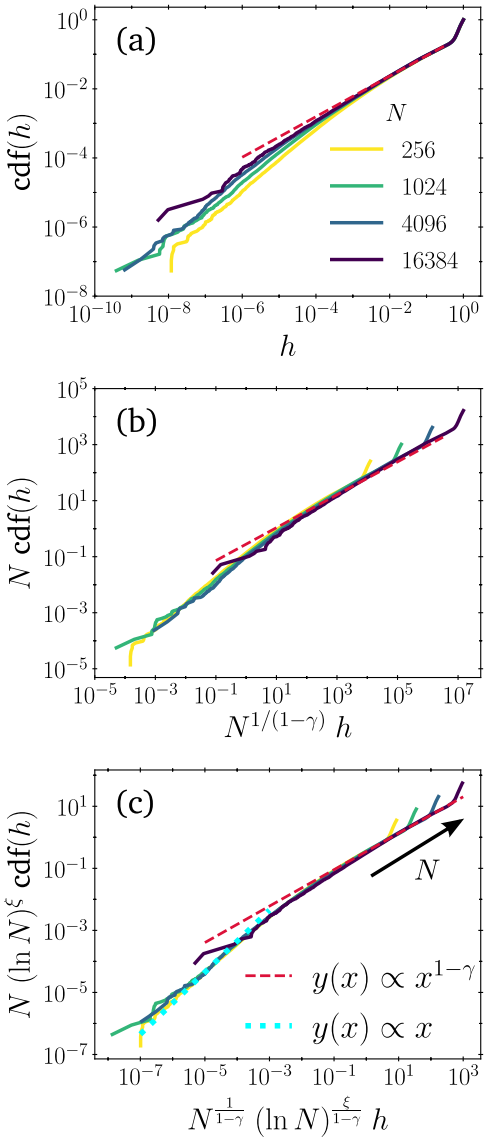

FIGURE 3.4. (a) Cumulative distributions of h of jammed configurations of $d = 2$ polydisperse disks and different size N. (b) Scaling of the different curves following Eq. (3.8) using the MF value of γ. (c) Same scaling as in (b) but including a logarithmic correction as in Eq. (3.12). Choosing $\xi = -2.5$ then best collapses the results. For reference, the expected power-law scaling is shown (red dashed line), as is the linear regime given by Eq. (3.13) at very small arguments (cyan dotted line).

Jammed configurations produced using the MK model exhibit a noticeable–albeit small–dependence on N, but this dependence can be removed by rescaling the cdfs according to Eq. (3.8) using the MF value of θ_e (see Fig. 3.3d). Interestingly, all three systems display an excess of very small contact forces for $f_e \lesssim 10^{-4}$, similarly to what was found for $d = 3$ configurations (see Sec. 3.3). Our results suggest that this effect is due to a crossover to a second regime, in which forces are distributed uniformly, as given by Eq. (3.14). A comparison with the corresponding linear behavior in each panel of Figure 3.3 presents a reasonably good agreement, in support of this hypothesis. A more careful analysis would nonetheless be needed to single out the true form of the left tails of $p(f_e)$.

We next consider the finite-size effects on the distribution of gaps of these three systems. From the spacing between different curves in $d = 2$ packings, it is clear that such effects are pronounced (Fig. 3.4a). Rescaling these distributions following Eq. (3.8) with MF value for γ yields a collapse (Fig. 3.4b) that is not as good as for their $d = 3$ counterparts. Section 3.2.4 anticipated this discrepancy on the basis that $d = 2$ is the upper critical dimension for jamming [64], and hence a logarithmic correction should be included, as in Eq. (3.12). As shown in Fig. 3.4c, with such correction the data can be robustly collapsed using the MF value of γ.

By contrast, gaps distributions in the FCC jammed configurations are best described by a completely different exponent. Figure 3.5 clearly shows that (a) finite-size corrections are important, but that (b) a poor collapse is obtained when curves are rescaled using Eq. (3.8) with the MF value of γ. Using (c) a different $\gamma_{FCC} \simeq 0.33$, however, satisfactorily captures the N dependence. This confirms previous reports that γ is changed in presence of an underlying crystalline structure [83, 84]. Reference [84] even found that γ depends on the

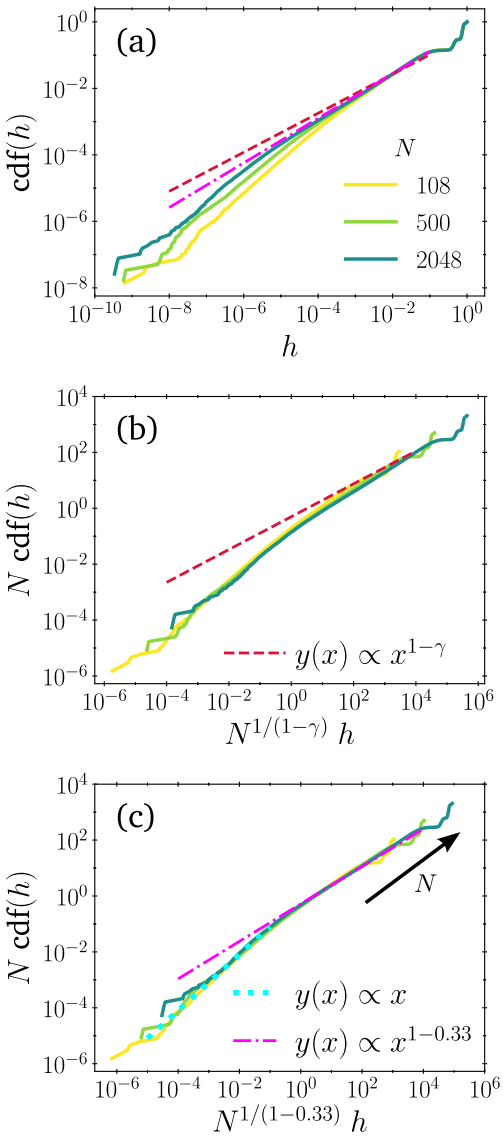

FIGURE 3.5. (a) Cumulative distributions of h for jammed configurations of polydisperse spheres with an FCC structure and different N. Scaling the different curves according to Eq. (3.8) using (b) the MF value of γ and and (c) $\gamma_{FCC} = 0.33$. For a clearer comparison, the trend for the expected power-law exponent (red dashed line) and for γ_{FCC} (pink dashed-dotted curve) are shown. For FCC configurations, unlike for $d = 2$ systems, the collapse obtained with the MF value of γ is poor over the whole interval considered of the scaled variables (see Fig. 3.4b). Note that when γ_{FCC} is used, a linear scaling at very small arguments is recovered (cyan dotted line).

system polydispersity, through the variance of the particle sizes. It is important to stress that finding a smaller γ is not merely a matter of scrupulous curve fitting. It also positively violates the marginal stability relations, Eqs. (3.3), and thus indicate that near-crystals belong to a different universality class than standard amorphous packings of spheres. We comment further on this point in Sec. 3.6.

Figure 3.6 presents the gap distributions for the MK model. Here again, finite-size corrections to $g(h)$ are significant, but now taking the MF value of γ in Eq. (3.8) yields a very good collapse, as expected from the MF nature of the model. It is important to note that although individual distributions of h suggest that a smaller exponent would better fit the curves in Fig. 3.6a, doing so worsens significantly the quality of the scaling collapse. This situation is typical of many critical scalings in finite-N systems [101, 102]. The most reliable way to determine critical exponents remains the finite-size scaling analysis. It is however surprising that the individual distributions in the MK model, which by construction should be closer to the MF solution, do not display the right gap exponent. Indeed, we observe from Fig. 3.6b that the scaling variable using the MF value of γ is the correct one (data do collapse when plotted versus $\tilde{h} = N^{1/(1-\gamma)}h$), but the slope of the curves in the range covered in our simulations ($10^{-3} < \tilde{h} < 10^{3}$) is not that predicted by MF theory. An important concern is thus whether this deviation is due to finite-size corrections or whether it indicates a failure of the MK model. In order to resolve the matter, we used the expected form of the scaling function, Eq. (3.15), to construct a fitting function, $F(\tilde{h})$, that *assumes* the correct behavior of the scaling function for large values of $\tilde{h}$; more specifically, $F(\tilde{h}) = \left[(a\tilde{h})^d + (b\tilde{h}^{1-\gamma})^d\right]^{1/d}$. The fitting function hence only depends on three parameters and fulfils the condition that $F(\tilde{h}) \propto \tilde{h}$ for $\tilde{h} \ll 1$, while the MF form, $\tilde{h}^{1-\gamma}$,

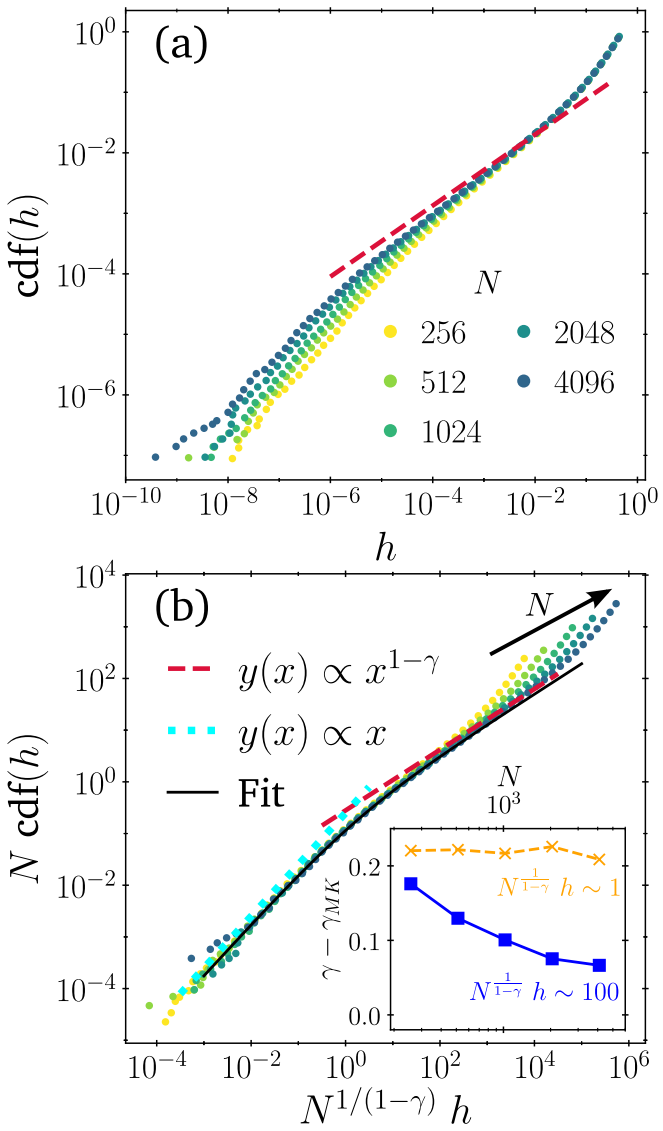

FIGURE 3.6. (a) Cumulative distributions of h for jammed configurations of $d = 3$ MK systems of different size N. (b) Same data but collapsed using the scaling in Eq. (3.8). Such scaling indicates that $\gamma_{MK} = \gamma$, in agreement with MF theory, although finite-size corrections are particularly important for this model (see main text for discussion). The MF (red dashed lined) and linear (cyan dotted line) behaviors are indicated, as well as the fitting function (solid black) based on Eq. (3.15), as discussed in the text. (Inset) Difference between the MF γ and the local slope estimate at two different values of the scaling variable, 1 (crosses, dashed) and 100 (squares, solid). These results suggest that systems orders of magnitude larger would be needed to recover the pure MF power law (see main text for details).

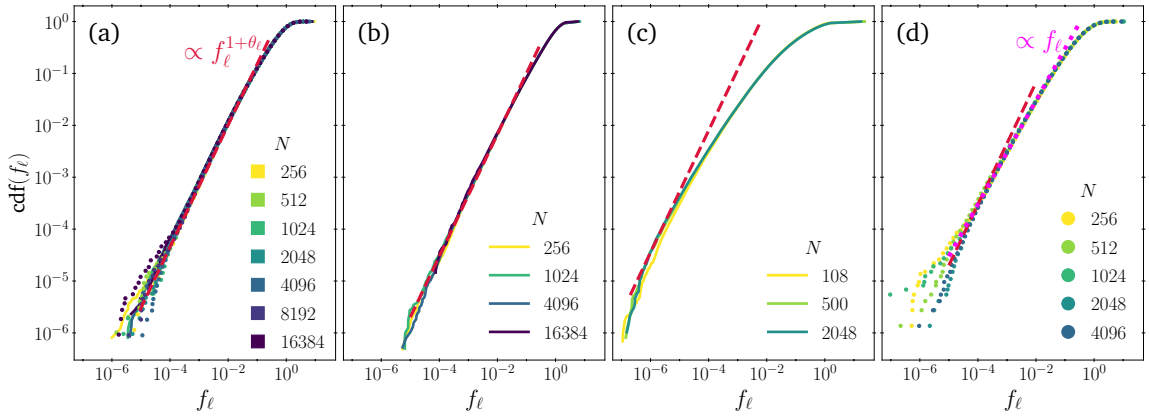

FIGURE 3.7. Cumulative distributions of f_ℓ for jammed packings of (a) $d = 3$ monodisperse spheres, (b) $d = 2$ polydisperse disks, (c) polydisperse spheres with FCC structure, (d) $d = 3$ MK model. Solid lines (circular markers) denote data obtained from configurations from the OC (UC) phase. For reference, the expected power law, $cdf(f) \sim f^{1+\theta_\ell}$, with $\theta_\ell = 0.17$, is shown (red dashed lines), and in panel (d) the power-law fit found by inspection for the MK model, $cdf(f) \sim f$, i.e., $\theta_{\ell,MK} = 0$, is also shown (pink dotted line). See text for more details.

is recovered for large values of the scaling variable. Fitting $F(\tilde{h})$ to the largest system size results gives the black line in Fig. 3.6b, which clearly interpolates nicely between both regimes. Therefore, the hypothesis that results for larger MK systems would eventually follow the MF power-law cannot be confuted. The convergence of the slope of the scaling function to the predicted value is nevertheless extremely slow, especially relative to that of other models (see, *e.g.* Figs. 3.2c, 3.5c) or to the distribution of forces in this same MK model (see Fig. 3.3d). One must thus reach very large values of the scaling variable in order to measure the right slope. More precisely, in the inset of Fig. 3.6b we report the difference of γ and our estimation of *local* γ_{MK} from the local slope as a function of N. Around $\tilde{h} = 1$, the slope clearly differs from the MF prediction, but even when $\tilde{h} \sim 10^2$ very large system sizes are needed for it to approach the theoretical exponent. This deviation results in an *apparent* size dependence of the global exponent, *i.e.* $\gamma_{MK} = \gamma_{MK}(N)$,

that is substantially more pronounced than for other models at similar N. Such discrepancy likely results from the MK system being fully connected. In contrast with their sparse counterparts, fully connected models indeed require much larger system sizes for thermodynamic power-law scalings to be visible [107, 108, 109]. This feature can be physically understood by recalling that the introduction of random shifts results in neighbors of a given particle (very likely) not being neighbors themselves. A particle can thus have many more contacts than normally allowed in Euclidean space. For instance, it is not uncommon ($\sim 1\%$) for particles at jamming to have as many as 12 contacts (the $d = 3$ kissing number) or more. In general, particles are thus surrounded by many more particles–both actual and near contacts–than usual hard spheres. Additionally, jamming densities in this model are much higher than can be achieved with hard spheres. Using our MD-LS+LP algorithm, as well as planting [99] to speed up the growing protocol, results in jamming packing fractions $\phi_{J,MK} \gtrsim 3.1$ (cf. $\phi_{J,3d} \simeq 0.64$). Now, given that $\phi \sim \sigma^{1/d}$, our MK configurations are made out of particles nearly twice as big as those of standard hard spheres. The combination of these two effects is that particles in MK packings are surrounded by a cluster of many relatively large neighbors. The effective size of the system being drastically reduced, finite-size corrections are correspondingly more pronounced. We thus conclude that gaps in the MK model will probably follow the MF power-law scaling, as expected, but only at system sizes orders of magnitude larger than those considered here. In practice the finite size effects are so important in the distribution of gaps in the MK model that its MF nature is, perhaps paradoxically, a strong limitation to study its MF behavior.

Looking at the whole set of gap distributions, an interesting feature is the robust emergence of a regime of uniform distribution at very small gaps, in a way

entirely analogous to the distributions of extended contact forces. We argued in Sec. 3.2.4 that this truncation of the leading power-law scaling in the distributions likely follows from the combined effect of the additional state of self stress and the system sizes being finite. All the models consistently exhibit this behavior and show very good agreement with the associated linear scaling (see Figs. 3.2c, 3.4c, 3.5c and 3.6b). The invariance of this secondary power-law scaling with dimensionality, inherent order or other system properties is reassuring, albeit somewhat surprising, given that the leading power-law scaling is more strongly affected by these same effects. The universality of this secondary scaling has been previously predicted [80] for all models that can be mapped to jamming of spherical particles, and it has been shown to occur even for non-spherical particles [85], provided that their jammed states remain sufficiently close to isostaticity. Such robustness can be understood in part by considering that isostaticity is a global property of the system related to a matching between constraints and degrees of freedom, and not to the specific distributions of its microstructural variables. Because we have restricted our analysis to packings with exactly $N_c = N_{dof} + 1$, the ubiquity of the linear left tails in our distributions supports the hypothesis that the form of $g_0(x)$ (Eq. (3.13)) and $p_0(x)$ (Eq. (3.14)) is determined by the single state of self stress alone, and not by the inherent structure. It is then remarkable that the same size scaling also seems to capture the behavior of the extremal part of the distributions of gaps and of extended forces, albeit not as evidently for the latter. Our findings are therefore in agreement with Eq. (3.15).

3.5. Cumulative distributions of f_ℓ

The last microstructural variable we consider is the set of localized forces. Figure 3.7 presents the probability distributions for all our results. As expected, this quantity exhibits no clear finite N signature for any of the models, even though some dispersion around the expected behavior is observed in the left tails of $d = 3$ monodisperse and MK configurations, (panels (a) and (d), respectively). This behavior is expected because the set $\{f_\ell\}$ corresponds to contact forces acting on bucklers, for which opening a weak contact mostly results in localized displacement field [37, 54]. Because opening any of the contacts associated with a buckler only has a non-negligible effect over a few particle layers away from its origin, it is reasonable to assume that their properties should be insensitive to N, or to any border or periodic effects.

An intriguing finding is that only the cdf of $d = 3$ monodisperse and $d = 2$ polydisperse particles follow the known value of $\theta_\ell \simeq 0.17$ (see Fig. 3.7a-b). By contrast, FCC structures give rise to no obvious power-law scaling. The FCC arrangement induces strong spatial correlations that seem to suppress the appearance of localized forces, as seen from the smaller slope of the cdf. Observing a distribution with an exponent different from θ_ℓ, or actually failing to scale as a power law, is in striking contrast with many other models, and even other crystalline structures [83]. It nonetheless echoes very recent reports of a dependence of θ_ℓ on geometry for other near-crystals [84]. These considerations highlight the need for further assessment of which aspects of jamming criticality are indeed universal, which are more generically conserved [55], and which disappear in the presence of long-range spatial constraints.

Although a power-law scaling is also obtained for MK configurations, the best fit to the data is achieved with a unit slope, i.e., $\theta_{\ell,MK} = 0$ (see Fig. 3.7d). Localized forces are thus distributed uniformly in this model. A careful analysis suggests that this unexpected distribution is in tune with the spatial properties of MK packings. First, note that even though bucklers follow a different pdf, selecting particles with $z_\ell = d + 1$ contacts is still a valid selection criterion. (If their contribution had not been isolated, the remaining forces would not follow the MF power-law scaling given in Eq. (3.2b), as it does in Fig. 3.3c, whereas if both kinds of forces are considered together, their joint pdf scales as ≈ 1.1, which differs from the analogous quantity for standard hard spheres [37].) Second, analyzing the distribution of dot products between contact vectors as in Ref. [93] reveals that particles with z_ℓ contacts in MK packings have a very similar distribution as those in standard hard sphere packings. Bucklers thus mainly give rise to a localized response thanks to them having three nearly coplanar contacts and one nearly orthogonal force. In order to understand why localized forces are uniformly distributed, we follow Ref. [54], which showed that the two types of contact forces are related to two types of floppy modes: extended forces are related to floppy modes that can couple strongly to external perturbations, and hence their response is bulk dominated; and buckling forces are associated to floppy modes of a rapidly decaying displacement field. (The value of $\theta_\ell \approx 0.17$ was estimated from the statistics of *displacements* in the latter.) There is therefore a strong connection between the distribution of forces in bucklers and the particle displacements their floppy modes produce. Now, let us assume that in an MK packing we open a buckling contact, $\langle ij \rangle$, between particles i and j, in order to describe the associated displacement field. In particular, let us focus on the remaining contacts of any of

Property	$d = 3$ Monodisperse UC and OC	$d = 2$ Polydisperse OC	FCC OC	MK UC
$p(f_e)$ with $\theta_e = 0.42311$	✓	✓	✓(but small range)	✓
$g(h)$ with $\gamma = 0.41629$	✓	✓	✗: $\gamma_{FCC} \simeq 0.33$	✓
$p(f_\ell)$ with $\theta_\ell = 0.17$	✓	✓	✗: no power law	✗: $\theta_{\ell,MK} = 0$
Eq. (3.8) scaling for forces	✗	✗	✗	✓(but small effect)
Eq. (3.8) scaling for gaps	✓	✓(Eq. (3.12))	✓(using γ_{FCC})	✓

TABLE 3.1. Summary of our main results for the various properties and models considered. In the heading we also indicate if the respective jamming point was reached from the under- (UC) or over-compressed (OC) phase. In the first three rows a check-mark (✓) denotes that the corresponding theoretical prediction was verified, and a cross (✗) that it was not. In the last two rows symbols denote whether the size scaling was verified or not. Results that contradict MF predictions, or results from previous studies, are highlighted in red.

these particles, say i. Because of the random shifts, the other particles touching i are (very likely) not constrained by each other nor by the other particles near i. Instead, the displacement of each neighbor of i is limited by its own contacts, which are not neighbors themselves, and are typically far apart. By the same token, the effect on the rest of particles in contact with j is determined by secondary contacts that–with high probability–are distant from each other and from $\langle ij \rangle$. As a result, opening a buckling contact produces a small series of uncorrelated displacements. No particular length scale is hence favored over any other. Because of the close relation between localized forces and displacements just mentioned, it is natural for f_ℓ to be uniformly distributed.

Before closing this section, we note that the distributions of f_ℓ for the FCC and MK packings violate the stability condition related to local excitations given by Eq. (3.3a). We comment further on this point in Sec. 3.6. For now, we simply note that broader classes of disorder need to be considered when studying the criticality associated with localized contact forces, even though their finite-size effects are unimportant.

3.6. Discussion

For clarity, we synthesize our results in Table 3.1. The first three rows, which consider the power-law scaling of the pdfs in Eqs. (3.1) and (3.2), assess the jamming criticality associated with microstructural variables for different types of systems. Recall that not only were different models considered, but so was the direction of approach to the jamming point. The systematic corroboration of the non-trivial distributions of forces and gaps for fully disordered systems at jamming completely supports the description derived from the exact MF theory. Systems with an underlying FCC symmetry, however, exhibit marked discrepancies. Our result thus validate earlier reports that crystalline structures fall outside the jamming universality [83, 84] , even though some of its critical features are conserved [55].

Our main finding is the contrasted system-size dependence of the distribution of gaps and contact forces, as summarized in the last two rows of Table 3.1. Size effects in $p(f_e)$ are practically nonexistent for all models, dimensionality, and interaction type, while $g(h)$ exhibits clear and systematic signatures of finite-N deviations from the expected power-law scaling. Logarithmic corrections to $g(h)$ are further observed in two-dimensional systems. We emphasize that testing for such size scalings not only rigorously assesses the critical scaling and its exponents [101, 102], but also provides key insight into the length scale of their correlations. Hence, we conclude that the MF exponents for all gap distributions and the f_e one in the MK model are correct. Yet–leaving aside for the moment the MK results–a second and more informative conclusion is that the distribution $p(f_e)$ reaches its thermodynamic limit behavior at smaller values of N than $g(h)$. Two different correlation lengths, ξ_{f_e} and ξ_h, therefore characterize the relevant length

scales of correlations of contact forces and gaps, respectively. This finding is rather unexpected, because the critical behavior of both quantities is controlled by the onset of isostaticity at the jamming transition. Moreover, theoretical approaches [7, 46, 80] suggest that forces and gaps can be studied from a unified viewpoint (essentially by considering forces as the zero limit of negative gaps), and thus they should share a common correlation length, ξ. Naturally, in the thermodynamic limit ξ should diverge at the jamming transition, thus signalling system-wide correlations between microscopic variables. Our results for finite-size systems, by contrast, suggest that correlations in gaps and forces have different length scales, namely $\xi_h \gtrsim N^{1/d} \gg \xi_{f_e}$. The fact that no known relation for ξ has been put forward (nor for ξ_h or ξ_{f_e} for that matter) partly obfuscates further analysis. A simple resolution could be to assume that both ξ_h and ξ_{f_e} are proportional to ξ, but with a prefactor that is much larger for the former than for the latter. Considering that forces and gaps are usually treated on an equal footing from the perspective of the SAT-UNSAT transition in the perceptron [74, 75], constraint satisfaction problems [80, 106], and neural networks [78] as well as from the point of view of marginal stability in amorphous solids [71, 72], the disparity in their correlation lengths is nevertheless surprising.

MK results also fit into this description if we consider that their very high densities and connectivity reduce the effective system size, as discussed in Sec. 3.4. Observing the scaling of Eq. (3.8) for the cdf of f_e is thus a manifestation of the smaller effective volume (for a similar N), which confirms that finite-size corrections for $p(f_e)$ are present at jamming, but disappear for relatively small system sizes. The significantly more pronounced N dependence of the distributions of h (Figs. 3.3c and 3.6b) thus supports our finding that $\xi_h \gg \xi_{f_e}$.

Interestingly, our results further suggest that the marginal stability bounds for the exponents, as expressed in Eqs. (3.3), should be modified when different types of disorder are present. For instance, our findings along with other works [83, 84] evince that these inequalities are prone to be violated when crystalline lattices are used to generate the jammed packings. The inherent geometry of jammed configurations therefore plays a significant role in formulating general stability criteria. Because the bounds in Eq. (3.3) were derived [54, 71, 72] assuming, implicitly, that particles positions are uncorrelated, it should not be overly surprising that γ_{FCC} violates both relations. It nevertheless suggests that, despite being likewise composed of frictionless spheres, near-crystals are not part of the same universality class.

The linear growth of cdf(f_ℓ) in the MK model is also at odds with the stability condition of Eq. (3.3a). This finding is more surprising because there is no long-range order in this type of system. At the end of Sec. 3.5 we used the peculiar geometry of these packings to suggest a physical explanation for the uniform distribution of f_ℓ, but this reasoning does not explain why the stability condition between γ and θ_ℓ is apparently violated. Given the drastic difference in the inherent structures of the FCC and MK packings, they highlight the need for more studies to better understand the role played by disorder in determining how the response to external perturbations is related to spatial correlations between particles in jammed systems.

The most persistent observation was that all cumulative distributions of both gaps and extended forces behave in a seemingly linear fashion at very small arguments, in agreement with the MF predictions, p_0 and g_0 in Eqs. (3.13) and (3.14), respectively. Such a cut-off of the main power-law scaling is due to the

extra contact of isostatic configurations and its effect in the scaling function can be captured using the same scaling transformation we performed for the main power-law scaling (see Sec. 3.2.4, especially Eq. (3.15)). It has been previously reported for the gaps distributions of disks packings [85], but we are not aware of analogous findings in any other model or for the f_e distributions. As discussed at the end of Sec. 3.4, our results suggest that scalings caused by the additional contact with respect to isostaticity are more robust against changes in the type of disorder and have a similar characteristic scale in both types of microstructural variables. However, because of undersampling of the left tails of these distributions, a more stringent analysis would need to be carried out to verify that $p_0(x) \sim g_0(x) \sim 1$ when $x \ll 1$. A previous work on the perceptron [87] also reported a similar transition to a uniform distribution of contact forces that depended on the type of algorithm used to reach the jamming point, but given that we have used two different algorithms to produce our packings, it is unlikely that both could produce the same systematic effect. This question is particularly interesting because it would directly affect the robustness of jamming universality, albeit only for the very smallest forces and gaps. Yet, given that the left tails of $g(h)$ and $p(f_e)$ determine the smallest gaps and contact forces, accurately describing their true distribution is key to assessing the stability of jammed packings away from the thermodynamic limit. We nevertheless leave this and other related issues as topics for future consideration.

Acknowledgments – We want to thank Franceso Zamponi for insightful comments and suggestions to our work. RDHR thanks Georgios Tsekenis for very useful discussions during the initial stage of this work and Beatriz Seoane for helpful suggestions regarding the molecular dynamics simulations of the MK

model. This work was supported by the Simons Foundation grant (# 454937, PC; # 454939, EC; # 454949 GP) as well as by the European Research Council under the European Unions Horizon 2020 research and innovation program (grant No. 694925, G.P.). H.I. was supported by JSPS KAKENHI No. 20J00289.

CHAPTER IV

DIONYSIAN HARD SPHERE PACKINGS ARE MECHANICALLY STABLE AT VANISHINGLY LOW DENSITIES

4.1. Introduction

When sand is densely packed, it is strong enough to support the weight of an elephant. But how loosely can one pack sand before this rigidity is lost? The answer is as loosely as one would like. That is, it is possible to rigidly pack hard spheres at any density, from filling all of space to filling none. In this manuscript we show a method for creating the sparsest possible hard sphere packings and demonstrate their impressive stability. Hard sphere packings are of particular interest because unlike other materials with a high strength-to-weight ratio such as tensegrity structures [110] and aerogels [111], hard spheres are purely compressive and do not rely on internal tensile forces.

There exist mechanically rigid packings with a density arbitrarily close to unity, such as the Apollonian gasket [112, 113]. We wish to find the foil to such a packing, that is, one with the smallest possible packing fraction that remains mechanically stable. As Dionysus is the nadir to the zenith that is Apollo [114], we refer to the sparsest possible mechanically stable packings as *Dionysian packings*. We present in this manuscript a construction for a Dionysian packing which has vanishingly low density in two and three dimensions.

Rigidity [115] describes a state in which no motion is possible. In the context of sphere packings, this is termed *strictly jammed* [49, 116, 117, 118, 119]. A

strictly jammed packing is resistant to all possible volume preserving deformations of the particles and boundaries.

Demonstrating that a packing is mechanically stable is commonly done using a linear programming algorithm [117, 118, 119]. In addition to demonstrating that our packings are stable through this same linear programming approach, we also compute the elastic moduli for the underlying spring network.

Finding a Dionysian packing is the same as finding the jamming threshold of sphere packings [49, 119]. The jamming threshold is the lowest density that can be achieved for strictly jammed configurations. However, while this threshold has mostly been explored for monodisperse configurations, we show that lower density packings can be found by expanding the search space to include polydispersity.

4.2. Methods

The method we employ is inspired by the construction of the Böröczky bridge packing [120, 121] for which locally stable bridges of circles can be constructed with arbitrary length. These bridges lead to packings with asymptotically zero density, but only satisfy the very weakest definition of stability; they are only *locally stable* or *locally jammed* [49, 116, 117, 118, 119, 120, 121]. Following the spirit of the Böröczky bridge packing and allowing for the radii of the spheres to be additional degrees of freedom, we achieve Dionysian packings subject to periodic boundary conditions at arbitrarily low densities. This demonstrates that the lower density bound for mechanically stable, repulsive circle and sphere packings is precisely zero.

To determine if a packing is strictly jammed, we model it as a spring network in which spheres interact through a harmonic contact potential in their overlaps. We examine whether or not the spring network represents a minimum with respect

to position degrees of freedom, x, as well as symmetric affine, volume-preserving strain degrees of freedom, ε [118, 122] where the potential is

$$U = \frac{1}{4}\sum_i \sum_{j \neq i} \xi_{ij}^2 \tag{4.1}$$

and ξ_{ij} is the normalized overlap between spheres i and j.

We require force balance on all degrees of freedom. The forces on the position degrees of freedom are

$$F_i^\alpha = -\frac{\partial U}{\partial x_i^\alpha} = \sum_{k \in \partial i} \left(\frac{\xi_{ik} n_{ik}^\alpha}{r_i + r_k} \right) = 0 \tag{4.2}$$

where n_{ik}^α is the α-component of the normalized contact vector pointing from particle k to particle i and r_i is the radius of sphere i. Forces on the strain degrees of freedom are

$$-\frac{\partial U}{\partial \varepsilon^{\alpha\beta}} = \frac{1}{4}\sum_i \sum_{j \in \partial i} \frac{\xi_{ij}}{r_i + r_j} \left(n_{ij}^\alpha x_{ij}^\beta + n_{ij}^\beta x_{ij}^\alpha \right) \tag{4.3}$$

for spheres i and j in Cartesian directions α and β where $\varepsilon^{\alpha\beta}$ is the strain degree of freedom and x_{ij}^α is the contact vector which is not normalized.

These forces are subject to the volume-preserving constraint, $\mathrm{Tr}\{(\varepsilon)\} = 0$ [118] so that force balance is achieved when

$$-\left.\frac{\partial U}{\partial \varepsilon^{\alpha\beta}}\right|_{\mathrm{Tr}\{(\varepsilon)\}=0} = -\frac{\partial U}{\partial \varepsilon^{\alpha\beta}} + \frac{\delta^{\alpha\beta}}{d}\sum_{\gamma=1}^{d} \frac{\partial U}{\partial \varepsilon^{\gamma\gamma}} = 0. \tag{4.4}$$

Because this derivative is proportional to overlap, it is trivially zero for any packing where overlaps do not occur. To ensure that these packings are at a critical point

due to a balancing of strain degrees of freedom, we evaluate the derivative with infinitesimal overlap.

The rigidity matrix [123] in conjunction with a linear programming algorithm [117, 118, 119] is used to determine if packings are strictly jammed. The rigidity matrix, R_x, relates a perturbation of the particles, $\vec{x}$, with the stresses on the bonds, $\vec{b}$, such that $\vec{b} = R_x\vec{x}$. However, perturbing the particles is not our only degree of freedom to explore when considering whether or not a packing is strictly jammed as we must also consider bulk deformations of the system as encoded in strain degrees of freedom. We define the extended rigidity matrix as $R = \begin{pmatrix} R_x & R_\varepsilon \end{pmatrix}$ where R_x is the ordinary rigidity matrix and R_ε relates the bond stresses to the strain degrees of freedom. (See supplementary materials for more information.) However, applying a strain that increases the volume of the periodic cell will allow all of the bonds to break, unjamming the packing. As such, we apply a constraint preventing the strain matrix, ε, from having volume changing deformations [118].

We quantify the degree of stability by calculating the resistance of the packing to compressive deformations and shear deformations via the bulk and shear moduli respectively. These quantities can be calculated simultaneously by computing the stiffness matrix, C, [124] for the packing. This matrix has the property $\vec{\sigma} = C\vec{\epsilon}$ where $\vec{\sigma}$ is the stress experienced by the packing when a particular strain, $\vec{\epsilon}$, is applied. The stiffness matrix can be computed in terms of the rigidity matrix as well as the states of self stress for R_x. The matrix of states of self stress, S, is an orthonormal basis for the zero modes of R_x^T such that $R_x^T S = \vec{0}$. The states of self stress represent the basis of stresses that can be placed on the bonds without causing particle perturbations. Using these terms, the stiffness matrix can

be computed as

$$C = R_\varepsilon^T S S^T R_\varepsilon. \tag{4.5}$$

(See supplementary materials for a derivation and an explanation of this equation.)

To explicitly satisfy the constraints for shear stability and jamming, we focus on creating a packing which is locally stable and has a high number of contacts per particle, z, and then test for stability. As illustrated in Figure 4.1 and described in more detail in the supplementary materials, this is achieved by placing n circles labeled a, where n is an odd integer greater than 2, on a strictly convex curve $\mathcal{C}$ such that they kiss their neighbors. A new row of circles, b, are then placed below so that each b circle kisses two a neighbors from below and a b neighbor on each side. Finally, the centers of circles c are placed on a line of zero slope and constrained to touch two b circles from below. Applying the appropriate symmetries, a stable bridge is formed. This construction can be replicated and the bridges can be joined such that a circle packing is formed without overlapping regions. This packing, with the addition of thirteen circles filling the largest void, is a Dionysian packing for particular construction parameters. Our bridge placement for the two dimensional Dionysian packing is based on the contact network of the triangular lattice.

In the limit of an infinitely large bridge, we find that every a circle has four contacts, every b has six, and every c has four. The asymptotic number ratio of this packing is $a : b : c = 2 : 2 : 1$. This means that there are $z = (2 \times 4 + 2 \times 6 + 4)/5 = 4\frac{4}{5}$ contacts per particle in two dimensions, which is larger than is required by the Maxwell rule for shear stable and jammed systems [125].

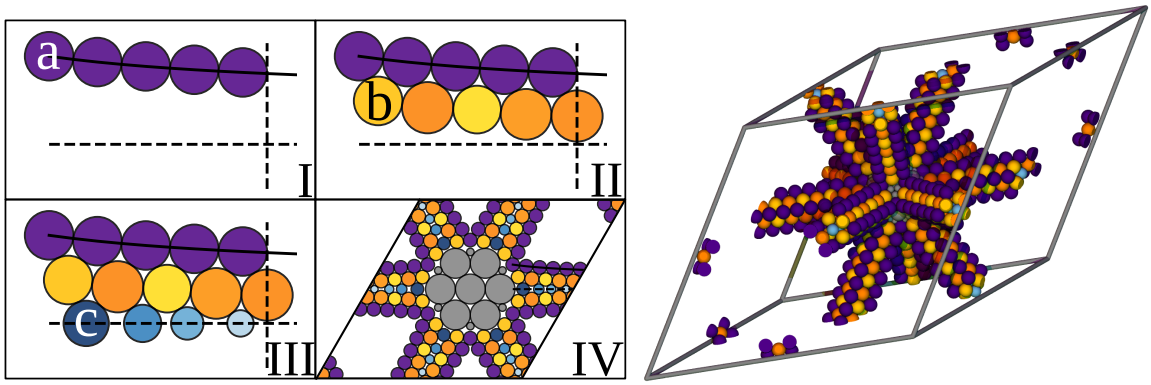

FIGURE 4.1. The construction of a Dionysian packing in two and three dimensions. **Left. I)** A row of $n = 5$ circles a (purple) lie on a strictly convex curve $\mathcal{C}$ such that each circle kisses its neighbors. **II)** A row of $n = 5$ circles b (orange/yellow) are placed such that they kiss two circles a from below and a circle b on either side. The rightmost b circle is constrained such that its center lies on the vertical line tangent to the rightmost a circle. **III)** A row of $n - 1 = 4$ circles c (blue) lie on a horizontal line and kiss two b circles above. **IV)** A bridge is formed by reflecting the circles about the dotted lines of symmetry. Three bridges are combined and their centers are filled as shown (gray). The resulting packing, which is jammed and shear stable, has a very low density and is a Dionysian packing in the limit as $n \to \infty$.
Right. A three dimensional mechanically stable packing at arbitrarily low densities. Such a construction contains the same three types of spheres as in the two dimensional analog but with additional symmetries and an entirely unrelated set of spheres filling the void region (gray). The three dimensional Dionysian packing has a much narrower set of convex curves $\mathcal{C}$ for which overlaps do not occur (as detailed in the supplementary materials). This requires a much more subtle curvature of $\mathcal{C}$ which is not apparent to the naked eye in this figure.

For the Böröczky locally jammed packing [120, 121], the two dimensional version can be used to create a locally jammed packing in any dimension by elevating the circles to spheres of the desired dimension and stacking the result. Such a trivial procedure will not work to extend the Dionysian construction because it results in structures which are not convex and so are subject to zero energy modes. To create a three dimensional Dionysian packing, we instead construct a set of six bridges in three dimensions and combine them as shown in Figure 4.1. A three dimensional bridge is constructed very similarly to the two dimensional bridge and exploits the symmetries of three dimensional space.

In the limit of an infinitely large bridge, we find that every a sphere has six contacts, every b has eight, and every c has eight. The asymptotic number ratio for these spheres is $a : b : c = 4 : 4 : 1$. This means that there are $z = (4 \times 6 + 4 \times 8 + 8)/9 = 7\frac{1}{9}$ contacts per particle in three dimensions, which is larger than is required by the Maxwell rule for shear stable and jammed systems [125].

Not all convex curves $\mathcal{C}$ result in viable packings; some choices of $\mathcal{C}$ result in overlapping of spheres in the limit as n approaches infinity. While infinitely many viable choices of $\mathcal{C}$ are possible, for simplicity we choose curves that fit the form

$$f(x) = \frac{(f_0 - h_\infty)^2}{(f_0 - h_\infty) - x\delta} + h_\infty \tag{4.6}$$

where f_0 is the height of the curve at $x = 0$, δ is the slope of the curve at $x = 0$, and $h_\infty = \lim_{x\to\infty} f(x)$. The values used in this manuscript are different between the two and three dimensional versions. (See supplementary materials.)

4.3. Results

For these parameters, we can track the smallest distance, w, between the b spheres and their reflected counterparts as seen in Figure 4.2. From this figure, we see a very clear power law and conclude that in the limit of infinitely large bridges, no unwanted additional contacts are created. This means that regardless of the value of n we choose, there are no overlaps for our Dionysian packing subject to the chosen curves $\mathcal{C}$. Because the length of our bridges increase with n but the other spatial dimensions do not, this construction results in packings with a density that falls like n^{1-d}.

Using the aformentioned linear programming algorithm on our Dionysian packings, we find that they are both jammed and shear stable for every n studied up to $n = 105$ ($N = 3145$) with packing fraction 0.0558 in two dimensions and $n = 25$ ($N = 2731$) with packing fraction 0.0128 in three dimensions.

In addition to demonstrating jamming and shear stability, we quantify the level of stability by calculating the shear, G, and bulk, K, moduli [126, 127] shown in Figure 4.3. The two dimensional dionysian packing is isotropic and has a single shear modulus, G. However, the three dimensional Dionysian packing, like the FCC crystal upon which it was based, has two independent shear moduli, G_{100} and G_{110}[128]. These moduli in two dimensions can be calculated from the stiffness matrix as $K = (C_{11} + C_{12})/2$ and $G = C_{33}$. In three dimensions, these are calculated as $K = (C_{11} + 2C_{12})/2$, $G_{100} = C_{44}$, and $G_{110} = (C_{11} - C_{12})/2$.

To compare the mechanical properties of Dionysian packings with other purely compressive solids, we also studied the properties of crystals and shear-stabilized jammed packings. We generated shear stabilized amorphous systems with monodisperse radii in three dimensions and 25% polydispersity in two

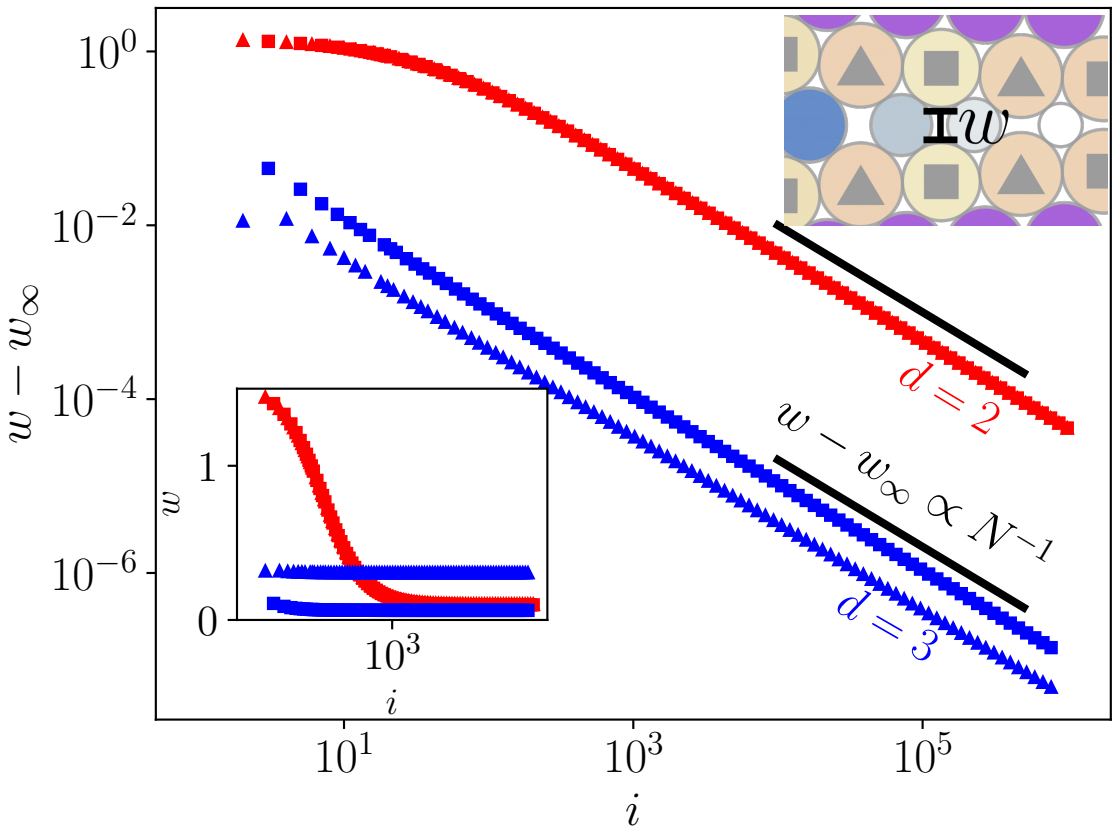

FIGURE 4.2. Top right inset: demonstration of the definition of a gap for a circle. The b circles, indexed by i, oscillate in size and are separated into two categories labelled by squares and triangles. Bottom left inset: The gap value for both square and triangular marked spheres asymptotes in two and three dimensions. When the asymptotic gap value is subtracted, the gap sizes follow a power law of N^{-1} as they reach their respective asymptotic values.

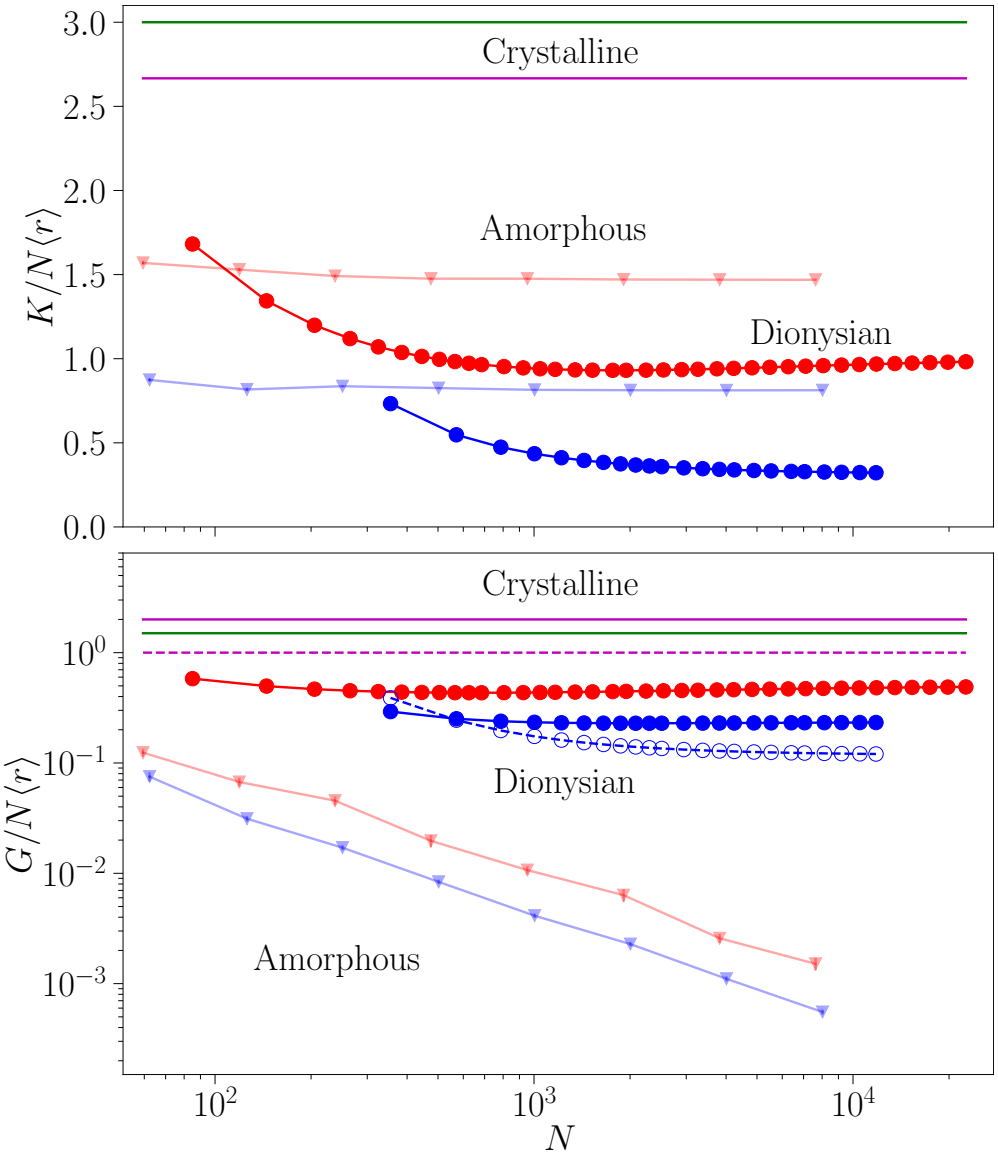

FIGURE 4.3. The dimensionless bulk, K, and shear, G, moduli per sphere for Dionysian and amorphous packings in a unit cell as a function of the number of spheres, N. The green line represents a two dimensional triangular packing, the magenta line represents a three dimensional FCC packing, and red and blue represent two dimensional and three dimensional packings respectively. The dashed curves with open symbols represent G_{110}, the shear modulus in direction $(1, 1, 0)$, whereas the solid curves with closed symbols represent G_{100}. The results are exact for the Dionysian packings and crystals. For the amorphous systems, sufficiently many systems were sampled to make the standard error bars smaller than the plot markers. In the limit of large N, the bulk modulus per sphere asymptotes to a positive value in two and three dimensions for all of the systems. The shear modulus for crystals and Dionysian packings plateaus for large N indicating that these remain very stiff. On the other hand, the amorphous packings have a shear modulus that decreases like $1/N$ [1].

dimensions drawn from a log-normal distribution. We then used a modified FIRE algorithm [33] that performs a constrained minimization with respect to both volume-preserving strains and positions as implemented in the pyCudaPacking software [29, 34, 35]. We created critically jammed and shear-stabilized packings by alternating between shear-stabilizing packings and uniformly decreasing the packing fraction and by extension the system pressure [37].

Figure 4.3 demonstrates that crystals, shear-stabilized jammed systems, and Dionysian packings all have a bulk modulus per particle that plateaus to a fixed value in the limit of large N. Similarly, the shear moduli per particle for crystals and Dionysian packings plateau for large N. In contrast, we confirm the claim by Dagois-Bohy et al. [1] that the shear modulus in shear-stabilized jammed systems decreases like $1/N$. These results indicate that Dionysian packings maintain their stability even as the density approaches zero whereas amorphous systems are only marginally stable in the thermodynamic limit. Remarkably, Dionysian packings can be created without sacrificing stiffness.

Extension of our procedure to higher dimensions can be proven to not be viable due to unavoidable overlapping of spheres (see supplementary materials). We conjecture that higher dimensional Dionysian packings also have arbitrarily low densities, but demonstrating this will require a novel construction.

4.4. Conclusions

We find that the lower bound on density for mechanical stability of purely repulsive spheres is 0 (Dionysian) and the upper bound is 1 (Apollonian) in two and three dimensional sphere packings. In addition to this solution and the extension of our understanding of the limits associated with the jamming energy

landscape, this discovery has implications for our fundamental understanding of mechanical stability. Where Apollonian packings can be used to create structures which fill space entirely, Dionysian packings can be used to create structures that utilize very little material and remain stiff. We prove that appreciably lighter weight materials can be constructed and give a road map for building them.

Acknowledgments – We thank Aileen Carroll-Godfrey, Sean Ridout, James Sartor, and Mike Thorpe for helpful discussions and feedback. This work was supported by National Science Foundation (NSF) Career Award DMR-1255370 and the Simons Foundation No. 454939.

4.5. Supplementary Materials

4.5.1. Constructing a Dionysian Packing in Two Dimensions

To construct a Dionysian packing in two dimensions, we do the following:

1. Create a chain of n kissing circles labeled $a_1 - a_n$ which have unit radius and centers that lie on a convex function $f(x)$ given by equation 6 such that the coordinates of each circle are $(x, f(x))$. The values used in this manuscript can be found in table 4.1. If we give the bridges $h_\infty = 1 + \sqrt{3}$, we end up with nice monodisperse crystalline structures at infinity. However, because the radii of b circles oscillate between two values, these values of h_∞ will eventually cause overlapping to occur. To prevent this, we perturb these values by 0.05

2. Place a circle b_1 of radius 1 that kisses a_1 and a_2

3. Place circle b_m, where $m \in [2, n-1]$, such that it kisses a_m, a_{m+1}, and b_{m-1}

4. Place circle b_n such that it kisses a_{n-1} and a_n and so that its center lies at $a_{nx} + 1$ where a_{nx} is the x coordinate of circle a_n

5. Place circle c_m, where $m \in [1, n-1]$, such that it lies on $y = 0$ and kisses circles b_m and b_{m+1}

6. Reflect the ensemble of circles about the x axis

7. Reflect the ensemble of circles about the line normal to the x axis that passes through the center of b_n

8. Generate three of these bridges and connect them such that they share a_1 circles and lie along the contact vectors of the triangular packing

9. Contain the circle ensemble in a rhombus with periodic boundary conditions

10. Place seven identical circles inside the cavity between bridges such that they form a honeycomb pattern and each of the six outer circles touch two copies of b_1

11. Place six identical circles in the cavity each of which touches an a circle and two of the circles in the honeycomb arrangement

4.5.2. Constructing a Dionysian Packing in Three Dimensions

The construction process is very similar in three dimensions, but with the following changes

1. The values for the curve are different and can be found in table 4.1

2. The coordinates of a spheres have the form $\left(a_x, a_y, 0\right)$, the coordinates of b spheres have the form $\left(b_x, b_y, b_y\right)$, and the coordinates of c spheres have the form $\left(c_x, 0, 0\right)$

3. The a and b spheres each have three copies that are rotated 45 degrees about the x axis

4. The sphere ensemble is reflected about the plane perpendicular to the x axis that passes through the center of b_n

5. Six of these bridges are created and connected such that they share sphere a_1 and lie along the contact vectors of the primitive cell for the FCC packing

6. The spheres in the empty cavity formed by the bridges are different. Generate thirteen equal sized spheres, f, in the shape of an fcc crystal such that one sphere is in the very middle of the cavity and the other twelve touch four b spheres associated with the ends of the bridges. Connecting these bridges will naturally create two differently sized holes. In the six larger holes, create a dimer of equally sized circles, m, such that they touch: each other, a b sphere, two a spheres, and an f sphere. Also in these larger holes, place a sphere, p, that touches eight of these m sphere and an f sphere. In the eight smaller holes, place a triangle of equally sized spheres, q, that touch each other, three a spheres and an f sphere

For a visual representation of the construction in two dimensions, see FIG. 1.

d	f_0	h_∞	δ
2	$2\sqrt{3}$	$\left(1+\sqrt{3}\right)+0.05$	0.01
3	$\sqrt{6}$	$\left(1+\sqrt{2}\right)+0.025$	0.01

TABLE 4.1. The values we used to parameterize curve $\mathcal{C}$ for various dimensions d according to equation 9

4.5.3. Trivial Extension to Higher Dimensions

We can prove that extending this construction to higher dimensions will not work. The generalized construction is given by parameterizing the positions of the a spheres as

$$\vec{a}_m = \left(a_{mx}, a_{my}, 0, 0, \dots\right) \text{ and } \vec{b}_m = \left(b_{mx}, b_{my}, b_{my}, b_{my}, \dots\right)$$

for $m \in [1, n]$. The a spheres will each have $2(d-1)$ copies given by

$$\left(a_{mx}, -a_{my}, 0, 0, \dots\right), \left(a_{mx}, 0, a_{my}, 0, \dots\right), \left(a_{mx}, 0, -a_{my}, 0, \dots\right), \left(a_{mx}, 0, 0, a_{my}, 0, \dots\right), \dots$$

and the b spheres will each have 2^{d-1} copies given by

$$\left(b_{mx}, -b_{my}, b_{my}, b_{my}, \dots\right), \left(b_{mx}, b_{my}, -b_{my}, b_{my}, \dots\right), \left(b_{mx}, -b_{my}, -b_{my}, b_{my}, \dots\right), \dots$$

We consider $\vec{a}_1 = \left(0, a_y, 0, \dots\right)$ with unit radius and $\vec{b}_1 = \left(1, b_y, b_y, \dots\right)$ with radius b_r. If we enforce that these two spheres kiss, we can solve for a_y. We can then find that b_y has a maximum value of

$$b_y^* = \sqrt{\frac{b_r(b_r+2)}{(d-2)(d-1)}}.$$

Because b_1 cannot overlap with one of it's copies, $b_y \geq b_r$. This along with the above equation means that

$$b_r \leq \sqrt{\frac{b_r(b_r+2)}{(d-2)(d-1)}}$$

or for $d > 2$,

$$b_r \leq \frac{2}{d^2-3d+1}.$$

We also know that in steady state, the sum of the radii for b_m and b_{m+1} will be 2. This means that setting b_m to have a radius less than 1 gives b_{m+1} a radius greater than 1. Therefore, if we substitute $b_r = 1$, we arrive at an upper bound for d :

$$d \leq \frac{3+\sqrt{13}}{2} \approx 3.30278$$

which means that this construction does not extend to dimensions higher than three. We do conjecture that a different construction procedure exists to generate Dionysian packings in higher dimensions.

4.5.4. Minimal Curvature for three dimensional Dionysian Packings

We remarked in the text that the curves $\mathcal{C}$ have a very subtle amount of curvature in three dimensions. Given a and b spheres of radius 1, the tightest Dionysian bridge configuration one can achieve has an a sphere with $a_y = (1+\sqrt{2})$. Any tighter and the b spheres will overlap. The loosest configuration has $a_y = \sqrt{6}$. Any looser and the b spheres will no longer be contained. (See table 4.1). If our

packing begins with the loosest configuration and ends with the tightest, the curve will decrease in height by $\sqrt{6}/(1+\sqrt{2}) - 1 = 1.46\%$ which is subtle.

4.5.5. Amorphous Shear Stabilized Systems

We generate amorphous shear stabilized systems by finding the traceless forces on strain degrees of freedom as given in equation 4 of the manuscript. We then use the FIRE algorithm on these strain degrees of freedom to adjust the lattice vectors and apply an affine strain. Because $\mathrm{Tr}(\varepsilon) = 0$ is just the linear approximation for volume conservation, we also rescale the lattice vectors after each minimization step. Once a shear stabilized packing is found, we alternate between minimizing the system and uniformly decreasing the radius of each particle in order to maintain the polydispersity. After rattlers are removed and the system is at one state of self stress, we find the mechanical properties.

4.5.6. Computing the Stiffness Matrix

We first consider our extended rigidity matrix for which

$$R_{x\langle ij\rangle(k\gamma)} = (\delta_{jk} - \delta_{ik})\, n_{ij}^{\gamma} \tag{4.7}$$

$$R_{\varepsilon\langle ij\rangle(\alpha\beta)} = n_{ij}^{\alpha} n_{ij}^{\beta} \sigma_{ij} \tag{4.8}$$

for contact $\langle ij\rangle$, particle k, and dimension γ. Here, also note that n_{ij}^{γ} is the normalized contact vector between particle j and particle i and σ_{ij} is the sum of the radii of particles i and j.

In order to find the stiffness matrix, we define the extended hessian, which is

$$H = \begin{pmatrix} H_{xx} & H_{x\varepsilon} \\ H_{x\varepsilon}^T & H_{\varepsilon\varepsilon} \end{pmatrix} \tag{4.9}$$

where H_{xx} is the second derivative of the energy function with respect to positional degrees of freedom, $H_{\varepsilon\varepsilon}$ is the second derivative with respect to strain degrees of freedom, and $H_{x\varepsilon}$ are mixed derivatives.

From Hooke's law, we know that

$$H \begin{pmatrix} \Delta\vec{x} \\ \vec{\varepsilon} \end{pmatrix} = \begin{pmatrix} -\vec{F} \\ \vec{\sigma} \end{pmatrix} \tag{4.10}$$

where $\Delta\vec{x}$ is a perturbation vector of the particles and $\vec{\sigma}$ is the stress. To find the stiffness matrix, we solve for the non-affine perturbation $\Delta\vec{x}_{\text{na}}$ that leave the spatial forces unchanged but imposes a stress:

$$H \begin{pmatrix} \Delta\vec{x}_{\text{na}} \\ \vec{\varepsilon} \end{pmatrix} = \begin{pmatrix} \vec{0} \\ \vec{\sigma} \end{pmatrix}. \tag{4.11}$$

If we solve this system of equations for $\vec{\sigma}$, we find that $C\vec{\varepsilon} = \vec{\sigma}$ where the stiffness matrix is

$$C = \left[H_{\varepsilon\varepsilon} - H_{x\varepsilon}^T \left(H_{xx} \right)^{-1} H_{x\varepsilon} \right]. \tag{4.12}$$

The term, $\left(H_{xx} \right)^{-1}$ is the Moore-Penrose pseudoinverse [129] of the singular matrix H_{xx}. While the algebra is simple, care must be taken to prove that it is valid to use the pseudoinverse for hyperstatic jammed packings.

We can take this result further by considering that for systems without prestresses, such as ours, the extended hessian can also be written as

$$H = R^T R \tag{4.13}$$

$$= \begin{pmatrix} R_x^T R_x & R_x^T R_\varepsilon \\ R_\varepsilon^T R_x & R_\varepsilon^T R_\varepsilon \end{pmatrix} \tag{4.14}$$

so that

$$C = \left[R_\varepsilon^T R_\varepsilon - R_\varepsilon^T R_x \left(R_x^T R_x \right)^{-1} R_x^T R_\varepsilon \right]. \tag{4.15}$$

This can be further simplified by applying the singular value decomposition [130] for R_x. We can define the left singular vectors as U which correspond to the linearly independent basis of bond stresses, the right singular vectors, V, which correspond to normal modes, and Σ which is the rectangular diagonal matrix of singular values. Given this,

$$R_x = U \Sigma V^T. \tag{4.16}$$

If we make this substitution in equation 4.15, we find that

$$C = \left[R_\varepsilon^T R_\varepsilon - R_\varepsilon^T U \Sigma \left(\Sigma^T \Sigma \right)^{-1} \Sigma^T U^T R_\varepsilon \right] \tag{4.17}$$

$$= R_\varepsilon^T \left(\mathbf{1} - U \Sigma \left(\Sigma^T \Sigma \right)^{-1} \Sigma^T U^T \right) R_\varepsilon \tag{4.18}$$

$$= R_\varepsilon^T \left(U U^T - U \Sigma \left(\Sigma^T \Sigma \right)^{-1} \Sigma^T U^T \right) R_\varepsilon \tag{4.19}$$

$$= R_\varepsilon^T U \left(\mathbf{1} - \Sigma \left(\Sigma^T \Sigma \right)^{-1} \Sigma^T \right) U^T R_\varepsilon. \tag{4.20}$$

The pseudoinverse of a diagonal matrix such as $\Sigma^T\Sigma$ is a diagonal matrix where the nonzero entries are inverted and the zero entries remain zero. To simplify this, we can rewrite Σ. If we let there be f floppy modes, s states of self stress, and z nonzero singular values, then we can choose to express Σ as

$$\Sigma = \begin{pmatrix} Q_{z\times z} & \mathbf{0}_{z\times f} \\ \mathbf{0}_{s\times z} & \mathbf{0}_{s\times f} \end{pmatrix} \tag{4.21}$$

where Q is the diagonal matrix of non-zero singular values and where we have explicitly assumed that $s > f$. This assumption will always hold for shear stabilized packings where $f = d$ corresponds to trivial floppy modes. Also note that this form of Σ assumes that the left and right singular vectors are arranged in a corresponding way. Substituting this equation into equation 4.20, we find that

$$C = R_\varepsilon^T U \left(\mathbf{1} - \begin{pmatrix} Q_{z\times z} & \mathbf{0}_{z\times f} \\ \mathbf{0}_{s\times z} & \mathbf{0}_{s\times f} \end{pmatrix} \begin{pmatrix} \left(Q_{z\times z}^2\right)^{-1} & \mathbf{0}_{z\times f} \\ \mathbf{0}_{f\times z} & \mathbf{0}_{f\times f} \end{pmatrix} \begin{pmatrix} Q_{z\times z} & \mathbf{0}_{z\times s} \\ \mathbf{0}_{f\times z} & \mathbf{0}_{f\times s} \end{pmatrix} \right) U^T R_\varepsilon \tag{4.22}$$

$$= R_\varepsilon^T U \left(\mathbf{1} - \begin{pmatrix} \mathbf{1}_{z\times z} & \mathbf{0}_{z\times s} \\ \mathbf{0}_{s\times z} & \mathbf{0}_{s\times s} \end{pmatrix} \right) U^T R_\varepsilon \tag{4.23}$$

$$= R_\varepsilon^T U \begin{pmatrix} \mathbf{0}_{z\times z} & \mathbf{0}_{z\times s} \\ \mathbf{0}_{s\times z} & \mathbf{1}_{s\times s} \end{pmatrix} U^T R_\varepsilon. \tag{4.24}$$

In this equation, the $\mathbf{1}_{s\times s}$ term corresponds to the entries associated with states of self stress. As such,

$$C = R_\varepsilon^T S S^T R_\varepsilon \tag{4.25}$$

where S is the matrix of states of self stress for R_x. Again, this expression is valid under the assumption that the packing has no prestress and is strictly jammed.

We can understand this result by considering how each term interacts with an arbitrary strain, $\vec{\varepsilon}$. This arbitrary strain results in bond stresses, $\vec{b} = R_\varepsilon \vec{\varepsilon}$. However, these bond stresses will very likely result in perturbations of the particles which will bring the packing out of force balance. The SS^T term removes any components of the bond stresses that are inconsistent with the states of self stress and therefore would cause particle movements. This new set of bond stresses is then passed through R_ε^T and gives the stress vector, $\vec{\sigma}$.

CHAPTER V

METHODS FOR CREATION AND LINEAR ELASTIC RESPONSE ANALYSIS OF PACKINGS OF SEMI-FLEXIBLE SOFT POLYMERS AND CHAINS

5.1. Introduction

Glasses, grains, foams, sand, particulates, and colloidal suspensions are all examples of amorphous systems that undergo complicated phase transitions. These transitions have been studied extensively through simulations with packings of soft, athermal, frictionless spheres that interact through a one-sided contact potential. The success of this simplified model in furthering our understanding of glasses and jamming cannot be overstated [1, 34, 35, 37, 48, 131, 132, 133]. However, many glassy systems are not comprised of soft spheres, but polymer chains that interact in more complex ways [134, 135, 136, 137].

While the use of soft sphere packings will not and should not subside in the future, I hope we can get further understand glassy systems if we begin simulating packings of soft chains of spheres. I show how this can be done through a simple modification to code for soft sphere simulations.

The importance of polymer studies ranges from the biology of complex biomolecules such as proteins and chains of DNA [138, 139, 140] to the polyethylene that is omnipresent in our daily lives [141, 142]. Packings of chains and polymers have been explored in experimental systems as well as in simulations [143, 144, 145, 146, 147, 148].

Here a novel method is proposed that can be more easily implemented and adapted to arbitrary cluster types and constraints. While real polymers are

comprised of components joined by various types of interparticle forces, the work in this manuscript is done for the limiting case where the interparticle linkages are much stronger than the interaction potential between unlinked particles. The methods in this manuscript are focused specifically on soft chains of spheres which interact via a one-sided harmonic potential. However, the methods can be easily generalized to include more sophisticated interactions. Beyond the simple simulations of clusters of rigid molecules and flexible polymeric chains, one can also simulate clumping, aggregation, and the cementing of particles.

In this manuscript, I demonstrate how to create overjammed and critically jammed packings of arbitrarily defined semi-rigid clusters of spheres. It is further explained how these can be prepared and shear stabilized as well as describe how to find features of the packing, such as the normal modes, rattling clusters, classification in the jamming hierarchy, and elastic moduli. This simple extension to the already successful soft sphere packing model opens the door for many avenues of exploration in the physical properties of glassy systems.

5.2. Generating the Packings

Below a procedure is presented for generating packings of soft polymer chains that are force balanced in a local energy minimum through the use of constraints.

5.2.1. Generating Polymers: Links

The polymer packings are comprised of individual sets (or clusters) of spheres of variable radii, r. The individual spheres in each cluster interact via a potential, U, that is a function of their normalized overlaps, ξ. To define these clusters,

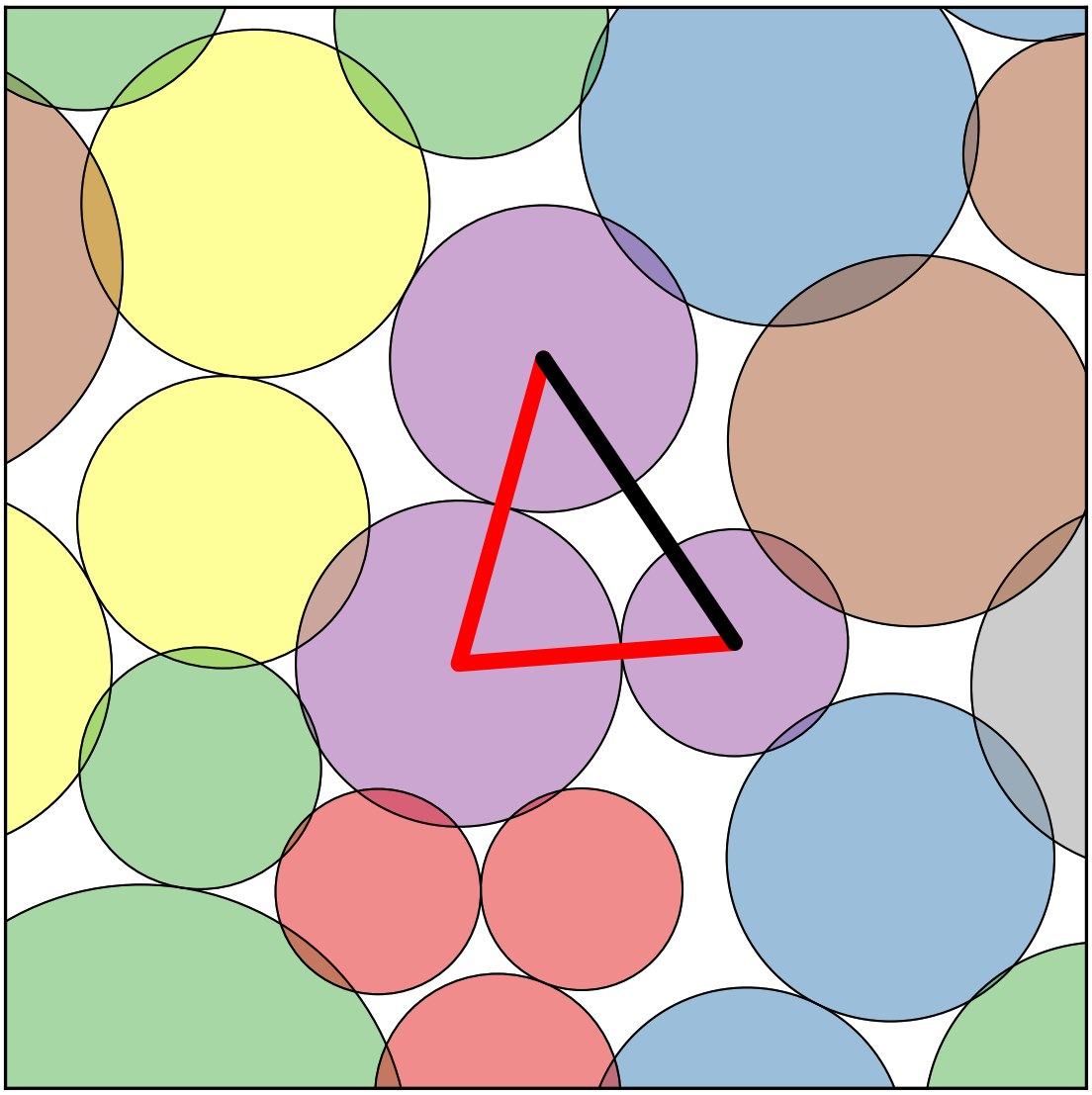

FIGURE 5.1. An example of a set of links in a packing. The red lines and the black line are all links, chosen to keep the purple cluster rigid. The red links join the particles together to form a cluster of three particles while the black link fixes the bond angle preventing the cluster from deforming. This rigid cluster only has three degrees of freedom: two translational and one rotational. However, three independent, unconstrained particles have six degrees of freedom. Adding the three links above effectively removes three degrees of freedom.

consider linkages between particles i and j of a fixed length. These are referred to as links.

By defining links, one is able to not only constrain the particles to be connected in arbitrary ways, but one can also fix the bond angles between particles. For example, given a triplet of circles, a, b, and c connected via links ab and bc, the bond angle can be fixed by creating a link of some fixed length l between a and c (see Figure 5.1).

5.2.2. The Orthonormalized Constraint Basis

Applying an arbitrary force to each of the particles in a packing would break their links and violate the constraints. The approach taken to prevent this is to project out the part of the force vector that violates the constraints to first order. Performing this projection will result in the forces that the chains actually experience and cause the appropriate cluster motions and torques in the simulation. Finding the projection requires finding an orthonormalized constraint basis.

In order to derive the orthonormal constraint basis, first consider the vector between two particles i and j that share a link, $\vec{x}_{ij}$. Because we are working in periodic boundary conditions for arbitrary lattice vectors, I define the lattice vector matrix, Λ, to be a $d \times d$ matrix where the columns are the lattice vectors. By considering a vector of integer lattice coordinates $\vec{z}_{ij} \in \mathbb{Z}^d$,

$$x_{ij}^{\alpha} = x_j^{\alpha} - x_i^{\alpha} + \Lambda^{\alpha}{}_{\gamma} z_{ij}^{\gamma} \tag{5.1}$$

where α and γ index the coordinates. It is also required that $\vec{z}_{ij}$ be an integer lattice vector which minimizes the norm of x. For particles in contact, this means

that $\vec{z}_{ij}$ is any integer vector that causes particle images i and j to be in contact. In general, this is degenerate, but without loss of generality, it can be asserted that every pair of overlapping spheres has exactly one $\vec{z}_{ij}$ and that $z_{ij}^{\alpha} \in \{-1, 0, 1\}$ for all coordinates α. If there is a link between particles i and j, our constraint is

$$c_{\langle ij \rangle} = \sqrt{\sum_{\alpha} \left(x_{ij}^{\alpha}\right)^2} - l_{\langle ij \rangle} = 0 \tag{5.2}$$

where $l_{\langle ij \rangle}$ is the constant length of bond $\langle ij \rangle$. Defining

$$\hat{\tau}_{ij}^{\alpha} = \frac{x_{ij}^{\alpha}}{l_{\langle ij \rangle}} \tag{5.3}$$

to be the normalized distance vector between particles i and j, the constraint Jacobian is

$$\Omega_{k\alpha\langle ij \rangle} = \hat{\tau}_{ij}^{\alpha} \left(\delta_{jk} - \delta_{ik}\right) \tag{5.4}$$

such that the columns of this matrix are given by the derivatives of c. If the packing does not contain degenerate links, then the constraint Jacobian has the property that the number of columns is equal to the rank. In practice, it is very easy to remove degenerate links, so to simplify computations and derivations, we assume there are no degenerate links.

This constraint Jacobian becomes very powerful in determining the forces on the unconstrained degrees of freedom. Because links in the same cluster share particles, the columns of this matrix will in general not be orthogonal. One can perform QR decomposition [149] on the constraint Jacobian to find an orthonormal basis for the constraints. QR decomposition can be fairly computationally

intensive, so a parallelized modified Gram-Schmitt process is employed [150] on each of the clusters individually. Since no two independent clusters share degrees of freedom, their columns will be automatically orthogonal. After performing the decomposition on our constraint Jacobian, the orthonormalized constraint basis, Ω_o is found. This matrix can be used to constrain the forces applied to the packing. Given an arbitrary force vector, $\vec{F}$, which acts on the particle positions, one can project out the part of the vector that lies along the constraints. This projection gives the constrained force vector:

$$\vec{F}_{\text{cons}} = \vec{F} - \Omega_o \Omega_o^T \vec{F} \tag{5.5}$$

$$= \left(\mathbf{1} - \Omega_o \Omega_o^T\right) \vec{F}. \tag{5.6}$$

For a system of rigid clusters, this constrained force removes the need to consider torques as it performs the correct angular rotation to first order. Similarly, for clusters with free bond angles, this alters the bond angles appropriately. It is worth noting that equation 5.6 does not apply only to forces, but other variables as well. For example, one can find a constrained velocity in the same manner.

5.2.3. Higher Order Corrections

The previously described constraint method is only correct for infinitesimal perturbations. As the goal is to perform a quench on these clusters, the non-linear contributions will accumulate over the course of the simulation causing our constraints to be violated. To combat this, the constraints are periodically reaffixed. This can be achieved numerically by employing the Newton-Rhapson method [151]. For simplicity, consider the positions of the particles to be

encapsulated by a single vector, $\vec{x}$. Practically, this can be achieved by simply flattening the matrix of positions. If the constraints are considered to be a vector, then the following recursive equation can be solved iteratively:

$$\Omega^T(\vec{x}_k)\left[\vec{x}_{k+1} - \vec{x}_k\right] = -\vec{c}(\vec{x}_k) \tag{5.7}$$

for $\vec{x}_{k+1}$ where k represents the iteration number. This equation can be solved using a method such as Gaussian elimination [149]. This algorithm is continued until iteration n where $|\vec{c}(\vec{x}_n)| < p$ for the desired precision p. When starting in a position that is very close to satisfying the constraints, this algorithm should terminate after just a few steps.

This now fully defines a method for generating semi-flexible soft polymer packings, however if one also wants to probe the linear elastic response, they should do so for packings that are stable with respect to strains.

5.2.4. Shear Stabilization

While true stress-strain isotropy is typically reserved only for certain perfect crystalline packings, the amorphous nature of large thermal systems of grains and polymers causes them to be approximately isotropic as well. However, this is only true if they are shear stabilized. That is, if the packing is not at a minimum with respect to all strain degrees of freedom, then there exists a strain which when applied causes the energy of the packing to decrease. This violates the isotropic assumption which means that the packings cannot be described with elastic moduli. While plenty of excellent research has been done on elastic response in

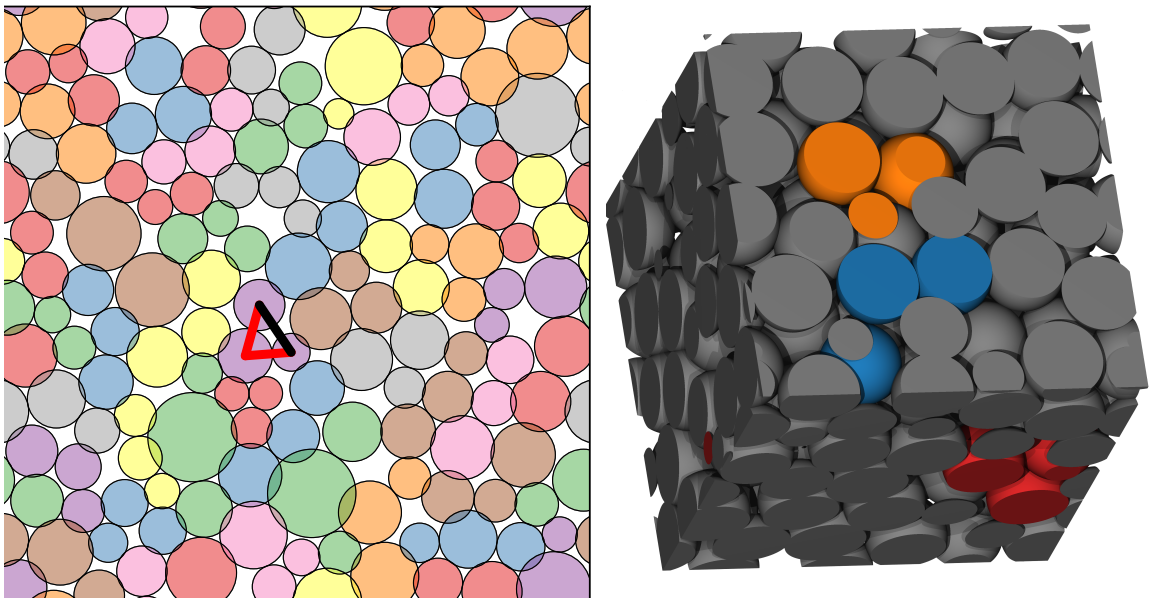

FIGURE 5.2. Polymer packings made up of 50 clusters of three particles with fixed bond angles in 2D (left) and 3D (right). For visualization purposes, only three of the rigid clusters are shown in the three dimensional packing.

systems which are not shear stabilized [124, 152, 153, 154, 155], the desire for shear stabilization is often warranted nonetheless [1, 117].

Shear stabilization is achieved by minimizing the energy of a packing with respect to both position and strain degrees of freedom. In other words, we also consider the packing's lattice vectors to be subject to change. Given the position of a node, $\vec{p}_0$, one can describe its lattice images as

$$\vec{p} = \vec{p}_0 + \Lambda \vec{z}. \tag{5.8}$$

A perturbation of the lattice vectors, $\Delta\Lambda$, results in

$$\Delta\vec{p} = (\Delta\Lambda)\,\vec{z}. \tag{5.9}$$

Solving equation 5.8 for $\vec{z}$ and making a substitution,

$$\Delta\vec{p} = (\Delta\Lambda)\,\Lambda^{-1}\,(\vec{p} - \vec{p}_0)\,. \tag{5.10}$$

Therefore, from the definition of the strain matrix,

$$\varepsilon \equiv \nabla_{\vec{p}}\,(\Delta\vec{p}) = (\Delta\Lambda)\,\Lambda^{-1}. \tag{5.11}$$

It's also important to notice that the strain matrix must be symmetric; this can be achieved by defining it's derivatives as

$$\frac{\partial\varepsilon_{ij}}{\partial\varepsilon_{kl}} \equiv \frac{1}{2}\left(\delta_{ik}\delta_{jl} + \delta_{il}\delta_{jk}\right). \tag{5.12}$$

It is crucial that the positions of particles be a function of the affine strain, so one can then find the distance between particle i and j as a function of position and strain,

$$\psi_{ij}^{\alpha} = \left(\delta^{\alpha}{}_{\beta} + \varepsilon^{\alpha}{}_{\beta}\right)\left(x_j^{\beta} - x_i^{\beta} + \Lambda^{\beta}{}_{\gamma} z_{ij}^{\gamma}\right). \tag{5.13}$$

The constraints, $c_{\langle ij\rangle}$, and constraint Jacobian, Ω, can also be redefined as functions of the strain degrees of freedom. This means that

$$c_{\langle ij\rangle}(\varepsilon) = \sqrt{\sum_{\alpha}\left(\psi_{ij}^{\alpha}(\varepsilon)\right)^2} - l_{\langle ij\rangle}. \tag{5.14}$$

The columns of Ω are comprised of derivatives of the constraints with respect to all of the degrees of freedom, positional and strain. The derivatives are evaluated at the current positions of the particles and the current strain of the packing. Because

the positions and lattice vectors are updated at every step of the minimization protocol, the constraint derivates can be evaluated at zero strain. One can derive that

$$\left.\frac{\partial c_{\langle ij\rangle}}{\partial x_k^\alpha}\right|_{\varepsilon=0} = \hat{\tau}_{ij}^\alpha \left(\delta_{jk} - \delta_{ik}\right) \tag{5.15}$$

as before. However,

$$\left.\frac{\partial c_{\langle ij\rangle}}{\partial \varepsilon^a{}_b}\right|_{\varepsilon=0} = \hat{\tau}_{ij}^a \hat{\tau}_{ij}^b l_{\langle ij\rangle} \tag{5.16}$$

after employing equation 5.12. It's important to note that all of the columns of our constraint Jacobian are linearly dependent which prevents the QR decomposition algorithm from taking advantage of the speed increase gained by assuming that the constraints between different clusters are orthogonal.

As the strain tensor is required to be a $d\times d$ symmetric matrix, there are $d(d+1)/2$ strain degrees of freedom. However, there is one final constraint to consider for shear stabilizing a packing of polymers: constraining the box volume. For a packing of monomers where the box volume is not constrained, the strain forces will always lead to the decompression of the box causing an unjamming event. It is therefore required that the applied strains keep the box volume constant. For infinitesimal strains, this constraint is simply $\mathrm{Tr}(\varepsilon) = 0$ [116, 117, 118]. The derivative of this constraint with respect to positional degrees of freedom is zero, but for the strain degrees of freedom, this means that

$$\frac{\partial}{\partial \varepsilon^a{}_b}\left(\sum_\alpha \varepsilon^\alpha{}_\alpha\right) = \delta_{ab}. \tag{5.17}$$

To avoid confusion, the constraint Jacobian is referred to as Ω if it only involves positional degrees of freedom and Γ if it involves both positional and strain degrees of freedom as well as the volume preserving constraint. Likewise, the othornormalized versions are called Ω_o and Γ_o respectively. Just as in equation 5.6, given an arbitrary force vector that involves the derivatives of positions and strain, $\vec{F}$, the constrained force is given by

$$\vec{F}_{\text{cons}} = \left(\mathbf{1} - \Gamma_o \Gamma_o^T\right) \vec{F}. \tag{5.18}$$

5.2.5. Performing Minimization

The constraints described above can be applied to any minimization algorithm that involves forces, such as gradient descent and FIRE [33] as well as molecular dynamics simulations. While this algorithm can be realized with any potential, I choose to direct my attention to a soft sphere potential of the form,

$$U(x, \varepsilon) = \frac{1}{2w} \sum_i \sum_{j \in \partial i} (\xi_{ij})^w \tag{5.19}$$

where w is some power and ξ_{ij} is the normalized overlap,

$$\xi_{ij} = 1 - \frac{\rho_{ij}}{\sigma_{ij}}. \tag{5.20}$$

In this equation $\rho_{ij} = \sqrt{\sum_\alpha \left(\psi_{ij}^\alpha\right)^2}$, σ_{ij} is the sum of the radii, and $j \in \partial i$ are defined to be those particles j which are in contact with particle i. This is understood to be a one-sided potential meaning that particles which are not overlapping do not interact. As a result, the contact network of our polymers changes throughout the minimization.

The positional forces are unchanged,

$$F^{\mu}_{x,k} = -\frac{\partial U}{\partial x^{\mu}_{k}}\bigg|_{\varepsilon=0} = \sum_{i\in\partial k} \xi^{w-1}_{ik} \frac{\hat{n}^{\mu}_{ik}}{\sigma_{ik}} \tag{5.21}$$

and the strain forces are

$$F_{\varepsilon,ab} = -\frac{\partial U}{\partial \varepsilon^{a}{}_{b}}\bigg|_{\varepsilon=0} = \frac{1}{2}\sum_{i}\sum_{j\in\partial i} \frac{\rho_{ij}}{\sigma_{ij}} \xi^{w-1}_{ij} \hat{n}^{a}_{ij} \hat{n}^{b}_{ij} \tag{5.22}$$

where $\hat{n}^{a}_{ij}$ is the normalized contact vector between particles i and j where a indexes the coordinates.

Now all that is left to do is to apply constraints to these forces and perform the minimization. After each minimization step, the positions and strains are updated. To simplify the scheme, the particle perturbations are applied first then the affine strain perturbs the particles further. The strain to our lattice vectors is also applied such that

$$\Lambda_{\text{new}} = (\mathbf{1} + \varepsilon)\,\Lambda. \tag{5.23}$$

Finally, the strain is reset to zero. However, applying a finite strain to the lattice vectors will only preserve the volume to first order. To correct this, the lattice vectors are uniformly rescaled after each step so that they have a determinant of one. The polymer constraints also become violated to higher order so the same scheme that appears in section 5.2.3 must be applied with our updated lattice vectors. To demonstrate the success of this methodology, two and three dimensional minimized system with 50 rigid clusters each containing three particles is shown in Figure 5.2.

5.2.6. Crossing Links, Rattling clusters, and Danglers

Careful initialization of two dimensional packings is important to avoid crossing links. If two dimers have links that cross, as seen in Figure 5.3, this forms a stable configuration that minimization will not affect. This behavior can occur between different clusters or even in a single cluster of adequate length. To avoid this behavior, one can initialize the system such that link crossings are forbidden prior to minimization. However, if large overlaps are present in a configuration prior to minimization, link crossings may still occur. This behavior becomes more likely for larger timesteps in the beginning of the quench. In a system of monomers at densities close to jamming, particles which are not locally constrained, termed rattlers, may introduce zero energy eigenmodes, or floppy modes, to the system. Rattlers are particles that are able to move independently of the other particles without affecting the system's energy. Polymer chain systems analogously can have rattling clusters. A rattling cluster is a cluster in which a subset of the cluster can move independently of the other clusters without affecting the system's energy. A particular type of rattling cluster that may appear is a dangler. A dangler is a single particle that does not interact with the other particles except by it's link (see Figure 5.4).

5.3. Finding Critically Jammed Systems

A critically jammed packing is a packing that is rigid and has zero energy. To create such a polymer packing, start with randomly distributed cluster positions and bond angles (avoiding link crossings in 2D) at a density which is much higher than the expected jamming density. These clusters are allowed to interact via a harmonic contact potential and the energy is minimized with the FIRE algorithm.

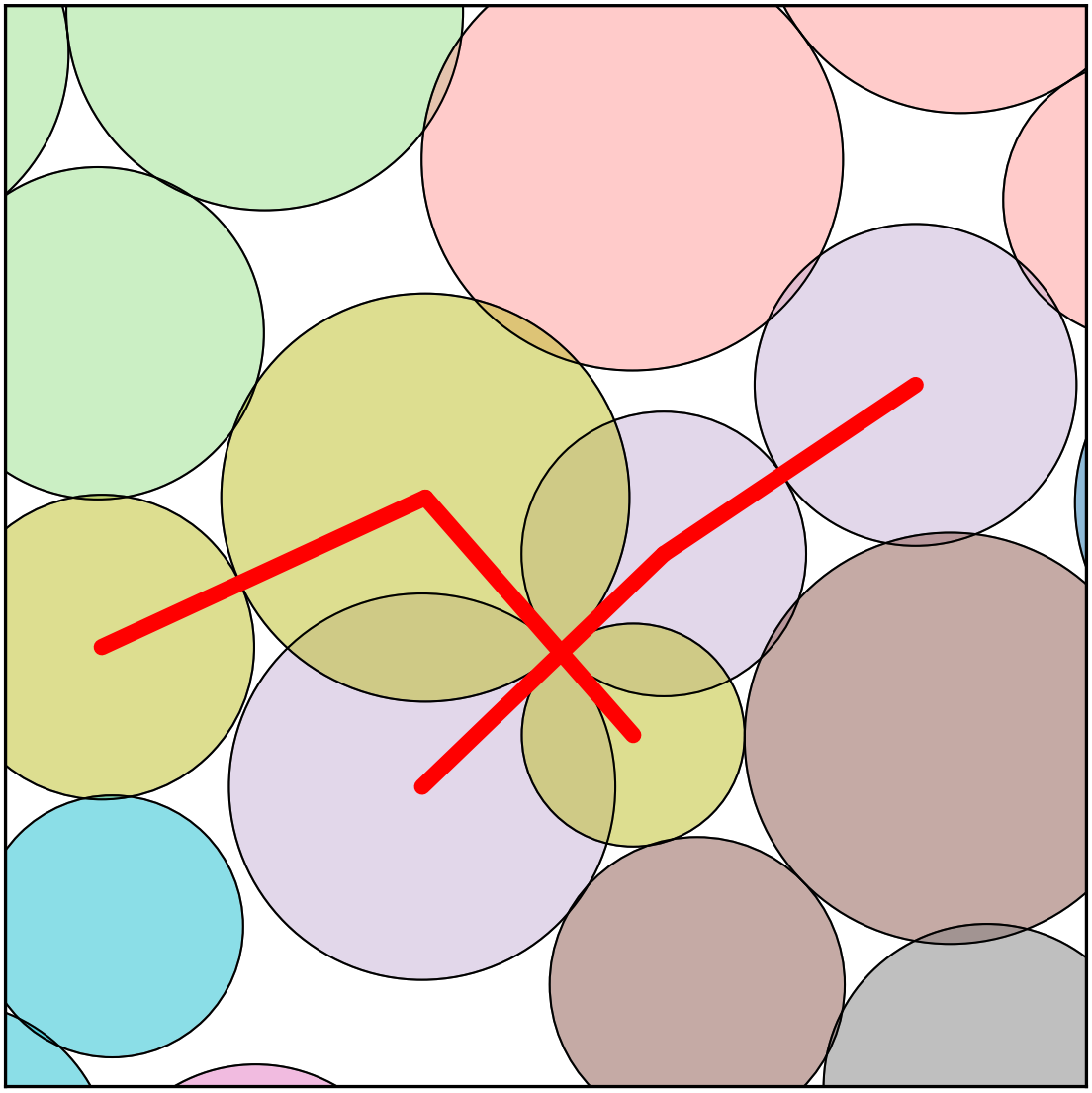

FIGURE 5.3. Two clusters and their links are shown in a packing of short chains. Two of the red links were crossing before minimization and these two links remain crossing after the minimization is finished. These two chains are in force balance despite being in a high energy configuration. This only occurs in two dimensions and can be mitigated by ensuring that there are no crossing links before beginning the quench.

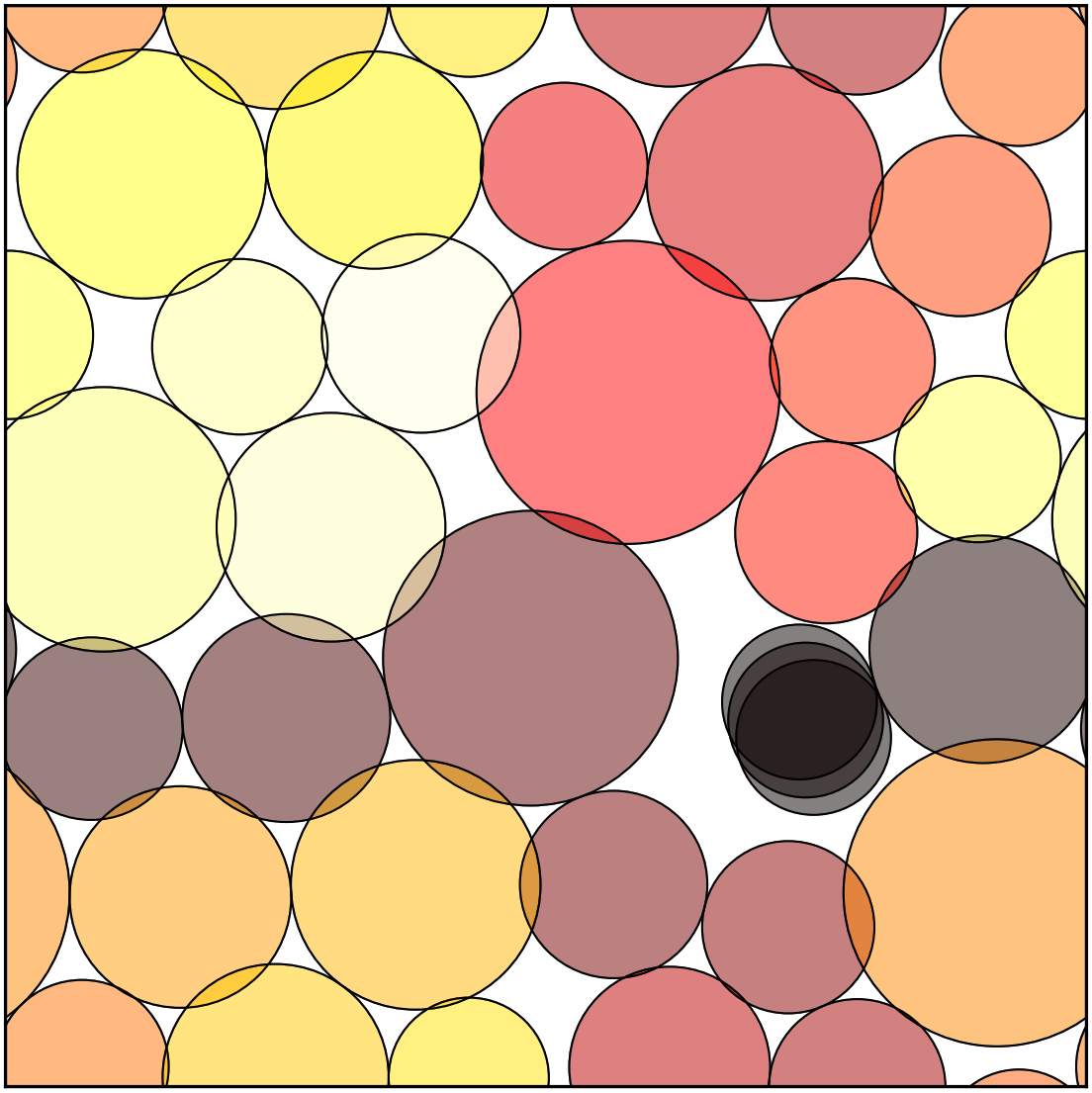

FIGURE 5.4. A chain of 30 particles in force balance. This chain is an example of a rattling cluster because one end of the chain (black) is constrained by its link, but still has a degree of freedom to move (as shown). This free motion is a floppy mode and this means that the packing is not collectively jammed. However, simply removing the end of the chain will remove this floppy mode from the system, leaving a subsystem that is collectively jammed.

The size of each cluster and the corresponding constraints are then uniformly decreased while maintaining their average positions. After minimizing this lower-density packing, the process is repeated until the energy reaches a low threshold. The amount by which the packing fraction is decreased at each step is decided by taking advantage of the scaling relationship between energy and distance to the jamming density for soft sphere systems, $\phi - \phi_j$, given in reference [37].

Because of the aforementioned rattling clusters, packings prepared in this manner will typically have some form of floppy mode present. This effect will be discussed in section 5.5.

5.4. Defining the constrained Hessian and Rigidity Matrices

5.4.1. The Constrained Hessian

For a packing of polymers, one may wish to find the normal modes, with or without strain degrees of freedom. In order to do that, one must first find the second derivatives of the energy function with respect to these degrees of freedom. These are as follows,

$$H_{xx} = \left.\frac{\partial^2 U}{\partial r_j^\nu \partial r_k^\mu}\right|_{\varepsilon=0} = \tag{5.24}$$
$$\delta_{kj} \sum_{i \in \partial k} \left[(w-1) \frac{\xi_{ik}^{w-2}}{\sigma_{ik}^2} n_{ik}^\mu n_{ik}^\nu + \frac{\xi_{ik}^{w-1}}{\rho_{ik}\sigma_{ik}} (n_{ik}^\mu n_{ik}^\nu - \delta^{\mu\nu}) \right]$$
$$- \delta_{\langle kj \rangle} \left[(w-1) \frac{\xi_{kj}^{w-2}}{\sigma_{kj}^2} n_{kj}^\mu n_{kj}^\nu + \frac{\xi_{kj}^{w-1}}{\rho_{kj}\sigma_{kj}} (n_{kj}^\mu n_{kj}^\nu - \delta^{\mu\nu}) \right],$$

$$H_{\varepsilon x} = \left.\frac{\partial^2 U}{\partial \varepsilon^a{}_b \partial r_k^\mu}\right|_{\varepsilon=0} = \tag{5.25}$$
$$\sum_i \frac{\delta_{\langle ik\rangle}}{\sigma_{ik}} \Bigg\{ \left[(w-1)\,\xi_{ik}^{w-2} - (w-2)\,\xi_{ik}^{w-1}\right] n_{ik}^\mu n_{ik}^\kappa n_{ik}^\beta$$
$$-\xi_{ik}^{w-1}\left(\delta^{\beta\mu} n_{ik}^\kappa + \delta^{\mu\kappa} n_{ik}^\beta\right)\Bigg\} \left(\frac{\partial \varepsilon^\kappa{}_\beta}{\partial \varepsilon^a{}_b}\right),$$

and

$$H_{\varepsilon\varepsilon} = \left.\frac{\partial^2 U}{\partial \varepsilon^g{}_h \partial \varepsilon^a{}_b}\right|_{\varepsilon=0} = \tag{5.26}$$
$$\frac{1}{2}\sum_i \sum_{j\in\partial i} (1-\xi_{ij}) \Bigg\{ \left[(w-1)\,\xi_{ij}^{w-2} - (w-2)\,\xi_{ij}^{w-1}\right] n_{ij}^\alpha n_{ij}^\mu$$
$$-\xi_{ij}^{w-1}\delta^{\alpha\mu}\Bigg\} n_{ij}^\beta n_{ij}^\nu \left(\frac{\partial \varepsilon^\mu{}_\nu}{\partial \varepsilon^g{}_h}\right)\left(\frac{\partial \varepsilon^\alpha{}_\beta}{\partial \varepsilon^a{}_b}\right).$$

In these equations, the term $\delta_{\langle km\rangle}$ is equal to one if particles k and m are in contact and zero otherwise. These terms can be combined to find the extended hessian, which is the second derivative of the energy function in terms of both positional and strain degrees of freedom:

$$H_0 = \begin{pmatrix} H_{xx} & H_{x\varepsilon} \\ H_{x\varepsilon}^T & H_{\varepsilon\varepsilon} \end{pmatrix}. \tag{5.27}$$

The extended hessian can be used to find the energy of a perturbation that is done to the positions of individual particles and the strains. However, with polymer packings, we do not have access to all of these degrees of freedom. If there are N particles in d dimensions with N_l nondegenerate links, the extended hessian will have $Nd + d(d+1)/2$ rows and columns whereas there are actually $N_{\text{dof}} = Nd + d(d+1)/2 - N_l - 1$ degrees of freedom (where the constraints

due to the links and the volume-preserving strain have been subtracted). In order to calculate the energy of a perturbation and the normal modes of the polymer packing, one needs to translate the perturbations of the particles and affine strains to some basis of the true degrees of freedom. This can be achieved by performing a change of basis from the original basis to a basis of the true degrees of freedom and the constraints.

Let $\vec{y}$ be a vector of length $Nd + d(d+1)/2$ that contains the position and strain variables, let $\vec{y}_t$ be a vector of length N_{dof} that contains the true degrees of freedom, and let $\vec{\lambda}$ be a vector of length $N_l + 1$ corresponding to the constraint degrees of freedom. We need a square matrix, Q, that decomposes $\vec{y}$ into $\vec{y}_t$ and $\vec{\lambda}$ such that

$$\begin{pmatrix} \vec{\lambda} \\ \vec{y}_t \end{pmatrix} = Q^T \vec{y}. \tag{5.28}$$

Without loss of generality, one can define a matrix,

$$\begin{pmatrix} \Gamma & \text{Null}(\Gamma^T) \end{pmatrix}. \tag{5.29}$$

This gives a non-singular matrix where the first $N_l + 1$ columns correspond to our constraints. This matrix can then be subjected to QR decomposition to give a matrix Q.

With this new matrix, Q, one can define a rectangular change of basis matrix as

$$B = \begin{pmatrix} \mathbf{0}_{N_l+1} & \mathbf{1}_{N_{\text{dof}}} \end{pmatrix} Q^T \tag{5.30}$$

such that

$$\vec{y}_t = B\vec{y}. \tag{5.31}$$

This basis is also useful for removing the components of a vector $\vec{y}$ that violate our constraints:

$$\vec{y}' = B^T B\vec{y}. \tag{5.32}$$

With this matrix, B, the constrained extended hessian becomes

$$H_{\mathrm{E}} = BH_0B^T. \tag{5.33}$$

Given some perturbation, $\vec{y}_t$ of our N_{dof} degrees of freedom, the change in energy can be computed as

$$\Delta E = \frac{1}{2}\vec{y}_t^T H_{\mathrm{E}}\vec{y}_t. \tag{5.34}$$

The extended hessian can also be diagonalized to find the normal modes. The only problem is that the normal modes are in terms of a rather confusing basis, but this can be easily rectified by taking the matrix of eigenvectors and multiplying them by B^T giving a set of N_{dof} eigenmodes in the familiar basis of positions of particles and strains. This entire procedure can also be easily adapted to use the matrix, Ω, and create an extended hessian that deals only with positional degrees of freedom.

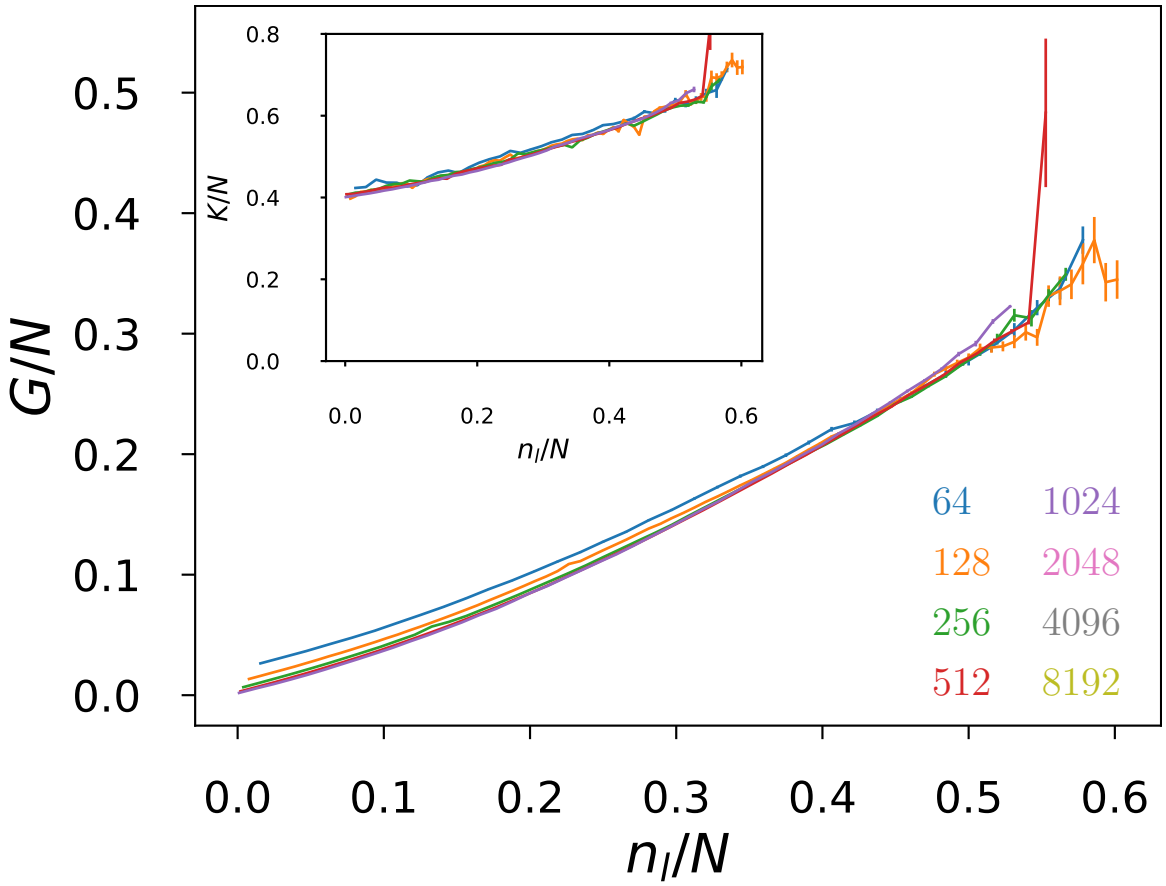

FIGURE 5.5. The shear and bulk (inset) moduli of three dimensional packings of clustered particles. Starting with shear stabilized, critically jammed systems of monomers, links are randomly added to the contact network and bond angles are frozen to simulate cementing events. The number of links at any given point is n_l and this does not include those links which are added to fix the bond angles. There are about 25 packings for each N (from 2^6 to 2^11) in which 50 independent percolation experiments were performed. The data for each N and n_l was subject to a weighted average where the Reuss and Voigt averages were used as a minimum and maximum respectively. The error bars show the weighted standard error.

5.4.2. The Constrained Rigidity Matrix

If one wanted to examine the underlying unnormalized, unstressed spring network of a packing and find the states of self stress, they could define the extended rigidity matrix. The rigidity matrix relates perturbations to bond stresses, so to derive it, consider the effect that perturbing or straining the packing has on the bond stresses. For particle perturbations, the rigidity matrix has the form

$$R_{x,\langle ij\rangle(k\gamma)} = (\delta_{jk} - \delta_{ik})\, n_{ij}^{\gamma}. \tag{5.35}$$

For strains, the rigidity matrix has the form

$$R_{\varepsilon,\langle ij\rangle(k\gamma)} = n_{ij}^{\alpha} n_{ij}^{\beta} \sigma_{ij}. \tag{5.36}$$

These two terms can be combined to get the rigidity matrix in terms of strains and positions,

$$R_{0,\langle ij\rangle} = \begin{pmatrix} R_{x,\langle ij\rangle} & R_{\varepsilon,\langle ij\rangle} \end{pmatrix} \tag{5.37}$$

such that for a vector $\vec{y} = \begin{pmatrix} \vec{x} \\ \vec{\varepsilon} \end{pmatrix}$,

$$R_{0,\langle ij\rangle}\vec{y} = R_{x,\langle ij\rangle}\vec{x} + R_{\varepsilon,\langle ij\rangle}\vec{\varepsilon}. \tag{5.38}$$

As before, one can perform a change of basis on this rigidity matrix to find the constrained extended rigidity matrix,

$$R_{\mathrm{E}} = R_0 B^T. \tag{5.39}$$

Note that the constrained extended rigidity matrix is only defined for the bonds in the system, not for the links. If the links were included, then R_{E} would return zero stress on those bonds regardless of the choice for $\vec{y}_t$.

Similarly, the states of self stress for the network are the left singular vectors that have a zero singular value. The constrained extended $\mathcal{N}$-matrix can be computed as $\mathcal{N}_{\mathrm{E}} = R_{\mathrm{E}} R_{\mathrm{E}}^T$ and the constrained extended dynamical matrix as $\mathcal{D}_{\mathrm{E}} = R_{\mathrm{E}}^T R_{\mathrm{E}}$ for the underlying unstressed spring network.

5.5. Testing for strict jamming

If one were to make a hard sphere polymer packing, such as those found by following the procedure described in section 5.3, one might want to know whether or not this packing remains stable against all possible combinations of strains and perturbations. One way to do this is to employ a linear programming algorithm based on the one found in reference [118] with the constrained extended rigidity matrix in place of the adjacency matrix. The linear program is:

$$\min \vec{b}^T \vec{y}_t \tag{5.40}$$

$$\text{such that } R_{\mathrm{E}} \vec{y}_t \leq \vec{0} \tag{5.41}$$

$$\text{where } |\vec{y}_t| \leq y_{\max}. \tag{5.42}$$

In this program, we are looking for the vector $\vec{y}_t$ which is subjected to some random load vector $\vec{b}$ that is bounded such that the length is less than some finite value $y_{\max}$. If this algorithm returns a nonzero vector, $\vec{y}_t$, then $\vec{y}_t$ describes an unjamming motion. Because of the presence of rattling clusters, this may be the case. To determine which particles are contributing to the nonzero $\vec{y}_t$, one can find the nonzero indices for $B^T\vec{y}_t$. Those rattling clusters should be removed from the packing before the linear program is executed again. This process can be repeating until $\vec{y}_t = \vec{0}$ is found. One must also run the same linear program for min $-\vec{b}^T\vec{y}_t$ to ensure that the polymer subpacking is strictly jammed [118]. As in the previous sections, the strain degrees of freedom do not need to be added; the same process can be adapted to R_x to test for collective jamming.

5.6. Computing the Compliance Matrix

Now that jamming and normal modes for the polymer systems have been discussed, the discussion can conclude by computing the elastic moduli. To compute the elastic moduli, the compliance matrix, S, is computed. This matrix relates the stress to the strain,

$$\vec{\varepsilon} = S\vec{\sigma}. \tag{5.43}$$

Before this is derived, consider Hooke's law for the unconstrained extended hessian,

$$H_0 \begin{pmatrix} \Delta\vec{x} \\ \vec{\varepsilon} \end{pmatrix} = \begin{pmatrix} -\vec{F} \\ \vec{\sigma} \end{pmatrix}. \tag{5.44}$$

Applying an arbitrary strain, $\vec{\varepsilon}$, and perturbation, $\Delta\vec{x}$, puts a stress, $\vec{\sigma}$, and interparticle forces, $\vec{F}$, on our packing. Not every combination of $\Delta\vec{x}$ and $\vec{\varepsilon}$ is allowed, so we need to project out the part of our vector that violates the constraints. From equation 5.32 one can achieve this with $B^T B$. However, this is not quite correct. When finding the elastic moduli, deformations which may affect the volume of the packing are allowed. As such, B is rederived with the volume-conserving constraint excluded from Γ. This new rectangular change of basis is referred to as B_{-1}. A new constrained hessian can be defined as

$$H_c = B_{-1}^T B_{-1} H_0 B_{-1}^T B_{-1} \tag{5.45}$$

such that it contains the same degrees of freedom as the original hessian.

To find the stress-strain relationship, it is not enough to apply an affine strain. Simply applying an affine strain will cause the packing to lose force balance. When the stress-strain relationship is probed in granular packings, minimization steps are taken between strain steps. What one must do is apply an arbitrary affine strain and a corresponding nonaffine perturbation, $\Delta\vec{x}_{\mathrm{na}}$, such that force balance is kept. For an unconstrained hessian, Hooke's law can be applied to achieve an equation such as the following:

$$H_0 \begin{pmatrix} \Delta\vec{x}_{\mathrm{na}} \\ \vec{\varepsilon} \end{pmatrix} = \begin{pmatrix} \vec{0} \\ \vec{\sigma} \end{pmatrix}. \tag{5.46}$$

However, for the constrained hessian, this relationship is false. To understand why, imagine applying a particular perturbation and strain that strictly violate our constraints; this would result in zero strain. This is the exact opposite of what

one would expect. It should be impossible to apply such a perturbation and strain, therefore one would expect the result of such a test to return an infinite stress. This is easily remedied by taking the Moore-Penrose pseudoinverse [129] of H_c. This works because the pseudoinverse preserves all of the zero eigenvalues. We can then conclude that

$$(H_c)^{-1} \begin{pmatrix} \vec{0} \\ \vec{\sigma} \end{pmatrix} = \begin{pmatrix} \Delta\vec{x}_{\text{na}} \\ \vec{\varepsilon} \end{pmatrix}. \tag{5.47}$$

This is much easier to understand as well because while certain strains may not be possible, any stress is allowed. The result will never violate our constraints, but may lead to zero strain. If $(H_c)^{-1}$ is partitioned,

$$\vec{\varepsilon} = S\vec{\sigma} \tag{5.48}$$

where

$$S = \begin{pmatrix} \mathbf{0}_{Nd\times Nd} & \mathbf{0}_{Nd\times s} \\ \mathbf{0}_{s\times Nd} & \mathbf{1}_{s\times s} \end{pmatrix} (H_c)^{-1} \tag{5.49}$$

is the compliance matrix.

For three dimensional polymer chain systems, the shear and bulk moduli can be found from the Voigt, Reuss, and Hill averages under the assumption that the configuration is nearly isotropic [156, 157]. From these averages, the poisson ratio and anisotropy can also be calculated. To understand this procedure, take three dimensional shear stabilized systems of monodisperse monomers at a single state of self stress and randomly replace some of their contacts with links. At a certain

point sufficiently many links are added to prevent certain stresses from causing strains. These impossible stresses show up as zero modes in the compliance matrix and indicate a direction in which the shear modulus is infinite. Adding additional links will also eventually cause the compliance matrix to become zero, indicating a completely rigid packing of polymer chains. The bulk and shear moduli for these systems as a function of the fraction of added links, n_l/N, (not including those added to preserve bond angles) are shown in Figure 5.5.

5.7. Conclusions

In this methods paper I have discussed how to generate packings of arbitrarily defined polymer chains. I described how to simulate the annealing of these packings and how they can be shear stabilized in the process. I gave examples of undesirable behaviors and how to prevent them as well as the definitions of rattling clusters and danglers. I then explained how to find the normal modes, classification in the jamming hierarchy, and elastic moduli. This work lays the foundations for a more thorough exploration of the mechanical properties of packings of polymer chains and molecules as well as a clear method for furthering our understanding of many important topics such as the polymer glass transition, clumping, and cementing events.

5.8. Acknowledgments

I thank Eric Corwin, James Sartor, and Heinrich Jaeger for helpful discussions and feedback. This work was supported by National Science Foundation (NSF) Career Award DMR-1255370 and the Simons Foundation No. 454939.

CHAPTER VI

PROPERTIES OF AMORPHOUS MATERIALS UNDER PERIODIC BOUNDARY CONDITIONS

6.1. Introduction

Periodic boundary conditions are a mainstay of the study of condensed matter systems as they ameliorate or eliminate many finite size effects, allowing one to infer bulk behavior from small systems. It is easy to take periodic boundary conditions for granted and think of them as capturing all of the physics of a repeated structure, but this is far from the truth. In essence, a system with periodic boundary conditions requires that all of the particle images move in concert whereas infinitely repeated structures have no such constraint.

For a finite-sized network (or packing) it is natural to ask how many constraining bonds (or contacts) are needed for rigidity. This question can be answered by the Maxwell-Calladine rule [158, 159, 160]:

$$F = Nd - N_c + S \tag{6.1}$$

where F is the total number of floppy modes (or zero modes), N is the number of nodes, d is the spatial dimension (making Nd the total number of degrees of freedom), N_c is the number of constraining bonds, and S is the number of redundant bonds which is equal to the number of states of self stress. For a physical system to be rigid, it must only have trivial rigid motions as floppy modes. For instance, a d dimensional finite network is considered rigid if it only has $F = d + d(d-1)/2$ floppy modes including d translations and $d(d-1)/2$ rotations.

For infinitely large systems, the only possible trivial rigid motion are translations. Thereby, a d dimensional network (or packing) under periodic boundary conditions can only have d floppy modes when rigid.

The Maxwell-Calladine constraint counting rule is not a suitable proxy for measuring rigidity in all types of physical systems. For instance, in second-order rigid systems, such as under-constrained networks that rigidify under tension, Eq. (6.1) cannot be used to describe the rigidity [161, 162, 163, 164]. Another example is networks with shear degrees of freedom or special symmetries (such as square lattices), where the alignment of states of self-stress leads to internal floppy modes that are accounted by the Maxwell-Calladine rule [165, 166]. However, for all systems studied in this paper, including over-constrained elastic networks and jammed packings of athermal soft particles, Eq. (6.1) is a sufficient proxy for measuring rigidity.

In this paper we rigorously examine the mathematical structure of periodic boundary conditions in jammed packings of soft athermal particles. Following the more statistical findings of Goodrich et al. [66, 67], who show that infinitely tiled two dimensional disk packings lead to anomolously low frequency modes, we demonstrate that infinitely tiled overjammed packings of soft spheres in any dimension can have not only anomolously low frequency modes, but negative modes. This result demonstrates that an overjammed sphere packing with periodic boundary conditions may not be jammed when tiling space. We also observe that the number of newly introduced zero modes when a system is used for tiling the space is directly related to its number of states of self-stress. We focus on three types of systems: 1) unstressed critically jammed packings that support just a single state of self-stress, 2) hyperstatic overjammed packings with a finite pre-

stress, and 3) the unstressed network representation of hyperstatic packings. We prove that jammed packings in d dimensions, whether stressed or unstressed, that support fewer than d states of self stress will never have a jammed tiling that is jammed and discuss the resulting floppy modes. We examine the contrapositive to discover the nature of jammed packings with d or more states of self stress. While these typically *do* have a jammed infinite lattice representation, we provide explicit counter-examples which do not.

We also explain the issues involved with overjammed packings with more d states of self stress by presenting the hessian in momentum space [67] via Bloch's Theorem [167]. We use this method to show that the infinite lattice representation of hyperstatic overjammed packings and even overjammed shear stabilized packings can have motions that lower the system energy. We conclude our discussion with a proof that the elastic properties of an infinitely repeated packing are fully captured by periodic boundary conditions.

6.2. Theorem I:

For an uncompressed, jammed spring network with $S < d$ states of self stress, the corresponding network that is duplicated across boundary x will not be jammed. Therefore infinitely tiled spring networks can only be jammed if the unit cell has $S > d$ states of self stress.

6.2.1. Proof

We proceed with a proof by contradiction. Assume that the original network has $F = d$ trivial floppy modes and $S < d$ states of self stress. Assume that the duplicated system is jammed and therefore will also have $F' = d$ trivial floppy

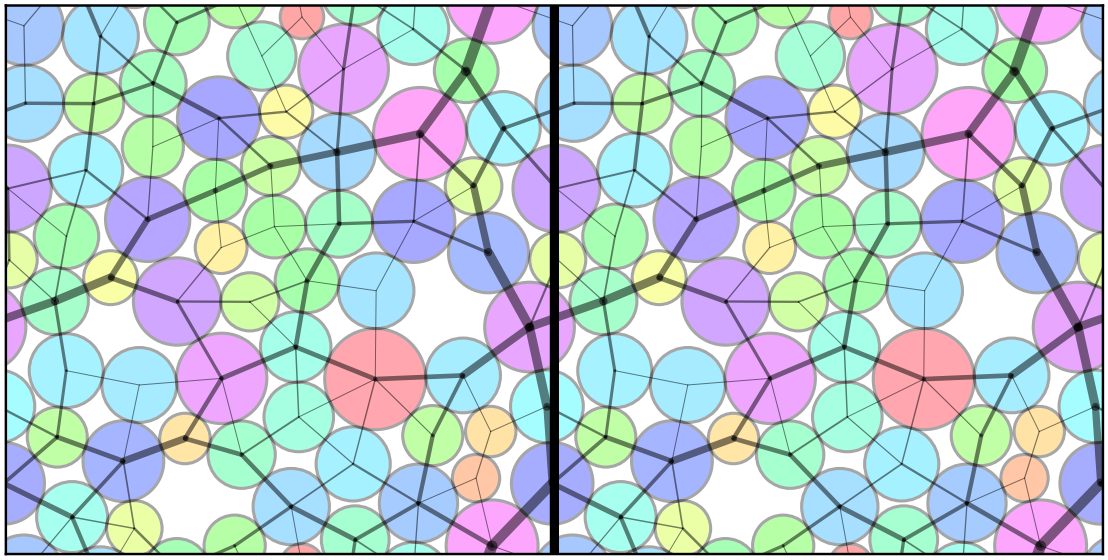

FIGURE 6.1. A packing of spheres that has been duplicated. The black lines are a state of self stress. The thickness of a line represents the magnitude of the stress on the corresponding bond. Replicating the state of self stress for the original system gives a state of self stress for the duplicated system.

modes and S' states of self stress. From the Maxwell-Calladine rule in equation 6.1,

$$Nd - N_c = F - S \tag{6.2}$$

$$\text{and } 2Nd - 2N_c = F' - S' \tag{6.3}$$

where Nd is the number of degrees of freedom and N_c is the number of contacts in the original network. If we substitute $F = F' = d$ and solve for S',

$$S' = 2S - d. \tag{6.4}$$

If we have a state of self stress for the original system, we can simply duplicate it to find a state of self stress for the replicated system [168] (as in figure 6.1). If applying a set of stresses to the bonds of the unreplicated packing

leads to force balance, then replicating those stresses to a duplicated packing must also lead to force balance. Note that the orthogonality is also preserved in this doubling procedure. With this in mind and the fact that we may find additional states of self stress not captured by this trivial doubling procedure, $S' \geq S$. Substituting this result into equation 6.4,

$$2S - d \geq S \tag{6.5}$$

$$S \geq d. \tag{6.6}$$

This is a contradiction which proves the above theorem.

6.3. Argument I:

Nearly all amorphous systems with fixed boundaries and non-zero prestress will destabilize under a sufficient number of replications

6.3.1. Reasoning

We have proven that amorphous systems with zero prestress and fewer than d states of self stress are not jammed upon replication, but many researchers are interested in overjammed packings. It turns out that these overjammed packings with more than d states of self stress typically represent saddle points in the energy landscape of the tiled system. We can show this by considering the hessian in momentum space, $H(\vec{q})$, found through Bloch's theorem [167]. For simplicity in calculating this quantity, we consider the interaction of a packing with its neighboring replicas. Each unit cell has $3^d - 1$ neighboring cells. We consider the interaction between a unit cell and it's neighbor, i as H_i. If we let the interaction

between the unit cell and itself be H_0, then this means that the original hessian, $H(\vec{0})$, can be written as:

$$H(\vec{0}) = H_0 + \sum_{i=1}^{3^d-1} H_i. \tag{6.7}$$

However, this can be simplified even further. If H_j is the hessian with respect to neighbor j and H_k is the hessian with respect to the opposing neighbor, then $H_k = H_j^T$ as in figure 6.2. This means that the hessian only needs to be split into $(3^d + 1)/2$ parts and

$$H(\vec{0}) = H_0 + \sum_{i=1}^{(3^d+1)/2} \left(H_i + H_i^T\right). \tag{6.8}$$

In general, from Bloch's theorem we can conclude that

$$\begin{aligned} H(\vec{q}) = H_0 + \sum_{i=1}^{(3^d+1)/2} \Big[&\left(H_i + H_i^T\right) \cos(\vec{q} \cdot \vec{r}_i) \\ &\left(H_i - H_i^T\right) \sin(\vec{q} \cdot \vec{r}_i) \Big] \end{aligned} \tag{6.9}$$

where $\vec{r}_i$ is the d dimensional vector corresponding to the position of cell i.

We can determine whether or not a tiled packing remains jammed upon replication by looking at the eigenvalues of the first branch. For a packing that remains jammed when tiled, all of these eigenvalues should be greater than zero except for the trivial zero modes that come from $H(\vec{0})$. Looking at a small jammed packing with 64 particles and 30 states of self stress in 2D, we can see that the eigenvalues in the first branch are negative for certain values of momentum (see figure 6.3). A negative eigenvalue means there is a direction that the particles can

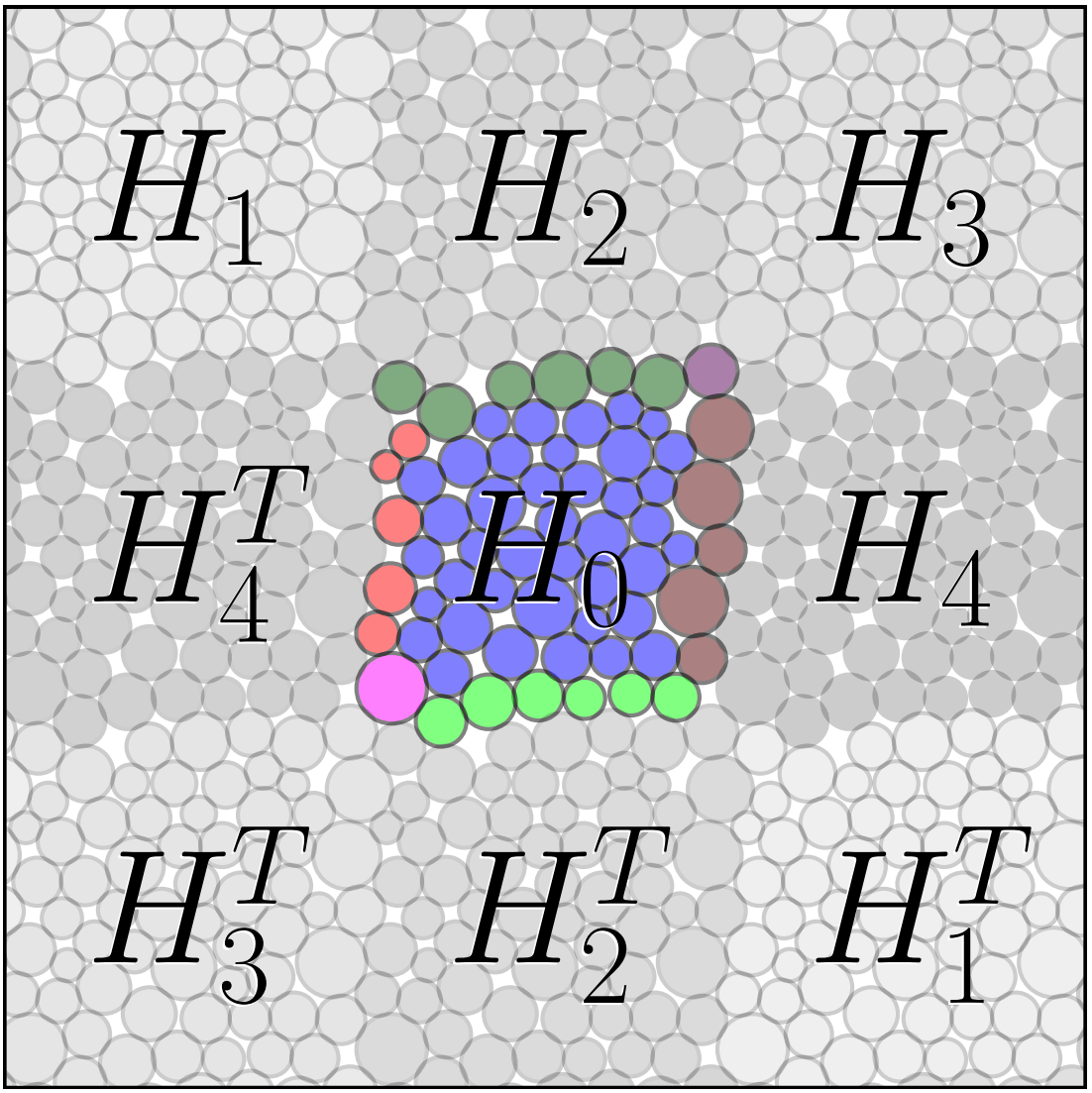

FIGURE 6.2. The hessian can be split into pieces corresponding to the interactions with neighboring cells. There are $(3^d + 1)/2$ independent hessian pieces which are shown in the center of their corresponding cells. In this example there is a single central hessian pieces as well as two vertices and two edges, each with opposing counterparts.

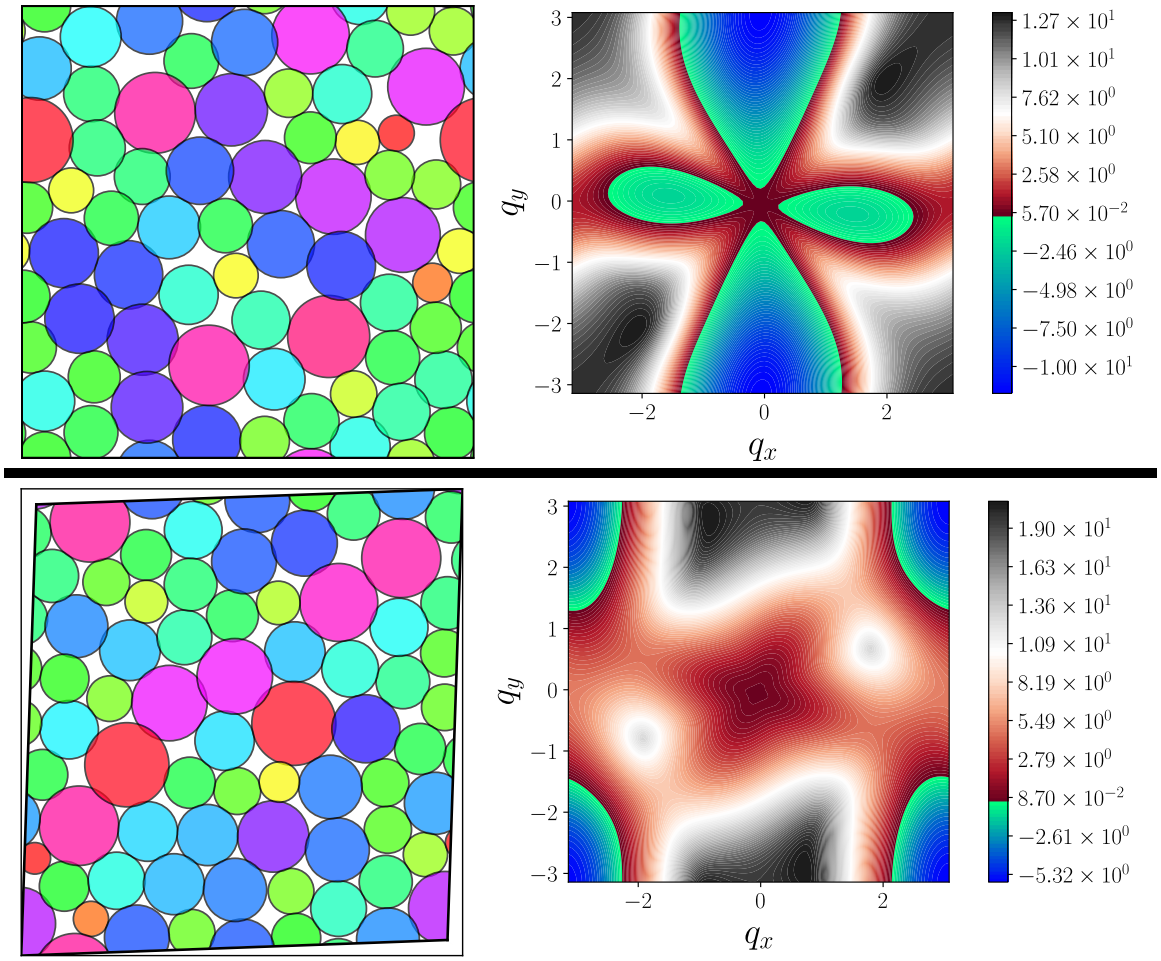

FIGURE 6.3. **Top Left**: An overjammed amorphous packing of 64 harmonic soft spheres at packing fraction $\phi = 0.9$ with 30 states of self stress.
Top Right: The eigenvalues in the first branch of the momentum-space hessian for this amorphous overjammed packing. The blue and green colors represent negative eigenvalues which corresond to perturbations that lower the system energy.
Bottom Left: A shear stabilized packing of harmonic soft spheres at $\phi = 0.9$ and 26 states of self stress.
Bottom Right: The corresponding contour plot of the first branch eigenvalues of the shear stabilized system's hessian in momentum space.

be perturbed which would lower the tiled system's energy. This means that the tiled packing, while in force balance, is not jammed.

Shear stabilized packings also may have negative modes in their first branch. This is also demonstrated in figure 6.3 with a shear stabilized packing with 64 particles and 26 states of self stress.

6.4. Lemma I

The rigidity matrix of any network can be written as

$$R = \begin{pmatrix} R_c & R_p \\ 0 & R_{b2} + R_{b1} \end{pmatrix}$$

where $\begin{pmatrix} 0 & R_{b2} + R_{b1} \end{pmatrix}$ **corresponds to the bonds that cross boundary** x. **This matrix has singular values** $\{\sigma_i\}$. **The matrix defined as**

$$R_{\mathbf{DHC}} \equiv \begin{pmatrix} R_c & R_p \\ 0 & R_{b2} - R_{b1} \end{pmatrix}$$

has singular values $\{\epsilon_i\}$. **Duplicating the network across boundary** x **results in a network where the rigidity matrix has singular values** $\{\sigma_i, \epsilon_i\}$.

6.4.1. Proof

If we consider the b bonds that cross boundary x, then we will find that there are p particles involved in making these bonds. We separate R into columns that do not involve these p boundary particles and columns that do. We further

separate R into rows that do not involve these b bonds and rows that do. This gives us

$$R = \begin{pmatrix} R_c & R_p \\ 0 & R_{b2} + R_{b1} \end{pmatrix} \tag{6.10}$$

where R_c are the bonds that are formed between particles not among the p boundary particles, R_p are the bonds that involve the p boundary particles and are not boundary bonds themselves, R_{b1} are the rows of the boundary bonds where the rightmost vectors in each row are zeroed out, and R_{b2} are the rows of the boundary bonds where the leftmost vectors in each rows are zeroed out.

If we replicate the network across boundary x, the rigidity matrix can be written as

$$R_{\mathrm{D}} = \begin{pmatrix} R_c & R_p & 0 & 0 \\ 0 & R_{b2} & 0 & R_{b1} \\ 0 & 0 & R_c & R_p \\ 0 & R_{b1} & 0 & R_{b2} \end{pmatrix}. \tag{6.11}$$

If we consider $\vec{u} = \begin{pmatrix} \vec{u}_1 \\ \vec{u}_2 \end{pmatrix}$ and $\vec{v} = \begin{pmatrix} \vec{v}_1 \\ \vec{v}_2 \end{pmatrix}$ to be left and right singular vectors (respectively) for R with corresponding singular value σ such that $\vec{u}^T R \vec{v} = \sigma$, then we can demonstrate that $\frac{1}{\sqrt{2}} \begin{pmatrix} \vec{u} \\ \vec{u} \end{pmatrix} = \frac{1}{\sqrt{2}} \begin{pmatrix} \vec{u}_1 \\ \vec{u}_2 \\ \vec{u}_1 \\ \vec{u}_2 \end{pmatrix}$ and $\frac{1}{\sqrt{2}} \begin{pmatrix} \vec{v} \\ \vec{v} \end{pmatrix} = \frac{1}{\sqrt{2}} \begin{pmatrix} \vec{v}_1 \\ \vec{v}_2 \\ \vec{v}_1 \\ \vec{v}_2 \end{pmatrix}$ are left and right singular vectors for R_{D} with singular value σ. Notice that these vectors

are orthonormal. Shown explicitly,

$$\begin{aligned}
&\frac{1}{2}\begin{pmatrix}\vec{u}^T & \vec{u}^T\end{pmatrix} R_{\mathrm{D}} \begin{pmatrix}\vec{v}\\ \vec{v}\end{pmatrix} \\
&\qquad = \frac{1}{2}\begin{pmatrix}\vec{u}^T & \vec{u}^T\end{pmatrix} \begin{pmatrix} R_c & R_p & 0 & 0 \\ 0 & R_{b2} & 0 & R_{b1} \\ 0 & 0 & R_c & R_p \\ 0 & R_{b1} & 0 & R_{b2}\end{pmatrix} \begin{pmatrix}\vec{v}_1\\ \vec{v}_2\\ \vec{v}_1\\ \vec{v}_2\end{pmatrix} \\
&\qquad = \frac{1}{2}\begin{pmatrix}\vec{u}^T & \vec{u}^T\end{pmatrix} \left(\begin{pmatrix} R_c & R_p \\ 0 & R_{b2}+R_{b1}\end{pmatrix} \begin{pmatrix}\vec{v}_1\\ \vec{v}_2\end{pmatrix} + \begin{pmatrix} R_c & R_p \\ 0 & R_{b2}+R_{b1}\end{pmatrix} \begin{pmatrix}\vec{v}_1\\ \vec{v}_2\end{pmatrix} \right) \\
&\qquad = \frac{1}{2}\begin{pmatrix}\vec{u}^T & \vec{u}^T\end{pmatrix} \begin{pmatrix} R\vec{v}\\ R\vec{v}\end{pmatrix} \\
&\qquad = \sigma.
\end{aligned}$$

This means that $\{\sigma_i\}$ are singular values for R_{D}. This is not surprising, as these are the modes that correspond to the particles moving in concert with their duplicate. In a similar fashion, consider $\vec{x}$ and $\vec{w}$ to be left and right singular vectors for R_{DHC} with singular value ϵ. We can now show that $\frac{1}{\sqrt{2}}\begin{pmatrix}\vec{x}\\ -\vec{x}\end{pmatrix}$ and $\frac{1}{\sqrt{2}}\begin{pmatrix}\vec{w}\\ -\vec{w}\end{pmatrix}$ are left and right singular vectors for R_{D} with singular value ϵ. Again, notice that these vectors

are orthonormal and consider

$$\begin{aligned}
\frac{1}{2}\begin{pmatrix}\vec{x}^T & -\vec{x}^T\end{pmatrix} R_{\mathrm{D}} \begin{pmatrix}\vec{w}\\ -\vec{w}\end{pmatrix} & \\
&= \frac{1}{2}\begin{pmatrix}\vec{x}^T & -\vec{x}^T\end{pmatrix} \begin{pmatrix}R_{\mathrm{DHC}}\vec{w}\\ -R_{\mathrm{DHC}}\vec{w}\end{pmatrix} \\
&= \vec{x}^T R_{\mathrm{DHC}}\vec{w} \\
&= \epsilon.
\end{aligned}$$

This means that $\{\epsilon_i\}$ are also singular values for R_{D}. Since R_{D} has exactly twice as many singular values as R, all of the singular values for R_{D} must be given by $\{\sigma_i, \epsilon_i\}$.

6.5. Lemma II:

Let the singular value decomposition of R be given by $R = \begin{pmatrix}U_c\\ U_b\end{pmatrix} \Sigma \begin{pmatrix}V_c\\ V_p\end{pmatrix}^T$ where U_b represents the final b rows of the left unitary singular vector matrix and V_p represents the final p rows of the right unitary singular vector matrix. We can prove that

$$Rank(R_{DHC}) = Rank(\Sigma - 2U_b^T R_{b1} V_p). \tag{6.12}$$

6.5.1. Proof

Let $U = \begin{pmatrix} U_c \\ U_b \end{pmatrix}$ and $V = \begin{pmatrix} V_c \\ V_p \end{pmatrix}$. Let X and W be left and right unitary singular vector matrices for R_{DHC} such that $R_{DHC} = X\Sigma_{\text{DHC}}W^T$. Further, consider α and β to be change of basis matrices such that

$$W = V\alpha$$

$$\text{and } X = U\beta.$$

Consider

$$\begin{aligned}
\Sigma_{\text{DHC}} &= X^T R_{\text{DHC}} W \\
&= \beta^T U^T R_{\text{DHC}} V\alpha \\
&= \beta^T U^T \left[R - \begin{pmatrix} 0 & 0 \\ 0 & 2R_{b1} \end{pmatrix} \right] V\alpha \\
&= \beta^T \left[U^T RV - U^T \begin{pmatrix} 0 \\ 2R_{b1}V_p \end{pmatrix} \right] \alpha \\
&= \beta^T \left(\Sigma - 2U_b^T R_{b1} V_p \right) \alpha.
\end{aligned}$$

Now we know that the rank of Σ_{DHC} is the same as the rank of R_{DHC} and that α and β must be full rank because they are change of basis matrices so we have

$$Rank(R_{\text{DHC}}) = Rank \left(\Sigma - 2U_b^T R_{b1} V_p \right).$$

6.6. Argument II:

For typical, unstressed, critically jammed systems with $s \geq d$ states of self stress, the corresponding system that is duplicated across boundary x will also be jammed. Therefore these systems will typically remain jammed when tiled.

6.6.1. Reasoning

We see from Lemma II that the rank of R_{DHC} comes from perturbing the rectangular matrix with a matrix that is typically dense. This means that it is extremely likely for the rank of R_{DHC} to be Nd. From Lemma I, we would have $Rank(R_{\mathrm{D}}) = (2N-1)d$. Since $Rank(R_{\mathrm{D}}) + F_{\mathrm{D}} = 2Nd$ where F_{D} is the number of floppy modes in the duplicated system, we have $F_{\mathrm{D}} = d$ and the duplicated system is therefore jammed.

6.6.2. Discussion

While we have explained why most amorphous, unstressed, critically jammed packings with d or more states of self stress are typically jammed upon replication, it is worth noting that this does indeed hinge on a statistical argument. It is possible to create non-amorphous packings of hard spheres which are not jammed upon replication. In figure 6.4, we create two packings based on the triangular lattice. These packings were proven to be jammed by using a linear programming algorithm [117, 118, 119]. However, when these packings are tiled, one finds that novel floppy modes are introduced.

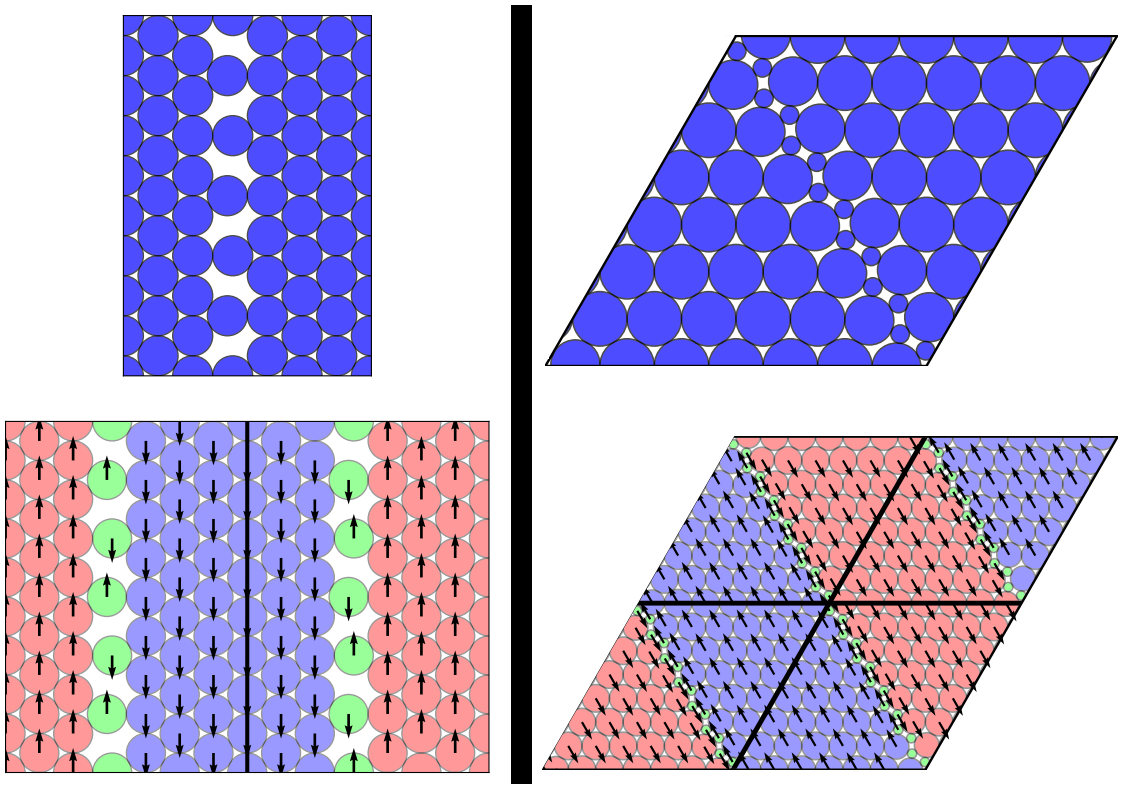

FIGURE 6.4. **Top Left**: A jammed packing of hard spheres with significantly more than d states of self stress based on a triangular lattice with a vertical line of particles with only three contacts each.
Bottom Left: The corresponding duplicated packing which is not jammed. There is a floppy mode in which the red and blue particles move in opposing directions.
Top Right: Another jammed packing of hard spheres with significantly more than d states of self stress. This packing is jammed even when duplicated once in either direction.
Bottom Right: The packing from above, but replicated in a 2x2 arrangement. This packing is not jammed as the red and blue regions are free to move in opposition, creating a floppy mode.

6.7. Theorem III:

The elastic moduli for a jammed packing are the same as the corresponding packing that is duplicated across boundary x up to a trivial scaling factor. This means that when tiling the system, the stiffness matrix is extensive.

6.7.1. Proof

The elastic properties of a packing can be understood from the stiffness matrix, C, where

$$\vec{\sigma} = C\vec{\varepsilon} \tag{6.13}$$

for the stress, $\vec{\sigma}$, and the strain, $\vec{\varepsilon}$. We can find this relationship for the original packing by considering the extended hessian, which is found from the second derivative of energy with respect to the positional and strain degrees of freedom. Let H be the extended hessian such that

$$H = \begin{pmatrix} H_{xx} & H_{x\varepsilon} \\ H_{x\varepsilon}^T & H_{\varepsilon\varepsilon} \end{pmatrix} \tag{6.14}$$

where H_{xx} is the second derivative of the energy with respect to the positions, $H_{\varepsilon\varepsilon}$ is the second derivative with respect to strain, and $H_{x\varepsilon}$ is the mixed second derivative. From Hooke's law, we can conclude that

$$H \begin{pmatrix} \vec{x} \\ \vec{\varepsilon} \end{pmatrix} = \begin{pmatrix} -\vec{F} \\ \vec{\sigma} \end{pmatrix} \tag{6.15}$$

where $\vec{F}$ represents the interparticle forces. If we want to find the stress-strain relationship as in equation 6.13, we need to ensure that through the process of applying a strain, force balance is never lost. Therefore, when applying a strain, we also need to apply a non-affine perturbation, $\vec{x}_{\text{na}}$, so that

$$H \begin{pmatrix} \vec{x}_{\text{na}} \\ \vec{\varepsilon} \end{pmatrix} = \begin{pmatrix} \vec{0} \\ \vec{\sigma} \end{pmatrix} \tag{6.16}$$

$$\begin{pmatrix} H_{xx}\vec{x}_{\text{na}} + H_{x\varepsilon}\vec{\varepsilon} \\ H_{x\varepsilon}^{T}\vec{x}_{\text{na}} + H_{\varepsilon\varepsilon}\vec{\varepsilon} \end{pmatrix} = \begin{pmatrix} \vec{0} \\ \vec{\sigma} \end{pmatrix}. \tag{6.17}$$

If we solve the first system of equations for $\vec{x}_{\text{na}}$ and substitute the solution in to the second system of equations, we find that

$$C = H_{\varepsilon\varepsilon} - H_{x\varepsilon}^{T} \left(H_{xx}\right)^{-1} H_{x\varepsilon} \tag{6.18}$$

where $\left(H_{xx}\right)^{-1}$ is the Moore-Penrose pseudoinverse [129] for the singular matrix H_{xx}.

Now that we have an expression for the stiffness matrix of the original packing, we need to find the stiffness matrix for the duplicated packing, C_D. We can express the positional second derivative of the duplicated system, H_{Dxx}, as

$$H_{Dxx} = \begin{pmatrix} H_A & H_B \\ H_B & H_A \end{pmatrix} \tag{6.19}$$

because the order in which we take the partial derivatives with respect to the positions of system A and B is inconsequential due to commutivity. The extended

hessian for the duplicated system is therefore

$$H_D = \begin{pmatrix} H_A & H_B & H_{x\varepsilon} \\ H_B & H_A & H_{x\varepsilon} \\ H_{x\varepsilon}^T & H_{x\varepsilon}^T & 2H_{\varepsilon\varepsilon} \end{pmatrix}. \tag{6.20}$$

If we let $\vec{x}_1$ be the non-affine motion of the original system and $\vec{x}_2$ be the non-affine motion of the replicated system, then

$$\begin{pmatrix} H_A\vec{x}_1 + H_B\vec{x}_2 + H_{x\varepsilon}\vec{\varepsilon} \\ H_B\vec{x}_1 + H_A\vec{x}_2 + H_{x\varepsilon}\vec{\varepsilon} \\ H_{x\varepsilon}^T(\vec{x}_1 + \vec{x}_2) + 2H_{xx}\vec{\varepsilon} \end{pmatrix} = \begin{pmatrix} \vec{0} \\ \vec{0} \\ \vec{\sigma} \end{pmatrix}. \tag{6.21}$$

If we add the first two equations, we find that

$$(H_A + H_B)(\vec{x}_1 + \vec{x}_2) + 2H_{\varepsilon\varepsilon}\vec{\varepsilon} = \vec{0}. \tag{6.22}$$

We can solve for $\vec{x}_1 + \vec{x}_2$ by using the fact that $H_{xx} = H_A + H_B$. Making this substitution into the third equation reveals that

$$C_D = 2C. \tag{6.23}$$

This means that when tiling the system, the stiffness matrix is extensive.

6.8. Conclusions

Using periodic boundary conditions is immensely useful in physics to reduce the impact of finite size effects. However, physicists need to be congnizant of

the limitations and pitfalls. We have demonstrated that hyperstatic overjammed packings often do not represent true minima when used to tile space. Likewise even packings that are shear stabilized can share this feature. We also demonstrated that critically jammed packings at a single state of self stress in periodic boundary conditions are never jammed when used to tile space. If these issues are important in a research endeavor, we argue that critically jammed shear stabilized systems will typically be jammed when used to tile space and we provide a method for checking if this is true. We finish this discussion with a proof that the elastic properties of an infinitely tiled packing are completely captured by periodic boundary conditions.

6.9. Acknowledgements

We thank Jayson Paulose for his perspective and useful discussions. This work is supported by the Simons Collaboration on Cracking the Glass Problem via award No. 454939.

CHAPTER VII

CONCLUSION

This work has focused on furthering our understanding of jammed solids and I'm proud to claim that I not only have contributed to this monumental effort, but I have the privilege of continuing to do so.

In chapter II, I wrote about the marginal Gardner phase, a mean-field result for glasses, and how jammed amorphous systems fit into this picture. By demonstrating that the jamming energy landscape is marginal, we showed how glasses and jamming are related as well as where marginality fits in the picture. Inspired by the mean-field theory, we showed that the jamming energy landscape is also hierarchical and ultrametric.

Chapter III was a much larger collaborative experience that was quite enjoyable. This chapter, like the previous, demonstrated that the mean-field theory of glasses is very relevant for low-dimensional jammed systems. We showed excellent agreement between several types of amorphous systems and the mean-field theory, further understanding the universality class.

In chapter IV, we discussed rigidity and what it means for a system to be jammed. We went on to show that there is no threshold for jamming, jammed systems exist at arbitrarily low densities. After explaining how to create one, we demonstrated that the construction works and examined the mechanical properties. Dionysian packings are jammed at arbitrarily low densities and display impressive elastic properties.

In chapter V, I demonstrated how one can simulate packings of semi-flexible polymers, chains, and molecules. By thinking in terms of constraints, I created a

simple modification that can be made to soft sphere packings simulations allowing polymers to be simulated, with or without shear stabilization. Crucially, I also explained and derived equations that can be used to calculate the normal modes and elastic response properties of polymer packings.

In chapter VI, we demonstrated a series of proofs involving periodic boundary conditions. It is our goal to help the jamming and glassy communities understand what exactly their results do and do not mean in terms of the infinitely tiled structure. We showed that critically jammed packings under periodic boundary conditions are never jammed when replicated. We also showed that overjammed packings (with prestresses) are rarely jammed when replicated and that shear stabilized packings with prestresses can also have unjamming motions.

REFERENCES CITED

[1] Simon Dagois-Bohy, Brian P. Tighe, Johannes Simon, Silke Henkes, and Martin van Hecke. Soft-Sphere Packings at Finite Pressure but Unstable to Shear. *Physical Review Letters*, 109(9):095703, August 2012. doi: 10.1103/PhysRevLett.109.095703. URL https://link.aps.org/doi/10.1103/PhysRevLett.109.095703. Publisher: American Physical Society.

[2] E. Gardner. Spin glasses with p-spin interactions. *Nuclear Physics B*, 257: 747–765, January 1985. ISSN 0550-3213. doi: 10.1016/0550-3213(85)90374-8. URL http://www.sciencedirect.com/science/article/pii/0550321385903748.

[3] M. Mezard, G. Parisi, and M. Virasoro. *Spin Glass Theory and Beyond: An Introduction to the Replica Method and Its Applications*. World Scientific Publishing Company, November 1987. ISBN 978-981-310-391-7. Google-Books-ID: DwY8DQAAQBAJ.

[4] Tommaso Castellani and Andrea Cavagna. Spin-glass theory for pedestrians. *Journal of Statistical Mechanics: Theory and Experiment*, 2005(05):P05012, 2005. ISSN 1742-5468. doi: 10.1088/1742-5468/2005/05/P05012. URL http://stacks.iop.org/1742-5468/2005/i=05/a=P05012.

[5] Jorge Kurchan, Giorgio Parisi, Pierfrancesco Urbani, and Francesco Zamponi. Exact Theory of Dense Amorphous Hard Spheres in High Dimension. II. The High Density Regime and the Gardner Transition. *The Journal of Physical Chemistry B*, 117(42):12979–12994, October 2013. ISSN 1520-6106. doi: 10.1021/jp402235d. URL https://doi.org/10.1021/jp402235d.

[6] Patrick Charbonneau, Jorge Kurchan, Giorgio Parisi, Pierfrancesco Urbani, and Francesco Zamponi. Fractal free energy landscapes in structural glasses. *Nature Communications*, 5:3725, April 2014. ISSN 2041-1723. doi: 10.1038/ncomms4725. URL https://www.nature.com/articles/ncomms4725.

[7] Patrick Charbonneau, Jorge Kurchan, Giorgio Parisi, Pierfrancesco Urbani, and Francesco Zamponi. Exact theory of dense amorphous hard spheres in high dimension. III. The full replica symmetry breaking solution. *Journal of Statistical Mechanics: Theory and Experiment*, 2014(10):P10009, 2014. ISSN 1742-5468. doi: 10.1088/1742-5468/2014/10/P10009. URL http://stacks.iop.org/1742-5468/2014/i=10/a=P10009.

[8] Patrick Charbonneau, Jorge Kurchan, Giorgio Parisi, Pierfrancesco Urbani, and Francesco Zamponi. Glass and Jamming Transitions: From Exact Results to Finite-Dimensional Descriptions. *Annual Review of Condensed Matter Physics*, 8(1):265–288, 2017. doi: 10.1146/annurev-conmatphys-031016-025334. URL https://doi.org/10.1146/annurev-conmatphys-031016-025334.

[9] Moumita Maiti and Michael Schmiedeberg. Ergodicity breaking transition in a glassy soft sphere system at small but non-zero temperatures. *Scientific Reports*, 8(1):1837, January 2018. ISSN 2045-2322. doi: 10.1038/s41598-018-20152-3. URL https://www.nature.com/articles/s41598-018-20152-3.

[10] Giorgio Parisi and Francesco Zamponi. Mean-field theory of hard sphere glasses and jamming. *Reviews of Modern Physics*, 82(1):789–845, March 2010. doi: 10.1103/RevModPhys.82.789. URL https://link.aps.org/doi/10.1103/RevModPhys.82.789.

[11] Corrado Rainone, Pierfrancesco Urbani, Hajime Yoshino, and Francesco Zamponi. Following the Evolution of Hard Sphere Glasses in Infinite Dimensions under External Perturbations: Compression and Shear Strain. *Physical Review Letters*, 114(1):015701, January 2015. doi: 10.1103/PhysRevLett.114.015701. URL https://link.aps.org/doi/10.1103/PhysRevLett.114.015701.

[12] Corrado Rainone and Pierfrancesco Urbani. Following the evolution of glassy states under external perturbations: the full replica symmetry breaking solution. *Journal of Statistical Mechanics: Theory and Experiment*, 2016(5): 053302, May 2016. ISSN 1742-5468. doi: 10.1088/1742-5468/2016/05/053302. URL https://doi.org/10.1088%2F1742-5468%2F2016%2F05%2F053302.

[13] Pierfrancesco Urbani and Francesco Zamponi. Shear Yielding and Shear Jamming of Dense Hard Sphere Glasses. *Physical Review Letters*, 118(3): 038001, January 2017. doi: 10.1103/PhysRevLett.118.038001. URL https://link.aps.org/doi/10.1103/PhysRevLett.118.038001.

[14] Giulio Biroli and Pierfrancesco Urbani. Liu-Nagel phase diagrams in infinite dimension. *SciPost Physics*, 4(4):020, April 2018. ISSN 2542-4653. doi: 10.21468/SciPostPhys.4.4.020. URL https://scipost.org/SciPostPhys.4.4.020.

[15] Camille Scalliet, Ludovic Berthier, and Francesco Zamponi. Marginally stable phases in mean-field structural glasses. *Physical Review E*, 99(1):012107, January 2019. doi: 10.1103/PhysRevE.99.012107. URL https://link.aps.org/doi/10.1103/PhysRevE.99.012107.

[16] Giulio Biroli and Pierfrancesco Urbani. Breakdown of elasticity in amorphous solids. *Nature Physics*, 12(12):1130–1133, December 2016. ISSN 1745-2481. doi: 10.1038/nphys3845. URL https://www.nature.com/articles/nphys3845.

[17] Ludovic Berthier, Patrick Charbonneau, Yuliang Jin, Giorgio Parisi, Beatriz Seoane, and Francesco Zamponi. Growing timescales and lengthscales characterizing vibrations of amorphous solids. *Proceedings of the National Academy of Sciences*, 113(30):8397–8401, July 2016. ISSN 0027-8424, 1091-6490. doi: 10.1073/pnas.1607730113. URL https://www.pnas.org/content/113/30/8397.

[18] Camille Scalliet, Ludovic Berthier, and Francesco Zamponi. Absence of Marginal Stability in a Structural Glass. *Physical Review Letters*, 119(20): 205501, November 2017. doi: 10.1103/PhysRevLett.119.205501. URL https://link.aps.org/doi/10.1103/PhysRevLett.119.205501.

[19] Beatriz Seoane and Francesco Zamponi. Spin-glass-like aging in colloidal and granular glasses. *Soft Matter*, 14(25):5222–5234, June 2018. ISSN 1744-6848. doi: 10.1039/C8SM00859K. URL https://pubs.rsc.org/en/content/articlelanding/2018/sm/c8sm00859k.

[20] C. L. Hicks, M. J. Wheatley, M. J. Godfrey, and M. A. Moore. Gardner Transition in Physical Dimensions. *Physical Review Letters*, 120(22):225501, May 2018. doi: 10.1103/PhysRevLett.120.225501. URL https://link.aps.org/doi/10.1103/PhysRevLett.120.225501.

[21] Yuliang Jin, Pierfrancesco Urbani, Francesco Zamponi, and Hajime Yoshino. A stability-reversibility map unifies elasticity, plasticity, yielding, and jamming in hard sphere glasses. *Science Advances*, 4(12):eaat6387, December 2018. ISSN 2375-2548. doi: 10.1126/sciadv.aat6387. URL https://advances.sciencemag.org/content/4/12/eaat6387.

[22] Qinyi Liao and Ludovic Berthier. Hierarchical Landscape of Hard Disk Glasses. *Physical Review X*, 9(1):011049, March 2019. doi: 10.1103/PhysRevX.9.011049. URL https://link.aps.org/doi/10.1103/PhysRevX.9.011049.

[23] Claudia Artiaco, Paolo Baldan, and Giorgio Parisi. An exploratory study of the glassy landscape near jamming. *arXiv:1908.06127 [cond-mat]*, August 2019. URL http://arxiv.org/abs/1908.06127. arXiv: 1908.06127.

[24] A. Seguin and O. Dauchot. Experimental Evidence of the Gardner Phase in a Granular Glass. *Physical Review Letters*, 117(22):228001, November 2016. doi: 10.1103/PhysRevLett.117.228001. URL https://link.aps.org/doi/10.1103/PhysRevLett.117.228001.

[25] Andrew P. Hammond and Eric I. Corwin. Experimental observation of the marginal glass phase in a colloidal glass. *Proceedings of the National Academy of Sciences*, 117(11):5714–5718, March 2020. ISSN 0027-8424, 1091-6490. doi: 10.1073/pnas.1917283117. URL https://www.pnas.org/content/117/11/5714. Publisher: National Academy of Sciences Section: Physical Sciences.

[26] Corey S. O'Hern, Leonardo E. Silbert, Andrea J. Liu, and Sidney R. Nagel. Jamming at zero temperature and zero applied stress: The epitome of disorder. *Physical Review E*, 68(1):011306, July 2003. doi: 10.1103/PhysRevE.68.011306. URL https://link.aps.org/doi/10.1103/PhysRevE.68.011306. Publisher: American Physical Society.

[27] T. S. Majmudar, M. Sperl, S. Luding, and R. P. Behringer. Jamming Transition in Granular Systems. *Physical Review Letters*, 98(5):058001, January 2007. doi: 10.1103/PhysRevLett.98.058001. URL https://link.aps.org/doi/10.1103/PhysRevLett.98.058001.

[28] Patrick Charbonneau, Eric I. Corwin, Giorgio Parisi, and Francesco Zamponi. Universal Microstructure and Mechanical Stability of Jammed Packings. *Physical Review Letters*, 109(20):205501, November 2012. doi: 10.1103/PhysRevLett.109.205501. URL https://link.aps.org/doi/10.1103/PhysRevLett.109.205501.

[29] Peter K. Morse and Eric I. Corwin. Geometric Signatures of Jamming in the Mechanical Vacuum. *Physical Review Letters*, 112(11):115701, March 2014. doi: 10.1103/PhysRevLett.112.115701. URL https://link.aps.org/doi/10.1103/PhysRevLett.112.115701. Publisher: American Physical Society.

[30] Enzo Marinari, Giorgio Parisi, Federico Ricci-Tersenghi, Juan J. Ruiz-Lorenzo, and Francesco Zuliani. Replica Symmetry Breaking in Short-Range Spin Glasses: Theoretical Foundations and Numerical Evidences. *Journal of Statistical Physics*, 98(5):973–1074, March 2000. ISSN 1572-9613. doi: 10.1023/A:1018607809852. URL https://doi.org/10.1023/A:1018607809852.

[31] Fionn Murtagh. On Ultrametricity, Data Coding, and Computation. *Journal of Classification*, 21(2):167–184, September 2004. ISSN 1432-1343. doi: 10.1007/s00357-004-0015-y. URL https://doi.org/10.1007/s00357-004-0015-y.

[32] Johannes J. Schneider, André Müller, and Elmar Schömer. Ultrametricity property of energy landscapes of multidisperse packing problems. *Physical Review. E, Statistical, Nonlinear, and Soft Matter Physics*, 79(3 Pt 1):031122, March 2009. ISSN 1539-3755. doi: 10.1103/PhysRevE.79.031122.

[33] Erik Bitzek, Pekka Koskinen, Franz Gähler, Michael Moseler, and Peter Gumbsch. Structural Relaxation Made Simple. *Physical Review Letters*, 97 (17):170201, October 2006. doi: 10.1103/PhysRevLett.97.170201. URL `https://link.aps.org/doi/10.1103/PhysRevLett.97.170201`. Publisher: American Physical Society.

[34] Patrick Charbonneau, Eric I. Corwin, Giorgio Parisi, Alexis Poncet, and Francesco Zamponi. Universal Non-Debye Scaling in the Density of States of Amorphous Solids. *Physical Review Letters*, 117(4):045503, July 2016. doi: 10.1103/PhysRevLett.117.045503. URL `https://link.aps.org/doi/10.1103/PhysRevLett.117.045503`. Publisher: American Physical Society.

[35] Peter K. Morse and Eric I. Corwin. Echoes of the Glass Transition in Athermal Soft Spheres. *Physical Review Letters*, 119(11):118003, September 2017. doi: 10.1103/PhysRevLett.119.118003. URL `https://link.aps.org/doi/10.1103/PhysRevLett.119.118003`. Publisher: American Physical Society.

[36] M. P Allen and author.) Tildesley, D. J. *Computer simulation of liquids*. Oxford : Oxford University Press, second edition edition, 2017. ISBN 978-0-19-184143-9. URL `https://trove.nla.gov.au/work/9142343`.

[37] Patrick Charbonneau, Eric I. Corwin, Giorgio Parisi, and Francesco Zamponi. Jamming Criticality Revealed by Removing Localized Buckling Excitations. *Physical Review Letters*, 114(12):125504, March 2015. doi: 10.1103/PhysRevLett.114.125504. URL `https://link.aps.org/doi/10.1103/PhysRevLett.114.125504`. Publisher: American Physical Society.

[38] G.-J. Gao, J. Blawzdziewicz, and C. S. O'Hern. Enumeration of distinct mechanically stable disk packings in small systems. *Philosophical Magazine*, 87(3-5):425–431, January 2007. ISSN 1478-6435. doi: 10.1080/14786430600851760. URL `https://doi.org/10.1080/14786430600851760`.

[39] S. S. Ashwin, Jerzy Blawzdziewicz, Corey S. O'Hern, and Mark D. Shattuck. Calculations of the structure of basin volumes for mechanically stable packings. *Physical Review E*, 85(6):061307, June 2012. doi: 10.1103/PhysRevE.85.061307. URL `https://link.aps.org/doi/10.1103/PhysRevE.85.061307`.

[40] Ning Xu, Daan Frenkel, and Andrea J. Liu. Direct Determination of the Size of Basins of Attraction of Jammed Solids. *Physical Review Letters*, 106(24): 245502, June 2011. doi: 10.1103/PhysRevLett.106.245502. URL https://link.aps.org/doi/10.1103/PhysRevLett.106.245502.

[41] Ludovic Berthier, Hugo Jacquin, and Francesco Zamponi. Microscopic theory of the jamming transition of harmonic spheres. *Physical Review E*, 84(5):051103, November 2011. doi: 10.1103/PhysRevE.84.051103. URL https://link.aps.org/doi/10.1103/PhysRevE.84.051103.

[42] R. Rammal, J.C. Angles d'Auriac, and B. Doucot. On the degree of ultrametricity. *Journal de Physique Lettres*, 46(20):945–952, 1985. ISSN 0302-072X. doi: 10.1051/jphyslet:019850046020094500. URL http://www.edpsciences.org/10.1051/jphyslet:019850046020094500.

[43] F. Murtagh. A Survey of Recent Advances in Hierarchical Clustering Algorithms. *The Computer Journal*, 26(4):354–359, November 1983. ISSN 0010-4620. doi: 10.1093/comjnl/26.4.354. URL https://academic.oup.com/comjnl/article/26/4/354/377434.

[44] Carl P. Goodrich, Andrea J. Liu, and Sidney R. Nagel. Finite-Size Scaling at the Jamming Transition. *Physical Review Letters*, 109(9):095704, August 2012. doi: 10.1103/PhysRevLett.109.095704. URL https://link.aps.org/doi/10.1103/PhysRevLett.109.095704.

[45] Joseph B. Kruskal. On the shortest spanning subtree of a graph and the traveling salesman problem. *Proceedings of the American Mathematical Society*, 7(1):48–50, 1956. ISSN 0002-9939, 1088-6826. doi: 10.1090/S0002-9939-1956-0078686-7. URL https://www.ams.org/proc/1956-007-01/S0002-9939-1956-0078686-7/.

[46] G. Parisi, P. Urbani, and F. Zamponi. Theory of Simple Glasses: Exact Solutions in Infinite Dimensions. *undefined*, 2020. URL https://www.semanticscholar.org/paper/Theory-of-Simple-Glasses%3A-Exact-Solutions-in-Parisi-Urbani/98e2d1f05eae274f745cf0831db9550b62e75a2c.

[47] Ludovic Berthier and Giulio Biroli. Theoretical perspective on the glass transition and amorphous materials. *Reviews of Modern Physics*, 83(2): 587–645, June 2011. doi: 10.1103/RevModPhys.83.587. URL https://link.aps.org/doi/10.1103/RevModPhys.83.587.

[48] Andrea J. Liu and Sidney R. Nagel. The Jamming Transition and the Marginally Jammed Solid. *Annual Review of Condensed Matter Physics*, 1(1): 347–369, 2010. doi: 10.1146/annurev-conmatphys-070909-104045. URL https://doi.org/10.1146/annurev-conmatphys-070909-104045.

[49] S. Torquato and F. H. Stillinger. Jammed hard-particle packings: From Kepler to Bernal and beyond. *Reviews of Modern Physics*, 82(3):2633–2672, September 2010. doi: 10.1103/RevModPhys.82.2633. URL https://link.aps.org/doi/10.1103/RevModPhys.82.2633. Publisher: American Physical Society.

[50] M. van Hecke. Jamming of soft particles: geometry, mechanics, scaling and isostaticity. *Journal of Physics: Condensed Matter*, 22(3):033101, December 2009. ISSN 0953-8984. doi: 10.1088/0953-8984/22/3/033101. URL https://doi.org/10.1088%2F0953-8984%2F22%2F3%2F033101. Publisher: IOP Publishing.

[51] Adrian Baule, Flaviano Morone, Hans J. Herrmann, and Hernán A. Makse. Edwards statistical mechanics for jammed granular matter. *Reviews of Modern Physics*, 90(1):015006, March 2018. doi: 10.1103/RevModPhys.90.015006. URL https://link.aps.org/doi/10.1103/RevModPhys.90.015006. Publisher: American Physical Society.

[52] A. J. Liu and S. Nagel. Nonlinear dynamics: Jamming is not just cool any more. *Nature*, 1998. doi: 10.1038/23819.

[53] J. Kurchan, G. Parisi, and F. Zamponi. Exact theory of dense amorphous hard spheres in high dimension I. The free energy. 2012. doi: 10.1088/1742-5468/2012/10/P10012.

[54] Edan Lerner, Gustavo Düring, and Matthieu Wyart. Low-energy non-linear excitations in sphere packings. *Soft Matter*, 9(34):8252–8263, 2013. doi: 10.1039/C3SM50515D. URL https://pubs.rsc.org/en/content/articlelanding/2013/sm/c3sm50515d. Publisher: Royal Society of Chemistry.

[55] Harukuni Ikeda. Jamming Below Upper Critical Dimension. *Physical Review Letters*, 125(3):038001, July 2020. doi: 10.1103/PhysRevLett.125.038001. URL https://link.aps.org/doi/10.1103/PhysRevLett.125.038001. Publisher: American Physical Society.

[56] Yuxiao Zhang, M. J. Godfrey, and M. A. Moore. Marginally jammed states of hard disks in a one-dimensional channel. *Physical Review E*, 102(4):042614, October 2020. doi: 10.1103/PhysRevE.102.042614. URL https://link.aps.org/doi/10.1103/PhysRevE.102.042614. Publisher: American Physical Society.

[57] Atsushi Ikeda, Ludovic Berthier, and Giulio Biroli. Dynamic criticality at the jamming transition. *The Journal of Chemical Physics*, 138(12):12A507, March 2013. ISSN 0021-9606. doi: 10.1063/1.4769251. URL https://aip.scitation.org/doi/10.1063/1.4769251. Publisher: American Institute of Physics.

[58] Adam B. Hopkins, Frank H. Stillinger, and Salvatore Torquato. Disordered strictly jammed binary sphere packings attain an anomalously large range of densities. *Physical Review E*, 88(2):022205, August 2013. doi: 10.1103/PhysRevE.88.022205. URL https://link.aps.org/doi/10.1103/PhysRevE.88.022205. Publisher: American Physical Society.

[59] Monica Skoge, Aleksandar Donev, Frank H. Stillinger, and Salvatore Torquato. Packing hyperspheres in high-dimensional Euclidean spaces. *Physical Review E*, 74(4):041127, October 2006. doi: 10.1103/PhysRevE.74.041127. URL https://link.aps.org/doi/10.1103/PhysRevE.74.041127. Publisher: American Physical Society.

[60] S. Torquato and Y. Jiao. Robust algorithm to generate a diverse class of dense disordered and ordered sphere packings via linear programming. *Physical Review E*, 82(6):061302, December 2010. doi: 10.1103/PhysRevE.82.061302. URL https://link.aps.org/doi/10.1103/PhysRevE.82.061302. Publisher: American Physical Society.

[61] Yang Jiao, Frank H. Stillinger, and Salvatore Torquato. Nonuniversality of density and disorder in jammed sphere packings. *Journal of Applied Physics*, 109(1):013508, January 2011. ISSN 0021-8979. doi: 10.1063/1.3524489. URL https://aip.scitation.org/doi/10.1063/1.3524489. Publisher: American Institute of Physics.

[62] E. DeGiuli, E. Lerner, and M. Wyart. Theory of the jamming transition at finite temperature. *The Journal of Chemical Physics*, 142(16):164503, April 2015. ISSN 0021-9606. doi: 10.1063/1.4918737. URL https://aip.scitation.org/doi/10.1063/1.4918737. Publisher: American Institute of Physics.

[63] Cristian F. Moukarzel. Isostatic Phase Transition and Instability in Stiff Granular Materials. *Physical Review Letters*, 81(8):1634–1637, August 1998. doi: 10.1103/PhysRevLett.81.1634. URL https://link.aps.org/doi/10.1103/PhysRevLett.81.1634. Publisher: American Physical Society.

[64] Carl P. Goodrich, Simon Dagois-Bohy, Brian P. Tighe, Martin van Hecke, Andrea J. Liu, and Sidney R. Nagel. Jamming in finite systems: Stability, anisotropy, fluctuations, and scaling. *Physical Review E*, 90(2):022138, August 2014. doi: 10.1103/PhysRevE.90.022138. URL https://link.aps.org/doi/10.1103/PhysRevE.90.022138. Publisher: American Physical Society.

[65] Carl P. Goodrich, Andrea J. Liu, and James P. Sethna. Scaling ansatz for the jamming transition. *Proceedings of the National Academy of Sciences of the United States of America*, 113(35):9745–9750, August 2016. ISSN 1091-6490. doi: 10.1073/pnas.1601858113.

[66] Carl P. Goodrich, Wouter G. Ellenbroek, and Andrea J. Liu. Stability of jammed packings I: the rigidity length scale. *Soft Matter*, 9(46):10993–10999, November 2013. ISSN 1744-6848. doi: 10.1039/C3SM51095F. URL https://pubs.rsc.org/en/content/articlelanding/2013/sm/c3sm51095f. Publisher: The Royal Society of Chemistry.

[67] Samuel S. Schoenholz, Carl P. Goodrich, Oleg Kogan, Andrea J. Liu, and Sidney R. Nagel. Stability of jammed packings II: the transverse length scale. *Soft Matter*, 9(46):11000–11006, November 2013. ISSN 1744-6848. doi: 10.1039/C3SM51096D. URL https://pubs.rsc.org/en/content/articlelanding/2013/sm/c3sm51096d. Publisher: The Royal Society of Chemistry.

[68] Daniel Hexner, Andrea J. Liu, and Sidney R. Nagel. Two Diverging Length Scales in the Structure of Jammed Packings. *Physical Review Letters*, 121(11): 115501, September 2018. doi: 10.1103/PhysRevLett.121.115501. URL https://link.aps.org/doi/10.1103/PhysRevLett.121.115501. Publisher: American Physical Society.

[69] Daniel Hexner, Pierfrancesco Urbani, and Francesco Zamponi. Can a Large Packing be Assembled from Smaller Ones? *Physical Review Letters*, 123(6): 068003, August 2019. doi: 10.1103/PhysRevLett.123.068003. URL https://link.aps.org/doi/10.1103/PhysRevLett.123.068003. Publisher: American Physical Society.

[70] Eric DeGiuli, Edan Lerner, Carolina Brito, and Matthieu Wyart. Force distribution affects vibrational properties in hard-sphere glasses. *Proceedings of the National Academy of Sciences of the United States of America*, 111(48): 17054–17059, December 2014. ISSN 1091-6490. doi: 10.1073/pnas.1415298111.

[71] Matthieu Wyart. Marginal Stability Constrains Force and Pair Distributions at Random Close Packing. *Physical Review Letters*, 109(12):125502, September 2012. doi: 10.1103/PhysRevLett.109.125502. URL https://link.aps.org/doi/10.1103/PhysRevLett.109.125502. Publisher: American Physical Society.

[72] Markus Müller and Matthieu Wyart. Marginal Stability in Structural, Spin, and Electron Glasses. *Annual Review of Condensed Matter Physics*, 6(1):177–200, 2015. doi: 10.1146/annurev-conmatphys-031214-014614. URL https://doi.org/10.1146/annurev-conmatphys-031214-014614. _eprint: https://doi.org/10.1146/annurev-conmatphys-031214-014614.

[73] Ludovic Berthier, Giulio Biroli, Patrick Charbonneau, Eric I. Corwin, Silvio Franz, and Francesco Zamponi. Gardner physics in amorphous solids and beyond. *The Journal of Chemical Physics*, 151(1):010901, July 2019. ISSN 0021-9606. doi: 10.1063/1.5097175. URL https://aip.scitation.org/doi/10.1063/1.5097175. Publisher: American Institute of Physics.

[74] Silvio Franz and Giorgio Parisi. The simplest model of jamming. *Journal of Physics A: Mathematical and Theoretical*, 49(14):145001, February 2016. ISSN 1751-8121. doi: 10.1088/1751-8113/49/14/145001. URL https://doi.org/10.1088/1751-8113/49/14/145001. Publisher: IOP Publishing.

[75] S. Franz, Antonio Sclocchi, and P. Urbani. Critical Jammed Phase of the Linear Perceptron. *Physical review letters*, 2019. doi: 10.1103/PhysRevLett.123.115702.

[76] S. Spigler, M. Geiger, Stéphane d'Ascoli, Levent Sagun, G. Biroli, and M. Wyart. A jamming transition from under- to over-parametrization affects loss landscape and generalization. *ArXiv*, 2018. doi: 10.1088/1751-8121/ab4c8b.

[77] Mario Geiger, Stefano Spigler, Stéphane d'Ascoli, Levent Sagun, Marco Baity-Jesi, Giulio Biroli, and Matthieu Wyart. Jamming transition as a paradigm to understand the loss landscape of deep neural networks. *Physical Review E*, 100(1):012115, July 2019. doi: 10.1103/PhysRevE.100.012115. URL https://link.aps.org/doi/10.1103/PhysRevE.100.012115. Publisher: American Physical Society.

[78] Silvio Franz, Sungmin Hwang, and Pierfrancesco Urbani. Jamming in Multilayer Supervised Learning Models. *Physical Review Letters*, 123(16): 160602, October 2019. doi: 10.1103/PhysRevLett.123.160602. URL https://link.aps.org/doi/10.1103/PhysRevLett.123.160602. Publisher: American Physical Society.

[79] Fabrizio Antenucci, Silvio Franz, Pierfrancesco Urbani, and Lenka Zdeborová. Glassy Nature of the Hard Phase in Inference Problems. *Physical Review X*, 9 (1):011020, January 2019. doi: 10.1103/PhysRevX.9.011020. URL https://link.aps.org/doi/10.1103/PhysRevX.9.011020. Publisher: American Physical Society.

[80] Giorgio Parisi, Maksim Sevelev, Pierfrancesco Urbani, and Francesco Zamponi. Universality of the SAT-UNSAT (jamming) threshold in non-convex continuous constraint satisfaction problems. *SciPost Physics*, 2, February 2017. doi: 10.21468/SciPostPhys.2.3.019.

[81] Florent Krzakala and Jorge Kurchan. Landscape analysis of constraint satisfaction problems. *Physical Review E*, 76(2):021122, August 2007. doi: 10.1103/PhysRevE.76.021122. URL https://link.aps.org/doi/10.1103/PhysRevE.76.021122. Publisher: American Physical Society.

[82] Silvio Franz, Antonio Sclocchi, and Pierfrancesco Urbani. Critical energy landscape of linear soft spheres. *SciPost Physics*, 9(1):012, July 2020. ISSN 2542-4653. doi: 10.21468/SciPostPhys.9.1.012. URL http://arxiv.org/abs/2002.04987. arXiv: 2002.04987.

[83] Patrick Charbonneau, Eric I. Corwin, Lin Fu, Georgios Tsekenis, and Michael van der Naald. Glassy, Gardner-like phenomenology in minimally polydisperse crystalline systems. *Physical Review E*, 99(2):020901, February 2019. doi: 10.1103/PhysRevE.99.020901. URL https://link.aps.org/doi/10.1103/PhysRevE.99.020901. Publisher: American Physical Society.

[84] G. Tsekenis. Jamming criticality of near–crystals. 2020. doi: 10.1209/0295-5075/ac0ffc.

[85] Harukuni Ikeda, Carolina Brito, and Matthieu Wyart. Infinitesimal asphericity changes the universality of the jamming transition. *Journal of Statistical Mechanics: Theory and Experiment*, 2020(3):033302, March 2020. ISSN 1742-5468. doi: 10.1088/1742-5468/ab74cb. URL https://doi.org/10.1088/1742-5468/ab74cb. Publisher: IOP Publishing.

[86] Carolina Brito, Harukuni Ikeda, Pierfrancesco Urbani, Matthieu Wyart, and Francesco Zamponi. Universality of jamming of nonspherical particles. *Proceedings of the National Academy of Sciences*, 115(46):11736–11741, November 2018. ISSN 0027-8424, 1091-6490. doi: 10.1073/pnas.1812457115. URL https://www.pnas.org/content/115/46/11736. Publisher: National Academy of Sciences Section: Physical Sciences.

[87] Yoav Kallus. Scaling collapse at the jamming transition. *Physical Review E*, 93 (1):012902, January 2016. doi: 10.1103/PhysRevE.93.012902. URL https://link.aps.org/doi/10.1103/PhysRevE.93.012902. Publisher: American Physical Society.

[88] Romain Mari and Jorge Kurchan. Dynamical transition of glasses: From exact to approximate. *The Journal of Chemical Physics*, 135(12):124504, September 2011. ISSN 0021-9606. doi: 10.1063/1.3626802. URL https://aip.scitation.org/doi/10.1063/1.3626802. Publisher: American Institute of Physics.

[89] Corey S. O'Hern, Stephen A. Langer, Andrea J. Liu, and Sidney R. Nagel. Random Packings of Frictionless Particles. *Physical Review Letters*, 88(7): 075507, January 2002. doi: 10.1103/PhysRevLett.88.075507. URL https://link.aps.org/doi/10.1103/PhysRevLett.88.075507. Publisher: American Physical Society.

[90] Varda F. Hagh, Eric I. Corwin, Kenneth Stephenson, and M. F. Thorpe. A broader view on jamming: from spring networks to circle packings. *Soft Matter*, 15(15):3076–3084, April 2019. ISSN 1744-6848. doi: 10.1039/C8SM01768A. URL https://pubs.rsc.org/en/content/articlelanding/2019/sm/c8sm01768a.

[91] Aleksandar Donev, Salvatore Torquato, and Frank H. Stillinger. Pair correlation function characteristics of nearly jammed disordered and ordered hard-sphere packings. *Physical Review E*, 71(1):011105, January 2005. doi: 10.1103/PhysRevE.71.011105. URL https://link.aps.org/doi/10.1103/PhysRevE.71.011105. Publisher: American Physical Society.

[92] Claudia Artiaco, Paolo Baldan, and Giorgio Parisi. Exploratory study of the glassy landscape near jamming. *Physical Review E*, 101(5):052605, May 2020. doi: 10.1103/PhysRevE.101.052605. URL https://link.aps.org/doi/10.1103/PhysRevE.101.052605. Publisher: American Physical Society.

[93] Rafael Díaz Hernández Rojas, Giorgio Parisi, and Federico Ricci-Tersenghi. Inferring the particle-wise dynamics of amorphous solids from the local structure at the jamming point. *Soft Matter*, 17(4):1056–1083, February 2021. ISSN 1744-6848. doi: 10.1039/C9SM02283J. URL https://pubs.rsc.org/en/content/articlelanding/2021/sm/c9sm02283j. Publisher: The Royal Society of Chemistry.

[94] Patrick Charbonneau and Peter K. Morse. Memory Formation in Jammed Hard Spheres. *Physical Review Letters*, 126(8):088001, February 2021. doi: 10.1103/PhysRevLett.126.088001. URL https://link.aps.org/doi/10.1103/PhysRevLett.126.088001. Publisher: American Physical Society.

[95] Daan Frenkel. Order through entropy. *Nature Materials*, 14(1):9–12, January 2015. ISSN 1476-4660. doi: 10.1038/nmat4178. URL https://www.nature.com/articles/nmat4178. Bandiera_abtest: a Cg_type: Nature Research Journals Number: 1 Primary_atype: Comments & Opinion Publisher: Nature Publishing Group Subject_term: Colloids;Self-assembly;Thermodynamics Subject_term_id: colloids;self-assembly;thermodynamics.

[96] Ning Xu, Jerzy Blawzdziewicz, and Corey S. O'Hern. Random close packing revisited: Ways to pack frictionless disks. *Physical Review E*, 71(6):061306, June 2005. doi: 10.1103/PhysRevE.71.061306. URL https://link.aps.org/doi/10.1103/PhysRevE.71.061306. Publisher: American Physical Society.

[97] Francesco Arceri and Eric I. Corwin. Vibrational Properties of Hard and Soft Spheres Are Unified at Jamming. *Physical Review Letters*, 124(23):238002, June 2020. doi: 10.1103/PhysRevLett.124.238002. URL https://link.aps.org/doi/10.1103/PhysRevLett.124.238002. Publisher: American Physical Society.

[98] Patrick Charbonneau, Yuliang Jin, Giorgio Parisi, and Francesco Zamponi. Hopping and the Stokes–Einstein relation breakdown in simple glass formers. *Proceedings of the National Academy of Sciences*, 111(42):15025–15030, October 2014. ISSN 0027-8424, 1091-6490. doi: 10.1073/pnas.1417182111. URL https://www.pnas.org/content/111/42/15025. Publisher: National Academy of Sciences Section: Physical Sciences.

[99] Patrick Charbonneau, Yuliang Jin, Giorgio Parisi, Corrado Rainone, Beatriz Seoane, and Francesco Zamponi. Numerical detection of the Gardner transition in a mean-field glass former. *Physical Review E*, 92(1):012316, July 2015. doi: 10.1103/PhysRevE.92.012316. URL https://link.aps.org/doi/10.1103/PhysRevE.92.012316. Publisher: American Physical Society.

[100] Mark Newman. Power Laws, Pareto Distributions and Zipf's Law. *Contemporary Physics - CONTEMP PHYS*, 46, December 2004. doi: 10.1080/00107510500052444.

[101] Daniel J. Amit and Victor Martin-Mayor. *Field Theory, the Renormalization Group, and Critical Phenomena: Graphs to Computers*. WSPC, Singapore, 3rd ed. edition edition, June 2005. ISBN 978-981-256-119-0.

[102] M. E. J. Newman. *Monte Carlo methods in statistical physics*. Clarendon Press ;, Oxford :, 2011. ISBN 978-0-19-851797-9. Pages: xiv, 475 pages :.

[103] J. Wang and A. P. Young. Monte Carlo study of the six-dimensional Ising spin glass. *Journal of Physics A: Mathematical and General*, 26(5):1063–1066, March 1993. ISSN 0305-4470. doi: 10.1088/0305-4470/26/5/025. URL `https://doi.org/10.1088/0305-4470/26/5/025`. Publisher: IOP Publishing.

[104] J. Ruiz-Lorenzo. Logarithmic corrections for spin glasses, percolation and Lee-Yang singularities in six dimensions. 1998. doi: 10.1088/0305-4470/31/44/006.

[105] R. Kenna. Finite size scaling for O(N) 4-theory at the upper critical dimension. 2004. doi: 10.1016/j.nuclphysb.2004.05.012.

[106] Harukuni Ikeda, Pierfrancesco Urbani, and Francesco Zamponi. Mean field theory of jamming of nonspherical particles. *Journal of Physics A: Mathematical and Theoretical*, 52(34):344001, July 2019. ISSN 1751-8121. doi: 10.1088/1751-8121/ab3079. URL `https://doi.org/10.1088/1751-8121/ab3079`. Publisher: IOP Publishing.

[107] Carlo Lucibello, Flaviano Morone, Giorgio Parisi, Federico Ricci-Tersenghi, and Tommaso Rizzo. Anomalous finite size corrections in random field models. *Journal of Statistical Mechanics: Theory and Experiment*, 2014, June 2014. doi: 10.1088/1742-5468/2014/10/P10025.

[108] C. Lucibello, F. Morone, G. Parisi, F. Ricci-Tersenghi, and Tommaso Rizzo. Finite-size corrections to disordered Ising models on random regular graphs. *Physical Review E*, 90(1):012146, July 2014. doi: 10.1103/PhysRevE.90.012146. URL `https://link.aps.org/doi/10.1103/PhysRevE.90.012146`. Publisher: American Physical Society.

[109] U. Ferrari, C. Lucibello, F. Morone, G. Parisi, F. Ricci-Tersenghi, and T. Rizzo. Finite-size corrections to disordered systems on Erd\"os-R\'enyi random graphs. *Physical Review B*, 88(18):184201, November 2013. doi: 10.1103/PhysRevB.88.184201. URL `https://link.aps.org/doi/10.1103/PhysRevB.88.184201`. Publisher: American Physical Society.

[110] R. Buckminster Fuller. *Synergetics: Explorations in the Geometry of Thinking*. Estate of R. Buckminster Fuller, 1982. ISBN 978-0-02-065320-2. Google-Books-ID: AKDgDQAAQBAJ.

[111] S. S. Kistler. Coherent Expanded Aerogels and Jellies. *Nature*, 127(3211): 741–741, May 1931. ISSN 1476-4687. doi: 10.1038/127741a0. URL https://www.nature.com/articles/127741a0. Number: 3211 Publisher: Nature Publishing Group.

[112] Paul Bourke. An introduction to the Apollonian fractal. *Computers & Graphics*, 30(1):134–136, February 2006. ISSN 0097-8493. doi: 10.1016/j.cag.2005.10.017. URL http://www.sciencedirect.com/science/article/pii/S0097849305002189.

[113] Jeffrey Lagarias, Colin Mallows, and Allan Wilks. Beyond the Descartes circle theorem (American Mathematical Monthly (2002) 109, 338-361)). 115, October 2008.

[114] Adrian Del Caro. Dionysian Classicism, or Nietzsche's Appropriation of an Aesthetic Norm. *Journal of the History of Ideas*, 50(4):589–605, 1989. ISSN 0022-5037. doi: 10.2307/2709799. URL https://www.jstor.org/stable/2709799. Publisher: University of Pennsylvania Press.

[115] Robert Connelly. Rigidity of packings. *European Journal of Combinatorics*, 29 (8):1862–1871, November 2008. ISSN 0195-6698. doi: 10.1016/j.ejc.2008.01.009. URL http://www.sciencedirect.com/science/article/pii/S0195669808000267.

[116] S. Torquato, A. Donev, and F. H. Stillinger. Breakdown of elasticity theory for jammed hard-particle packings: conical nonlinear constitutive theory. *International Journal of Solids and Structures*, 40(25):7143–7153, December 2003. ISSN 0020-7683. doi: 10.1016/S0020-7683(03)00359-7. URL http://www.sciencedirect.com/science/article/pii/S0020768303003597.

[117] Aleksandar Donev, Salvatore Torquato, Frank H. Stillinger, and Robert Connelly. Jamming in hard sphere and disk packings. *Journal of Applied Physics*, 95(3):989–999, January 2004. ISSN 0021-8979. doi: 10.1063/1.1633647. URL https://aip.scitation.org/doi/10.1063/1.1633647. Publisher: American Institute of Physics.

[118] Aleksandar Donev, Salvatore Torquato, Frank H. Stillinger, and Robert Connelly. A linear programming algorithm to test for jamming in hard-sphere packings. *Journal of Computational Physics*, 197(1):139–166, June 2004. ISSN 0021-9991. doi: 10.1016/j.jcp.2003.11.022. URL http://www.sciencedirect.com/science/article/pii/S0021999103006235.

[119] Sal Torquato and Frank H. Stillinger. Toward the jamming threshold of sphere packings: Tunneled crystals. 2007. doi: 10.1063/1.2802184.

[120] K Böröczky. Über stabile Kreis- und Kugelsysteme. *Annales Universitatis Scientiarium Budapestinensis de Rolando Eötvös Nominatae Sectio Mathematica*, 7:79–82, 1964.

[121] Matthew Kahle. Sparse Locally-Jammed Disk Packings. *Annals of Combinatorics*, 16(4):773–780, December 2012. ISSN 0219-3094. doi: 10.1007/s00026-012-0159-0. URL https://doi.org/10.1007/s00026-012-0159-0.

[122] Aleksandar Donev and Salvatore Torquato. Energy-efficient actuation in infinite lattice structures. *Journal of the Mechanics and Physics of Solids*, 51 (8):1459–1475, August 2003. ISSN 0022-5096. doi: 10.1016/S0022-5096(03)00048-6. URL http://www.sciencedirect.com/science/article/pii/S0022509603000486.

[123] Robert Connelly, Asia Ivić Weiss, and Walter Whiteley, editors. *Rigidity and Symmetry*. Fields Institute Communications. Springer-Verlag, New York, 2014. ISBN 978-1-4939-0780-9. doi: 10.1007/978-1-4939-0781-6. URL https://www.springer.com/gp/book/9781493907809.

[124] Ching-Lung Liao, Ta-Peng Chang, Dong-Hwa Young, and Ching S. Chang. Stress-strain relationship for granular materials based on the hypothesis of best fit. *International Journal of Solids and Structures*, 34(31):4087–4100, November 1997. ISSN 0020-7683. doi: 10.1016/S0020-7683(97)00015-2. URL http://www.sciencedirect.com/science/article/pii/S0020768397000152.

[125] T. C. Lubensky, C. L. Kane, Xiaoming Mao, A. Souslov, and Kai Sun. Phonons and elasticity in critically coordinated lattices. *Reports on Progress in Physics*, 78(7):073901, June 2015. ISSN 0034-4885. doi: 10.1088/0034-4885/78/7/073901. URL https://doi.org/10.1088%2F0034-4885%2F78%2F7%2F073901. Publisher: IOP Publishing.

[126] Donald Askeland and Pradeep Fulay. *The Science & Engineering of Materials*. Cengage Learning, April 2005. ISBN 978-0-534-55396-8. Google-Books-ID: fRbZslUtpBYC.

[127] Beer. *Mechanics Of Materials (Si Units) 5E*. McGraw-Hill Education (India) Pvt Limited, 2009. ISBN 978-0-07-015389-9.

[128] A. Ballato. Poisson's ratio for tetragonal, hexagonal, and cubic crystals. *IEEE Transactions on Ultrasonics, Ferroelectrics, and Frequency Control*, 43(1): 56–62, January 1996. ISSN 1525-8955. doi: 10.1109/58.484463. Conference Name: IEEE Transactions on Ultrasonics, Ferroelectrics, and Frequency Control.

[129] Existence and Construction of Generalized Inverses. In Adi Ben-Israel and Thomas N. E. Greville, editors, *Generalized Inverses: Theory and Applications*, CMS Books in Mathematics, pages 40–51. Springer, New York, NY, 2003. ISBN 978-0-387-21634-8. doi: 10.1007/0-387-21634-0_3. URL https://doi.org/10.1007/0-387-21634-0_3.

[130] V. Klema and A. Laub. The singular value decomposition: Its computation and some applications. 1980. doi: 10.1109/TAC.1980.1102314.

[131] Andrea J. Liu and Sidney R. Nagel. Jamming is not just cool any more. *Nature*, 396(6706):21–22, November 1998. ISSN 1476-4687. doi: 10.1038/23819. URL https://www.nature.com/articles/23819. Number: 6706 Publisher: Nature Publishing Group.

[132] Jie Lin, Ivane Jorjadze, Lea-Laetitia Pontani, Matthieu Wyart, and Jasna Brujic. Evidence for Marginal Stability in Emulsions. *Physical Review Letters*, 117(20):208001, November 2016. doi: 10.1103/PhysRevLett.117.208001. URL https://link.aps.org/doi/10.1103/PhysRevLett.117.208001. Publisher: American Physical Society.

[133] R. C. Dennis and E. I. Corwin. Jamming Energy Landscape is Hierarchical and Ultrametric. *Physical Review Letters*, 124(7):078002, February 2020. doi: 10.1103/PhysRevLett.124.078002. URL https://link.aps.org/doi/10.1103/PhysRevLett.124.078002. Publisher: American Physical Society.

[134] Shoji Ichihara, Akihiko Komatsu, Yoshiharu Tsujita, Takuhei Nose, and Toshio Hata. Thermodynamic Studies on the Glass Transition and the Glassy State of Polymers. I. Pressure Dependence of the Glass Transition Temperature and Its Relation to Other Thermodynamic Properties of Polystyrene. *Polymer Journal*, 2(4):530–534, July 1971. ISSN 1349-0540. doi: 10.1295/polymj.2.530. URL https://www.nature.com/articles/pj197159. Bandiera_abtest: a Cg_type: Nature Research Journals Number: 4 Primary_atype: Research Publisher: Nature Publishing Group.

[135] D. Cangialosi. Dynamics and thermodynamics of polymer glasses. *Journal of Physics. Condensed Matter: An Institute of Physics Journal*, 26(15):153101, April 2014. ISSN 1361-648X. doi: 10.1088/0953-8984/26/15/153101.

[136] Xavier Monnier, Juan Colmenero, Marcel Wolf, and Daniele Cangialosi. Reaching the Ideal Glass in Polymer Spheres: Thermodynamics and Vibrational Density of States. *Physical Review Letters*, 126(11):118004, March 2021. doi: 10.1103/PhysRevLett.126.118004. URL https://link.aps.org/doi/10.1103/PhysRevLett.126.118004. Publisher: American Physical Society.

[137] Guozhang Wu, Yuanbiao Liu, and Gaopeng Shi. New Experimental Evidence for Thermodynamic Links to the Kinetic Fragility of Glass-Forming Polymers. *Macromolecules*, 54(12):5595–5606, June 2021. ISSN 0024-9297. doi: 10.1021/acs.macromol.1c00670. URL https://doi.org/10.1021/acs.macromol.1c00670. Publisher: American Chemical Society.

[138] J. D. Watson and F. H. C. Crick. Molecular Structure of Nucleic Acids: A Structure for Deoxyribose Nucleic Acid. *Nature*, 171(4356):737–738, April 1953. ISSN 1476-4687. doi: 10.1038/171737a0. URL https://www.nature.com/articles/171737a0. Bandiera_abtest: a Cg_type: Nature Research Journals Number: 4356 Primary_atype: Research Publisher: Nature Publishing Group.

[139] Cyrille Boyer, Xin Huang, Michael R. Whittaker, Volga Bulmus, and Thomas P. Davis. An overview of protein–polymer particles. *Soft Matter*, 7 (5):1599–1614, February 2011. ISSN 1744-6848. doi: 10.1039/C0SM00412J. URL https://pubs.rsc.org/en/content/articlelanding/2011/sm/c0sm00412j. Publisher: The Royal Society of Chemistry.

[140] Keiji Numata. How to define and study structural proteins as biopolymer materials. *Polymer Journal*, 52(9):1043–1056, September 2020. ISSN 1349-0540. doi: 10.1038/s41428-020-0362-5. URL https://www.nature.com/articles/s41428-020-0362-5. Bandiera_abtest: a Cc_license_type: cc_by Cg_type: Nature Research Journals Number: 9 Primary_atype: Reviews Publisher: Nature Publishing Group Subject_term: Biomaterials – proteins;Polymers Subject_term_id: biomaterials-proteins;polymers.

[141] Sarah-Jeanne Royer, Sara Ferrón, Samuel T. Wilson, and David M. Karl. Production of methane and ethylene from plastic in the environment. *PLoS ONE*, 13(8):e0200574, August 2018. ISSN 1932-6203. doi: 10.1371/journal.pone.0200574. URL https://www.ncbi.nlm.nih.gov/pmc/articles/PMC6070199/.

[142] Sunil Ghatge, Youri Yang, Jae-Hyung Ahn, and Hor-Gil Hur. Biodegradation of polyethylene: a brief review. *Applied Biological Chemistry*, 63(1):27, May 2020. ISSN 2468-0842. doi: 10.1186/s13765-020-00511-3. URL https://doi.org/10.1186/s13765-020-00511-3.

[143] Ling-Nan Zou, Xiang Cheng, Mark L. Rivers, Heinrich M. Jaeger, and Sidney R. Nagel. The Packing of Granular Polymer Chains. *Science*, 326 (5951):408–410, October 2009. doi: 10.1126/science.1177114. URL https://www.science.org/doi/full/10.1126/science.1177114. Publisher: American Association for the Advancement of Science.

[144] Jean-Louis Barrat, Jörg Baschnagel, and Alexey Lyulin. Molecular dynamics simulations of glassy polymers. *Soft Matter*, 6(15):3430–3446, July 2010. ISSN 1744-6848. doi: 10.1039/B927044B. URL https://pubs.rsc.org/en/content/articlelanding/2010/sm/b927044b. Publisher: The Royal Society of Chemistry.

[145] Nikos Karayiannis, Katerina Foteinopoulou, and Manuel Laso. Spontaneous Crystallization in Athermal Polymer Packings. *International journal of molecular sciences*, 14:332–58, December 2012. doi: 10.3390/ijms14010332.

[146] Robert S. Hoy. Jamming of Semiflexible Polymers. *Physical Review Letters*, 118(6):068002, February 2017. doi: 10.1103/PhysRevLett.118.068002. URL https://link.aps.org/doi/10.1103/PhysRevLett.118.068002. Publisher: American Physical Society.

[147] Thomas E. Gartner and Arthi Jayaraman. Modeling and Simulations of Polymers: A Roadmap. *Macromolecules*, 52(3):755–786, February 2019. ISSN 0024-9297. doi: 10.1021/acs.macromol.8b01836. URL https://doi.org/10.1021/acs.macromol.8b01836. Publisher: American Chemical Society.

[148] Vlasis G. Mavrantzas. Using Monte Carlo to Simulate Complex Polymer Systems: Recent Progress and Outlook. *Frontiers in Physics*, 9:173, 2021. ISSN 2296-424X. doi: 10.3389/fphy.2021.661367. URL https://www.frontiersin.org/article/10.3389/fphy.2021.661367.

[149] Lloyd Nicholas Trefethen and David Bau. *Numerical Linear Algebra*. Society for Industrial and Applied Mathematics, 1997. ISBN 978-0-89871-487-6. Google-Books-ID: 5Y1TPgAACAAJ.

[150] Andrew Kerr, Dan Campbell, and Mark Richards. QR decomposition on GPUs. pages 71–78, January 2009. doi: 10.1145/1513895.1513904.

[151] Johan Verbeke and Ronald Cools. The Newton-Raphson method. *International Journal of Mathematical Education in Science and Technology*, 26(2):177–193, March 1995. ISSN 0020-739X. doi: 10.1080/0020739950260202. URL https://doi.org/10.1080/0020739950260202. Publisher: Taylor & Francis _eprint: https://doi.org/10.1080/0020739950260202.

[152] M. Lisa Manning. Vibrational modes identify soft spots in a sheared model glass. March 2011.

[153] M. L. Manning and A. J. Liu. Vibrational Modes Identify Soft Spots in a Sheared Disordered Packing. *Physical Review Letters*, 107(10):108302, August 2011. doi: 10.1103/PhysRevLett.107.108302. URL https://link.aps.org/doi/10.1103/PhysRevLett.107.108302. Publisher: American Physical Society.

[154] Edward J. Banigan, Matthew K. Illich, Derick J. Stace-Naughton, and David A. Egolf. The chaotic dynamics of jamming. *Nature Physics*, 9(5): 288–292, May 2013. ISSN 1745-2481. doi: 10.1038/nphys2593. URL https://www.nature.com/articles/nphys2593. Bandiera_abtest: a Cg_type: Nature Research Journals Number: 5 Primary_atype: Research Publisher: Nature Publishing Group Subject_term: Particle physics;Statistical physics, thermodynamics and nonlinear dynamics Subject_term_id: particle-physics;statistical-physics-thermodynamics-and-nonlinear-dynamics.

[155] Corrado Rainone, Eran Bouchbinder, and Edan Lerner. Pinching a glass reveals key properties of its soft spots. *Proceedings of the National Academy of Sciences*, 117(10):5228–5234, March 2020. ISSN 0027-8424, 1091-6490. doi: 10.1073/pnas.1919958117. URL https://www.pnas.org/content/117/10/5228. Publisher: National Academy of Sciences Section: Physical Sciences.

[156] R. Hill. The Elastic Behaviour of a Crystalline Aggregate. *Proceedings of the Physical Society. Section A*, 65(5):349–354, May 1952. ISSN 0370-1298. doi: 10.1088/0370-1298/65/5/307. URL https://doi.org/10.1088/0370-1298/65/5/307. Publisher: IOP Publishing.

[157] J. Peter Watt, Geoffrey F. Davies, and Richard J. O'Connell. The elastic properties of composite materials. *Reviews of Geophysics*, 14(4):541–563, 1976. ISSN 1944-9208. doi: 10.1029/RG014i004p00541. URL https://agupubs.onlinelibrary.wiley.com/doi/abs/10.1029/RG014i004p00541.

[158] J. Clerk Maxwell F.R.S. L. On the calculation of the equilibrium and stiffness of frames. *The London, Edinburgh, and Dublin Philosophical Magazine and Journal of Science*, May 2009. doi: 10.1080/14786446408643668. URL https://www.tandfonline.com/doi/abs/10.1080/14786446408643668. Publisher: Taylor & Francis Group.

[159] C. R. Calladine. Buckminster Fuller's "Tensegrity" structures and Clerk Maxwell's rules for the construction of stiff frames. *International Journal of Solids and Structures*, 14(2):161–172, January 1978. ISSN 0020-7683. doi: 10.1016/0020-7683(78)90052-5. URL https://www.sciencedirect.com/science/article/pii/0020768378900525.

[160] Justin Malestein and Louis Theran. Generic combinatorial rigidity of periodic frameworks. *Advances in Mathematics*, 233(1):291–331, January 2013. ISSN 0001-8708. doi: 10.1016/j.aim.2012.10.007. URL https://www.sciencedirect.com/science/article/pii/S000187081200388X.

[161] Robert Connelly and Walter Whiteley. Second-Order Rigidity and Prestress Stability for Tensegrity Frameworks. *SIAM Journal on Discrete Mathematics*, 9(3):453–491, August 1996. ISSN 0895-4801. doi: 10.1137/S0895480192229236. URL https://epubs.siam.org/doi/abs/10.1137/S0895480192229236. Publisher: Society for Industrial and Applied Mathematics.

[162] Miranda Holmes-Cerfon, Louis Theran, and Steven J. Gortler. Almost-Rigidity of Frameworks. *Communications on Pure and Applied Mathematics*, 74(10): 2185–2247, 2021. ISSN 1097-0312. doi: 10.1002/cpa.21971. URL https://onlinelibrary.wiley.com/doi/abs/10.1002/cpa.21971. _eprint: https://onlinelibrary.wiley.com/doi/pdf/10.1002/cpa.21971.

[163] Ojan Khatib Damavandi, Varda F. Hagh, Christian D. Santangelo, and M. Lisa Manning. Energetic rigidity II: Applications in examples of biological and underconstrained materials. *arXiv:2107.06868 [cond-mat, physics:physics]*, July 2021. URL http://arxiv.org/abs/2107.06868. arXiv: 2107.06868.

[164] Ojan Khatib Damavandi, Varda F. Hagh, Christian D. Santangelo, and M. Lisa Manning. Energetic rigidity I: A unifying theory of mechanical stability. *arXiv:2102.11310 [cond-mat, physics:physics]*, July 2021. URL http://arxiv.org/abs/2102.11310. arXiv: 2102.11310.

[165] S. D Guest and J. W Hutchinson. On the determinacy of repetitive structures. *Journal of the Mechanics and Physics of Solids*, 51(3):383–391, March 2003. ISSN 0022-5096. doi: 10.1016/S0022-5096(02)00107-2. URL https://www.sciencedirect.com/science/article/pii/S0022509602001072.

[166] J. C. Owen and S. C. Power. Frameworks symmetry and rigidity. *International Journal of Computational Geometry & Applications*, 20(06):723–750, December 2010. ISSN 0218-1959. doi: 10.1142/S0218195910003505. URL https://www.worldscientific.com/doi/abs/10.1142/S0218195910003505. Publisher: World Scientific Publishing Co.

[167] Charles Kittel. *Introduction to Solid State Physics*. Wiley, Hoboken, NJ, 8th edition edition, November 2004. ISBN 978-0-471-41526-8.

[168] Ciprian Borcea and Ileana Streinu. Liftings and Stresses for Planar Periodic Frameworks. *Discrete & Computational Geometry*, 53(4):747–782, June 2015. ISSN 1432-0444. doi: 10.1007/s00454-015-9689-7. URL https://doi.org/10.1007/s00454-015-9689-7.